SHIP

SCIENCE & TECHNOLOGY

CIENCIA & TECNOLOGÍA DE BUQUES

ISSN 1909-8642

COTECMAR
COLOMBIA

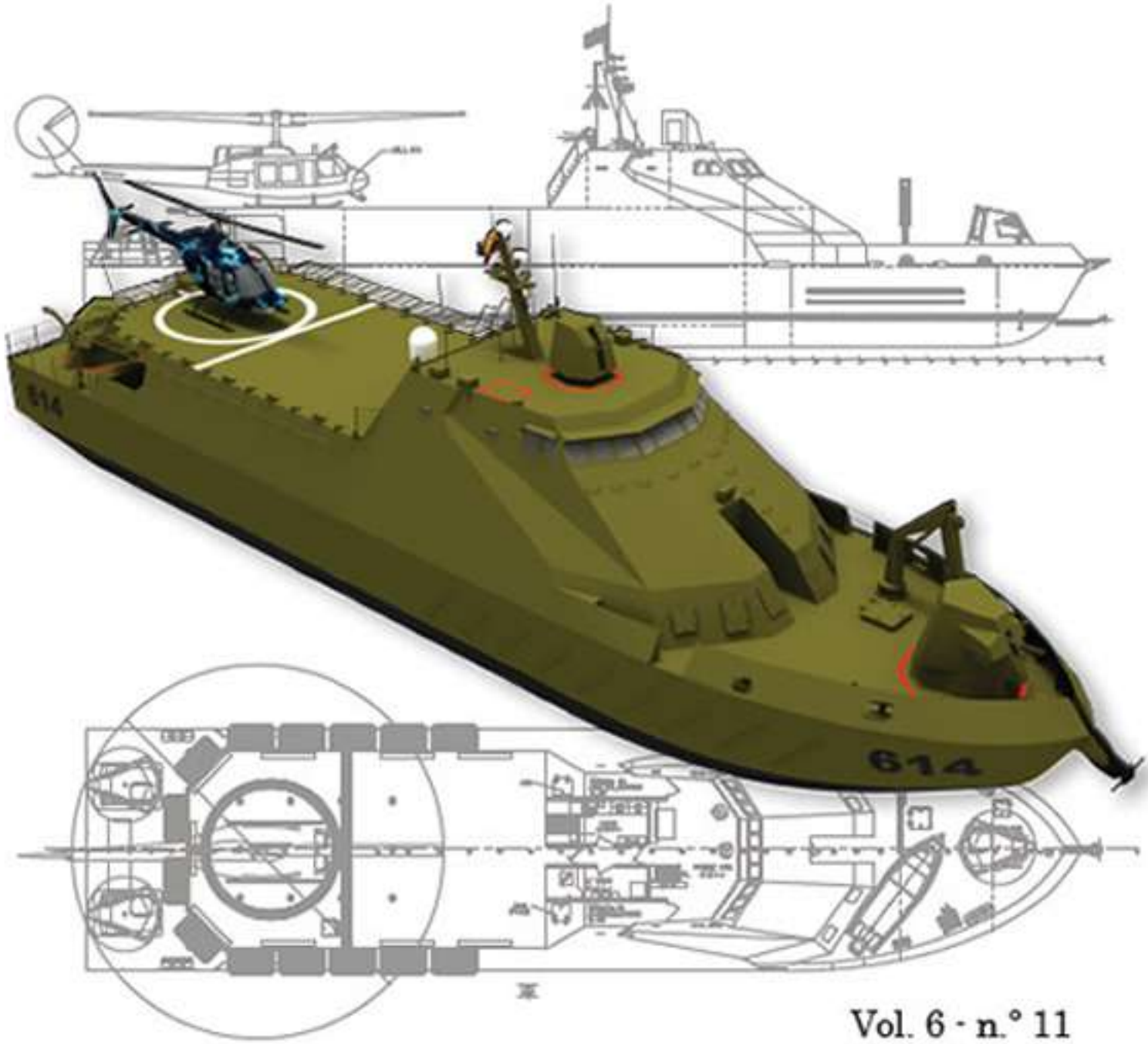

Vol. 6 - n.° 11
(1 - 112) July 2012

Ship Science & Technology ISSN 1909-8642 Vol. 6 - No. 11 - July 2012 Colombia

SHIP
SCIENCE & TECHNOLOGY
CIENCIA & TECNOLOGÍA DE BUQUES

Volume 6, Number 11 July 2012 ISSN 1909-8642

Ship Science & Technology is a specialized journal in topics related to naval architecture, and naval, marine and ocean engineering. Every six months, the journal publishes scientific papers that constitute an original contribution in the development of the mentioned areas, resulting from research projects of the Science and Technology Corporation for the Naval, Maritime and Riverine Industries, and other institutions and researchers. It is distributed nationally and internationally by exchange or subscription.

A publication of

Corporación de Ciencia y Tecnología para el Desarrollo de la Industria Naval, Marítima y Fluvial - Cotecmar
Electronic version: www.shipjournal.co

Editorial Coordinator
Karen Domínguez Martínez. M.Sc.
Jimmy Saravia Arenas. M.Sc. (c)

Layout and design
Mauricio Sarmiento Barreto

Printed by
C&D Publicidad & Marketing. Bogotá, D.C.

COTECMAR
COLOMBIA

SHIP
SCIENCE & TECHNOLOGY
CIENCIA & TECNOLOGÍA DE BUQUES

Volume 6, Number 11 July 2012 ISSN 1909-8642

9 Project and Construction of Oceanographic and Faisheries Research Vessels in Spain
Proyecto y Construcción de Buques Oceanográficos y de Investigación Pesquera en España
José Fernando Núñez Basáñez

35 Analysis and Prediction of Welding Distortion in complex Structures Using Elastic Finite Element Method
Análisis y Predicción de Distorsiones en Estructuras Soldadas complejas por medio de Análisis Elástico de Elementos Finitos
Adán Vega Sáenz, Carlos Plazaola, Ilka Banfield, Sherif Rashed, Hidekazu Murakawa

43 Study of the weldability of Aluminum Alloy 5083 H116 with Pulsed Arc GMAW (GMAW-P)
Estudio de soldabilidad de aleación de aluminio 5083 H116 con arco pulsado GMAW (GMAW-P)
Cueca, F., Morales, A., Muñoz, R., Patarroyo, A., Rojas, F., Solano, E.

57 Shooting Simulator for Fluvial Combat Training
Sistema de simulación de tiro para entrenamiento de combate fluvial
Carlos F. Rodríguez, José Tiberio Hernández, Pablo Figueroa

67 Side-boat tow to Test the Influence of Flaps in a 2-meter Planing Craft Model
Remolque lateral de embarcación para comprobar la influencia de dispositivos sustentadores (flaps) sobre un modelo de embarcación de planeo de 2 metros
José R. Marín, Daniela A. Benites

79 Dynamic modeling of trawl fishing gear components
Modelación Dinámica de componentes de Aparejos de Pesca de Arrastre
Jorge Freiria Pereira

91 Analysis of radar cross section assessment methods and parameters affecting it for surface ships
Análisis de Métodos de Evaluación de la Sección Transversal de Radar y de los Parámetros que Inciden en Ella para Buques de Superficie
Vladimir Díaz Charris, José Manuel Gómez Torres

SHIP
SCIENCE & TECHNOLOGY
CIENCIA & TECNOLOGÍA DE BUQUES

Editorial Note

Cartagena de Indias, 23 July 2012.

Cotecmar has over the last 12 years constituted itself as an institution that innovates and learns to undertake the big responsibility of designing and building the Strategic Surface Platform (PES, for the term in Spanish), the ships that will replace our current frigates. As indicated by Rear Admiral Roberto Sáchica Mejía, President of Cotecmar, during this anniversary's commemoration last July 21st, we must bear in mind that Cotecmar is not merely an organization that builds and repairs ships, it is an organization that generates skills in science and technology for the development of a strategic industry that generates employment and security, which results in great social benefit for all Colombians.

With this perspective, the *Ship Science and Technology* journal contributes by being one of the scientific publication media that helps to introduce updated knowledge on themes related to naval engineering, naval architecture, and related topics that contribute to increase the performance of ships and shipyards. In this edition, we are introducing research related to oceanographic and fishing research vessels in Spain, analysis and prediction of distortions in complex welded structures, weld ability of aluminum alloy, tow simulation systems, flap influence tests, dynamic modeling of fishing rig components, and – finally – assessment methods of the radar cross section.

We hope these contents are of great benefit to the national and international community and we also hope they contribute to Cotecmar's challenge of becoming an innovation leader in Latin America. We urge you to keep contributing with research results in order to consolidate the *Ship Science and Technology* journal as a world-class publication.

Commander OSCAR DARÍO TASCÓN MUÑOZ

SHIP
SCIENCE & TECHNOLOGY
CIENCIA & TECNOLOGÍA DE BUQUES

Nota Editorial

Cartagena de Indias, 23 de julio de 2012.

Cotecmar ha cumplido 12 años constituyéndose en una institución que innova y que aprende para llevar a cabo la gran responsabilidad de diseñar y construir la Plataforma Estratégica de Superficie PES, embarcación que reemplazará las actuales fragatas. Como lo indicaba el Señor CALM Roberto Sáchica Mejía, Presidente de Cotecmar durante la conmemoración de este aniversario, el pasado 21 de Julio, debemos tener presente que Cotecmar no es sólo una organización que construye y repara buques, es una organización que genera capacidades en Ciencia y Tecnología para el desarrollo de una industria estratégica generadora de empleo y seguridad que redunda en un gran beneficio social para todos los colombianos.

Con esta perspectiva la *Revista Ciencia y Tecnología de Buques* contribuye siendo uno de los medios de divulgación científica que ayuda a presentar conocimiento actualizado sobre temas relacionados con la ingeniería naval, arquitectura naval y temas afines que contribuyan al desempeño efectivo de los buques y astilleros.

Es por eso que para esta edición les presentamos investigaciones relacionadas con Buques oceanográficos y de investigación pesquera en España, Análisis y predicción de distorsiones en estructuras soldadas complejas, Soldabilidad de aleación de aluminio, Sistemas de simulación de tiro, Pruebas de influencia de Flaps, Modelación dinámica de componentes de aparejos de pesca y finalmente, Métodos de evaluación de la sección transversal de radar.

Esperamos que estos contenidos sean de amplio provecho para la comunidad científica nacional e internacional y que aporten al reto de Cotecmar de ser un líder innovador en América Latina. Los exhortamos a continuar contribuyendo con resultados de investigación para seguir consolidando a la *Revista Ciencia y Tecnología de Buques* como una publicación de clase mundial.

Capitán de Fragata OSCAR DARÍO TASCÓN MUÑOZ

Project and Construction of Oceanographic and Faisheries Research Vessels in Spain

Proyecto y Construcción de Buques Oceanográficos y de Investigación Pesquera en España

José Fernando Núñez Basáñez [1]

Abstract

The objective of the paper is to analyze and present the specific and innovative characteristics of the multipurpose oceanographic vessels that are currently being built in Spain. The main requirement in these types of vessels is the low level of noise radiated to the water, Silent Platform, according to ICES 209, to satisfactorily exploit the evaluation of the Fishing Resources and its dynamic position capacity for operations with remote operating vehicles. These vessels are designed to carry out a wide range of research activities and have, therefore, the most modern facilities, laboratories, and equipment to undertake scientific missions in the different marine disciplines: Marine Geology, Physical Oceanography, Chemical Oceanography, Pollution, Marine Biology, and Fisheries.

Key words: Multipurpose Oceanographic Vessels (MOV), Noise radiated, Marine Scientific Missions (MSM)

Resumen

Con este trabajo, se pretende analizar y presentar las características específicas e innovadoras de los Buques Oceanográficos Multipropósito que, actualmente, se están construyendo en España. El principal requerimiento en este tipo de buques es su bajo nivel de ruido radiado al agua, *Plataforma Silenciosa*, de acuerdo con ICES 209, para explotar satisfactoriamente la evaluación de los Recursos Pesqueros y su capacidad de posición dinámica para operaciones con vehículos de operación remota. Los buques son diseñados para llevar a cabo un amplio rango de actividades de investigación y disponen, por tanto, de las más modernas instalaciones, laboratorios y equipos, para realizar misiones científicas en las diferentes disciplinas marinas: Geología Marina, Oceanografía Física, Oceanografía Química, Contaminación y Biología Marina y Pesquerías.

Palabras claves: Buques Multipropósitos Oceánicos, Ruido radiado, Misiones Marítimas Científicas

Date Received: December 2nd, 2010 - *Fecha de recepción: 2 de Diciembre de 2010*
Date Accepted: March 6th, 2012 - *Fecha de aceptación: 6 de Marzo de 2012*

[1] Escuela Técnica Superior de Ingenieros Navales. Universidad Politécnica de Madrid. Doctor Ingeniero Naval. Catedrático de Universidad. Madrid, España. e-mail: josefnunez2005@hotmail.com

Introduction

Oceanographic ships are research vessels designed to collect quantitative data from the sea surface, its depths, the sea floor, and the overlying atmosphere. Their primary purpose is to transport scientists and increasingly sophisticated equipment to and from study sites on the ocean's surface, and in some cases below the surface. The ships must have the ability to lower and retrieve instruments by using winches and wires. The ship's equipment and instrumentation must precisely determine the location on the sea surface, and provide suitable communication, data gathering, archiving, and computational facilities for the scientific party.

The requirements list includes **seakeeping** (sea-kindliness, a measure of the ship's responses to severe seas; and station-keeping, the ability of a ship to maintain its fixed location on the sea surface); **work environment**; **endurance** (range, days at sea); **scientific complement** (number of researchers accommodated); **operating economy and scientific effectiveness**; **subdued acoustical characteristics**; **payload** (scientific storage, weight handling); **speed**; and **ship control**. These requirements often conflict; thereby, necessitating compromise.

Ships can typically be considered within three major groups based on use: **general purpose** (classical biological, physical, chemical, geological, and ocean engineering research, or a combination); **dedicated special purpose** (hydrographic survey, mapping, geophysical, or fisheries); or unique (deep-sea drilling, crewed spar buoy, or support of submersible operations). They can be used simply as delivery and support systems for exploratory devices, such as floats and bottom landers, as well as crewless remote operating vehicles (ROVs—tethered, powered, surface-controlled robots), or autonomous underwater vehicles (AUVs—freely operating robots, using computer programmed guides).

In the world, fisheries and oceanographic research vessels are not very numerous. In Spain, oceanographic ships depend on two Government Agencies: the Spanish Institute of Oceanography (IEO, for its name in Spanish), and the General Secretariat of the Sea.

The IEO, which belongs to the Ministry of Education and Science, is responsible for studying marine resources, problems related to Oceanography and marine pollution and crops. The Institute guides its research for the purpose of its results to support the consultant role and to respond specifically to the public function in relationship to the sea, rational use, and protection. Given its characteristic as a State authority, the IEO represents the Spanish Government in International Oceanographic Commissions and Organizations. To date, the IEO has six ships and two more are under construction.

The General Secretariat of the Sea, which belongs to the Ministry of the Environment, Rural and Marine, MARM, has three fishery and oceanographic research ships. MARM obtains accurate and reliable data to evaluate the state of stocks, resource, and seabed, as well as data for the preparation of fishing maps of the Spanish continental shelf and the stocks of fishing grounds of interest to the Spanish fleet.

Definition And Characteristics of the Vessels

Scientific Missions. General Arrangement

These vessels were designed for a wide range of research activities in the Spanish coastal and regional area, as well as in other more remote areas. Each vessel is qualified to develop multi-purpose research and provides basic facilities for the marine disciplines of the coastal and regional areas:

Marine Geology: Study of the seabed and structure of the bottom, through sample collection and analysis.

Physical Oceanography: Study of the movement of water masses. Thermal measurement and sea water acoustics and optical properties. Description of basic properties of the ocean, such as: boundary coastal conditions, water depth, seabed profile,

etc., and study of the variation of the properties of seawater.

Chemical Oceanography: Chemical analysis of particulate matter in suspension in sea water; including polluting agents.

Marine Biology and Fisheries: Collection and analysis of phyto and zooplankton, fish, other marine species, etc.; benthonic and pelagic sampling. Ecosystem integrated studies. Fishery research and stock assessment by acoustic means.

Pollution: Observation and measurement of marine pollution, atmospheric air and water analysis. Collection of polluting agent samples.

Fig. 1 presents the general arrangement of oceanographic ship **Miguel Oliver**. In the deck sections, it can be seen that different facilities and compartments are arranged according to their function. Thus, on the lower deck or double bottom are most of the systems and naval equipment; in it, there is space for the engines, alternators, pumps, and compressors. The Fishing Park, the Biology Laboratory (due to the advantages resulting from this location for their activities) and cabins for crew and scientists are located on the main deck. The Upper deck will be mainly dedicated to research activities. The remaining laboratories will be located in this deck, as well as the galley, dining room, and pantry. This working area will be located aft on this deck. The Deck castle also serves for accommodation, nursing, conference room, and cabins for the captain and chief engineer. The navigation bridge is loactaed above the castle deck.

Along the ship length, areas more aft are dedicated to work and research activities; whereas, the more fore areas are dedicated to hotel and crew leisure activities.

Fig. 1. General Arrangement

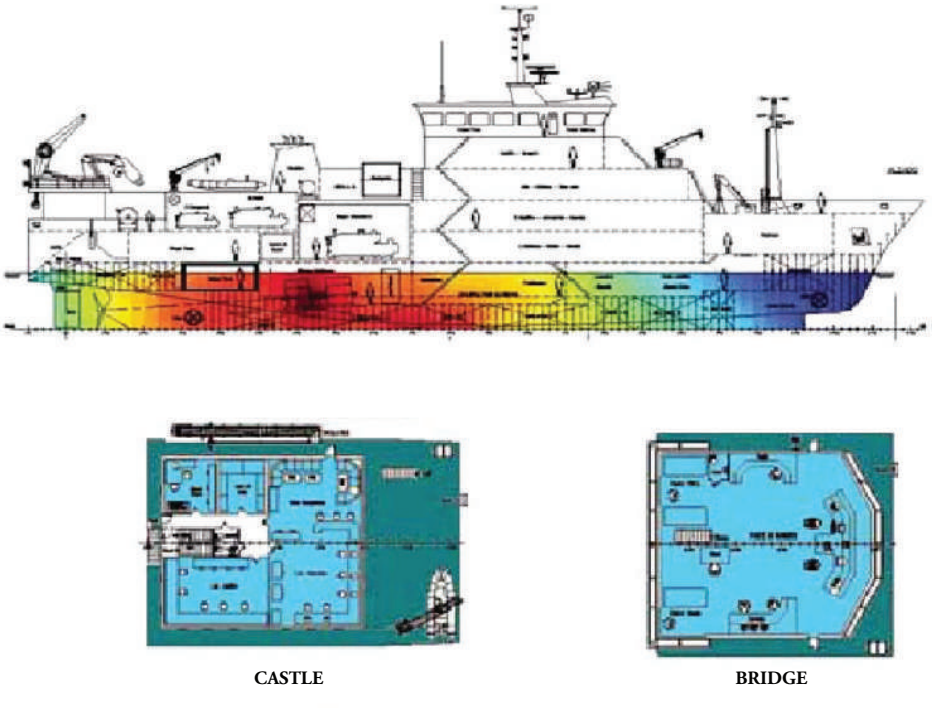

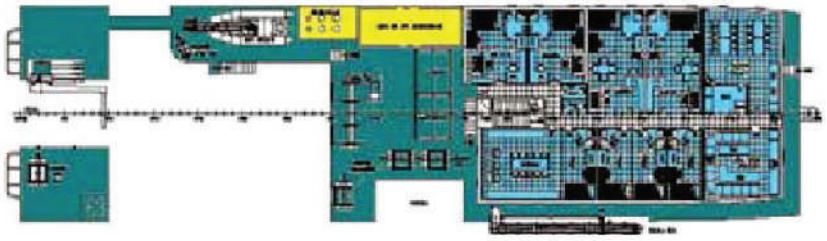

UPPER DECK

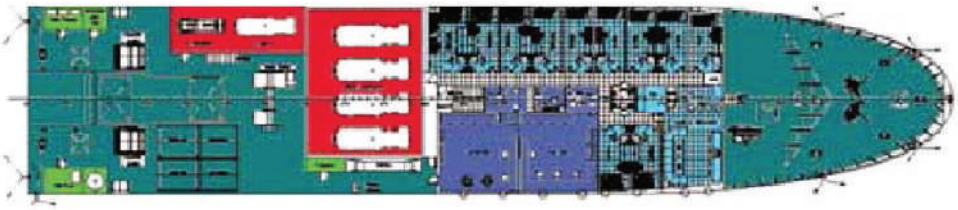

MAIN DECK

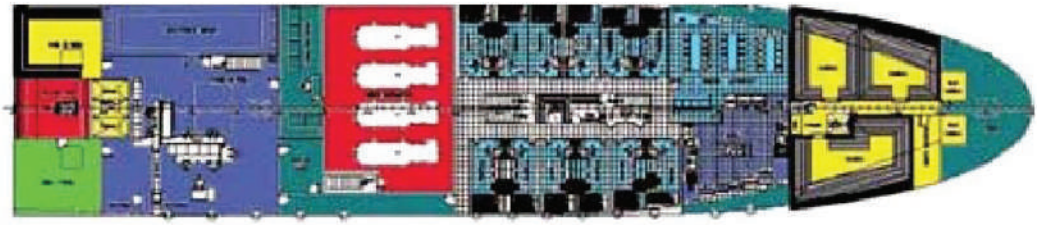

LOWER DECK

Hull Shape and Appendages

Demands for speed, fuel economy during the exploitation of the ship, and low hydrodynamic noise level lead to choosing fine and very slender forms with a prismatic coefficient of 0.62 - 0.65.

Low noise requirements make imperative a very soft water run to promote a uniform flow of entry to blades, without separation and vortex generation.

The bow flare will be accentuated to improve seakeeping and habitability in this area. The waterplane entrance half-angle should be low (no more than 18°) to minimize resistance by wave formation and, thus, achieve the speed ordered with the least possible power.

The ship will have a transom stern to increase the volume of this area for the greatest possible useful space.

At the bottom of the hull a **retractable keel** is installed, which hangs a gondola where transducers for acoustic detection and control of other equipment are installed. Being 4/4.5 m away from the ship, the vibration and noise reduction generated by the vessel allows reliable assessments of fish stocks. As an additional provision, the retractable keel allows operations for repair and replacement of equipment without the need to take the ship out of the water (Fig. 2).

The pod does not have to be affected by air bubbles. Transducers have to protrude below the boundary layer. The drag of this equipment has to be minimized, as well as the hull pressure fluctuations and cavitation inception.

Diesel-Electric Propulsion

The propulsion power is provided by generators located in total isolation, actuated by diesel engines

Fig. 2. Retractable Keel and Transducer

that feed to electric motors coupled to the propeller axes. A diesel-electric installation consists of one or more engines coupled to an equal number of generators that supply power to the engine or electric motors responsible for propulsion (Fig. 3).

Fig. 3. Diesel-Electric Installation

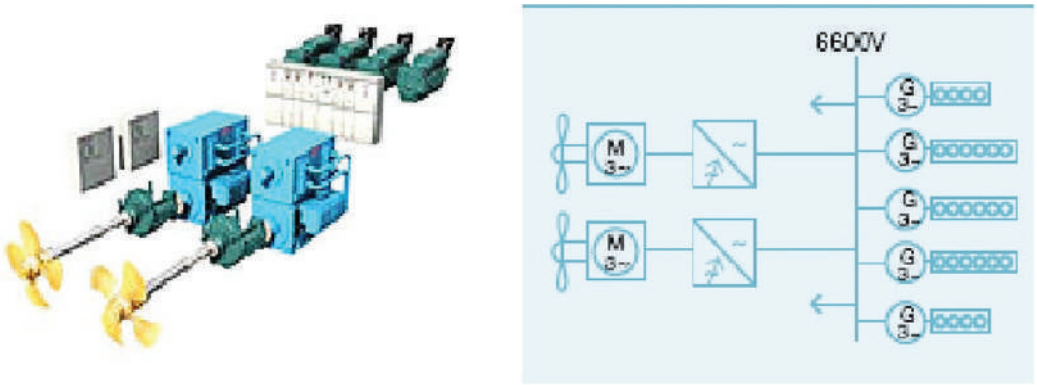

Diesel engines are irreversible, *i.e.*, they always rotate in the same direction; for that reason, their construction is simpler. The rotation regime is between 250 and 600 rpm and the current used can be direct or alternating. Regulating speed of the propulsion engines, when they are DC, is performed by acting on excitation of generators by resistors turning these generators at constant speed and, when several generators feed a same engine, their excitations are connected in parallel for unified command. For the regulation of speed with alternating current, it acts on the resistors of excitation, engine, and alternator.

From the acoustic point of view, this propulsion system allows for silent navigation with respect to instruments detection and evaluation of 'stock' of marine species. This ensures that research teams get their readings free from vibration and noise.

Dynamic Positioning System

Dynamic positioning (DP) systems enable, through the integration of multiple on-board systems, obtaining precise maneuverability for a ship under changing conditions. DP Systems can be defined as systems that automatically control

the position or direction of a ship by using active thrust devices. DP keeps the ship heading in a fixed point or makes it maneuver accurately. DP also provides monitoring or other positioning or precise movement needs.

Sensors connected to different elements (anemometers and windmills, wire tensors, pressure gauge monitors, etc.) allow direct feedback of these "external" forces and, thus, feed the DP system so the necessary corrections can be made by using the propulsion. The system connected to differential GPS equipment commands two transverse thrusters, as well as the main propeller and the active rudder.

A computer-controlled system automatically maintains the position of a ship by using its own propellers and thrusters. The software contains a mathematical model of the boat, which includes information related to the wind and current drag of the vessel and the location of the thrusters. This knowledge, together with the sensor information allows the computer to calculate the rudder angle and the suitable rpm for each propeller.

Sensor position of reference, in combination with wind sensors, sensors of movement and compass signal provides computer information related to the position of the vessel and the magnitude and direction of environmental forces affecting its position.

Fig. 4 presents a block diagram of a control for a dynamic positioning system.

Scientific Equipment

The vessels are equipped with the following scientific equipment, appropriate to the tasks described above:

Doppler Current meter and Profiler, (150 kHz) for current monitoring in specific sections of the water column, measuring the following parameters: direction and speed, temperature and pressure. Installed in the retractable keel. Fig. 5 shows some models of this instrument.

Complete Meteorology station, which includes at least sensors of air temperature, humidity,

Fig. 4. Control System Block Diagram

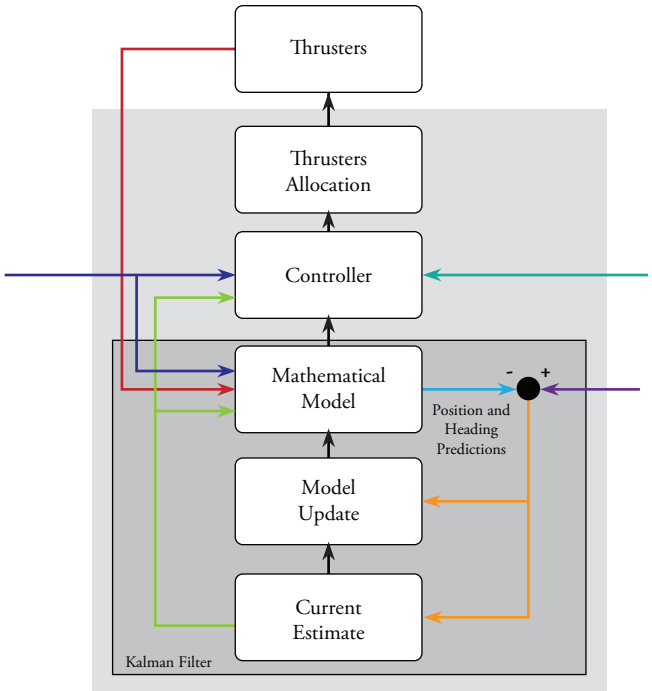

radiation, speed and direction of wind, and water temperature. The water temperature sensor will be assembled in the retractable keel to facilitate its access and maintenance.

Fig. 5. Doppler Current meter

Multi-frequency Biological Sounder. It is now an international standard for the scientific evaluation of fishing resources. The system allows knowing the size of targets starting from the echo intensity received and, hence, knowing the distribution of sizes of individuals and fish biomass bank. Fig. 6 shows a screen with several echograms corresponding to a bank of krill; records allow comparing frequencies used in the response: 18, 38, 70, 120, and 200 kHz. It will be installed in the retractable keel.

Fig. 6. Krill Bank Echograms

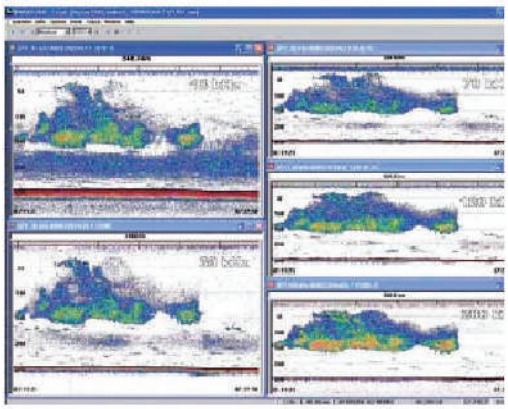

Multi-beam Scientific Echosounder. Its role will be to increase precision in the biomass estimation and the definition of structures of the fishing banks and their dispersion when detecting the vessel presence. It will be installed in the retractable keel. This probe can incorporate a bathymetric option through which a high-resolution bottom map can be elaborated (Fig. 7).

Fig. 7. Scientific Echosounder

Multi-frequency Hydrographic Echosounder. Its function is to determine the depth of the sea and discover the features of the seabed in the portion of acoustic energy reflected by the bottom. It will be compatible with the previous equipment.

Side Scan Sonar. Uses a sonar device that emits conical or fan-shaped pulses from a torpedo or "dragged fish", towards the seafloor across a wide angle perpendicular to the path of the sensor through the water. The equipment may be towed from a surface vessel or submarine, or mounted on the ship's hull. The signal to be returned after bouncing off the bottom builds an acoustic image of the bottom or phonograph, which informs us about the morphology of the seafloor (Figs. 8 and 9).

Fig. 8a. Side Scan Sonar

Fig. 8b. Winch

Net Sonar; towed with trawl riding 1500-m driver cables with double armored steel coating. The Net Sonar is capable of detecting the shoal found at the mouth of the net used in large-scale pelagic trawls. Provides real-time images from the information received from the sonar head (Fig.10).

Hull Hydrophones; connected by cables to the winch's control zone. One or two hydrophones oriented towards the stern of the ship, paying particular attention to the location away from the noise generated by the ship's propellers (Fig. 11).

Fig. 11. Hull Hydrophone

Sampling Equipment. During each oceanographic campaign, samples are taken at different depths to, subsequently, determine the various parameters of

Fig. 9. Hull-mounted Multi-beam Sonar (left) and Towed Side Scan Sonar (right)

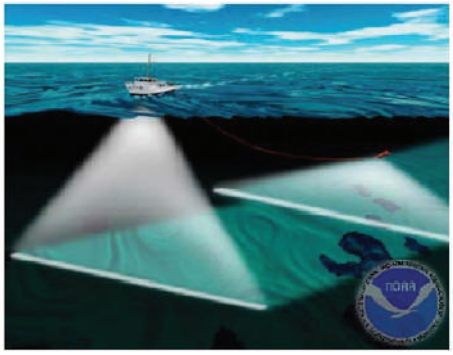

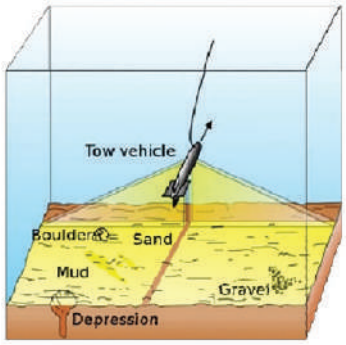

Fig. 10. Net sonar Disposition (left) and Sonar Head (right)

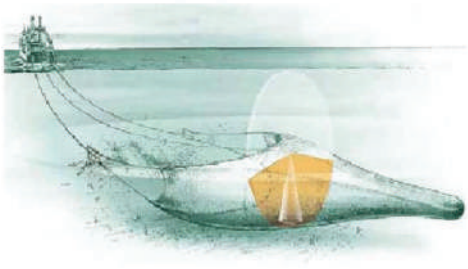

the water (salinity, oxygen content, temperature, turbidity, etc.) through analysis and through the quantity of suspended matter (nutrient, phytoplankton and zooplankton, etc.). To sum up, the main components of this equipment include:

- ***Oceanographic Rosette***. A carousel water sampler, which integrates all the devices is used for sampling. It dives into the sea through a specific trawl located on the deck (Fig. 12).

Fig. 12. Oceanographic Rosette

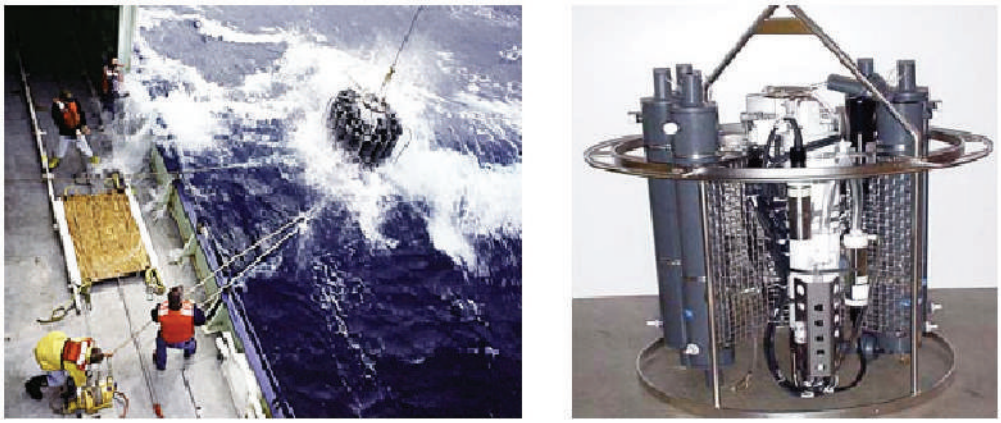

- ***CTD***. It is the acronym for conductivity, temperature, and depth. It is the primary tool for determining essential physical properties of seawater, giving scientists a precise and comprehensive charting of the distribution and variation of water temperature, salinity, and density that helps to understand how the oceans affect life. The CTD mounted sensors will measure up to 6 different parameters: dissolved oxygen, CO_2, fluormeter, turbidity meter, radiometer, and pH/ORP (pH + Redox potential) (Fig. 13).

Fig. 13. CTD (left) and Fluorometer Sensor (right)

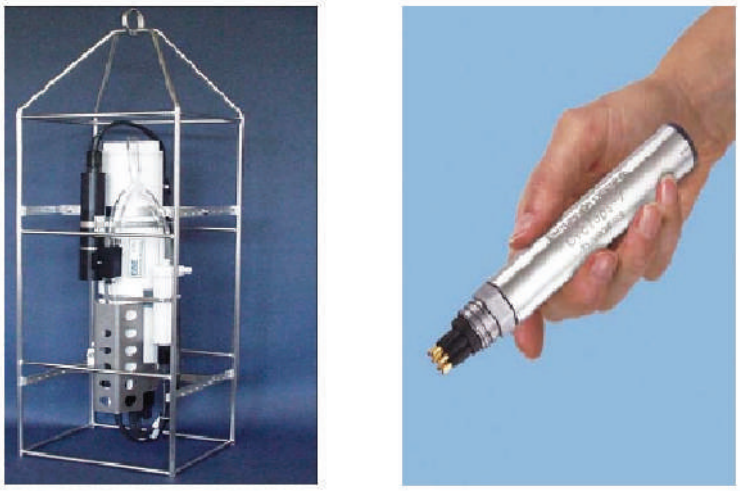

- ***Niskin Bottle.*** It is a tool widely used in Oceanography to sample water at different depths. Opening and closing of bottles can be done manually, through a steel cable and a

counterweight to lead. Often, in sea launching from oceanographic vessels, Niskin batteries are joined in a rosette with which various bottles at different depths are filled (Fig. 14).

Fig. 14. Hull-mounted Multi-beam Sonar (left) and Towed Side Scan Sonar (right)

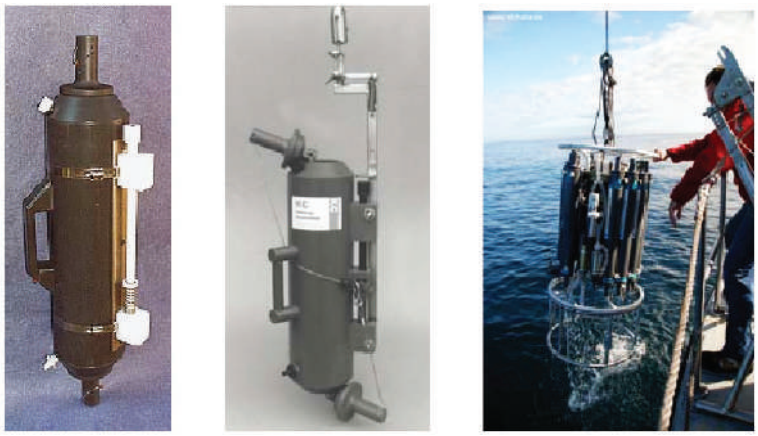

- ***Van Veen Dredger***. It allows the collection of sediment from the vessel. All Van Veen Dredges have the same operation mode: the clamps are open, held by a hook, and slowly enter the water and upon touching the sea bed, the hook is liberated and the clamps close, leaving the sample inside. (Fig. 15).

Fig. 15. Van Veen Dredger

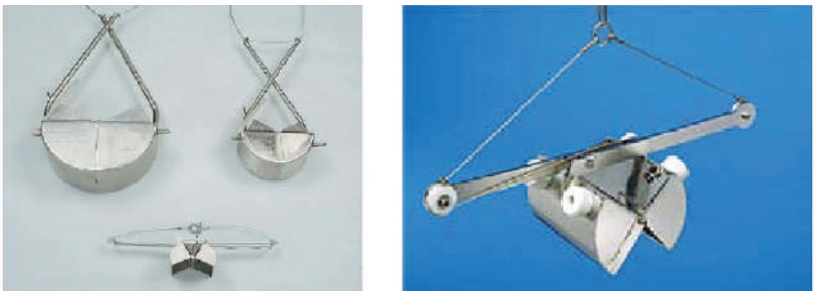

- ***Secchi Disk***. Water transparency is determined by using a Secchi disk; depending on the depth to which this disk will no longer be visible. Fig. 16 shows how the disk is used to measure water transparency.

Fig. 16. VSecchi Disk

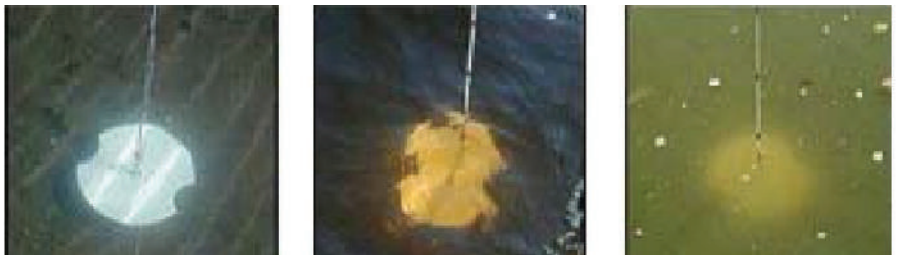

- ***Oceanographic Buoys***. According to the missions described in the corresponding section, oceanographic buoys are also necessary. Buoys must be stored on board near to the launching area. These buoys will be used for missions related to pollution, oceanography, and marine biology. To reach the place where the buoys must be anchored, they shall be hauled down with a davit located on the upper deck (Fig.17).

Fig. 17. Oceanographic Buoys

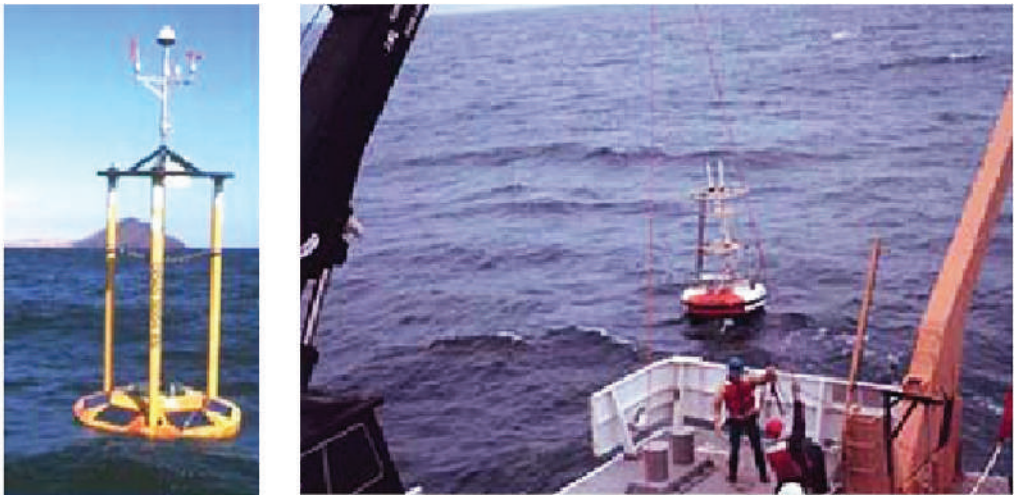

- ***ROV (Remote Operated Vehicle)***. It is an unmanned tethered underwater robot, highly maneuverable and operated by a person aboard a vessel. It is linked to the ship by a tether (umbilical cable), a group of cables that carry electrical power, video and data signals back and forth between the operator and the vehicle. Most ROVs are equipped with at least a video camera and lights. Additional equipment is commonly added to expand the vehicle's capabilities. These may include sonar, magnetometers, a still camera, a manipulator or cutting arm, water samplers, and instruments that measure water clarity, light penetration, and temperature (Fig.18).

Fig. 18. ROV

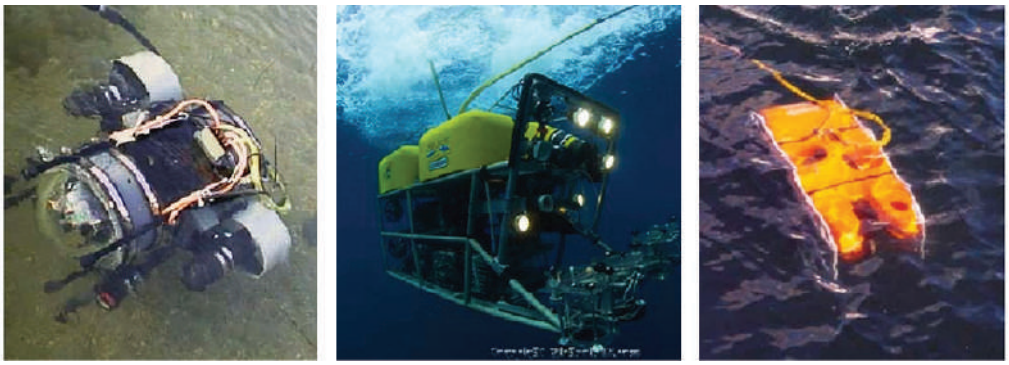

- ***Data Management System***. Regardless of the above, an integrated scientific data management system (MDM 400) will be installed (including a redundant server) with

the ability to work integrated with different scientific teams, as well as oceanographic winches and the fishing winch control information.

Noise and Vibration

Noise transmitted to the water from a vessel, in form of vibrations, scare marine beings and can, consequently, affect the results of investigations carried out in the sea. It is therefore important to regulate and control these vibrations from the earliest stages of ship design. With this in mind, the ship must be designed to minimize air, structural, and radiated noise to the water. It must also comply with the requirements of Silent Platform ICES 209.

Sources that generate noise are primarily structural or hydrodynamic. Airborne noise also generates underwater noise due to vibrations induced in the hull. As the speed of the vessel increases, the contributions from these sources to the resulting noise increase. Therefore, a given speed must be set for noise level measurement. It is also normal to set at what distance from the hull induced pressure sound is measured, which typically is 1 m from the hull. Pressure levels are usually measured in decibels referenced to 1μPa.

Generated noise can have specific frequencies or a continuous form in the frequency spectrum. Among the first sources are unbalanced rotating elements, repetitive discontinuities like gears or blades of turbines or alternative movements of mechanical elements like pistons. The latter include cavitation or turbulence in pipes, valves or pumps and friction produced by sliding and shaft bearing.

In vessels, the main sources of noise on board are propelling machinery, diesel generator groups, auxiliary machinery, and propellers. To achieve the low acoustic detectability platform design below summarizes a number of basic design criteria:

- ***Selection of low-noise air and structural machinery.*** The main mission of these ships is to investigate the aquatic environment; therefore, acoustic signature requirements are high. This makes it convenient to take a diesel-electric propulsion system with direct coupled shafts. If adoption of gearboxes is required, they must have very strict manufacturing standards to reduce structural noise levels.

- ***Selection of appropriate mounting propelling machinery and diesel generator groups***. Once the machinery to be installed has been determined, it is necessary to define the type of mounting on which said equipment will be installed. Mounts can be simple, rigid elastic on a basis that is elastically attached to the engine-bearers of the motor and double elastic on a mid-term basis. On the other hand, to reduce airborne noise the machinery has to be isolated by means of acoustic wrapping.

- ***Selection of appropriate flexible connections*** to connect the propelling machinery and the diesel generator group with the rest of the ship. To minimize the acoustic signature, flexible hoses between the different services (fuel, oil, cooling water, connections of expansion of air ducts for combustion and exhaust, etc.,) will be used.

- ***Selection of auxiliary machinery*** which has a remarkable contribution to radiated noise, taking into account their noise vibration levels and airborne noise, as well as defining their elastic mounts properly.

- ***Appropriate design of hydrodynamic*** forms of the hull and their appendages to minimize hydrodynamic noise and also obtain satisfactory wake distribution in the propellers.

- ***Wake-Adapted Propeller Design***, finding an appropriate radial load distribution to prevent the onset of cavitation in the speed margin required.

- ***Application of new*** system based on masking noise radiated by the hull by using bubbles generated with compressed air.

To ensure compliance with the acoustic-dynamic objectives, the shipyard builder uses in-house

noise and vibration personnel or may hire external personnel, has to carry out integral management of vibrations and noise, covering the following aspects:

1. Information and sensitivity awareness-raising of the shipyard and the main suppliers for the dynamic-acoustic criteria required for the ship.
2. Implementation of a protocol to prevent and minimize vibrations and noise.
3. Implementation, during early phases of the project, of tools and studies of vibration prediction, airborne and noise radiated to the water.
4. Establishment of a reception test program of components and/or main equipment in accordance with the dynamic-acoustic criteria.
5. Establishment of an inspection points program (IPP), to ensure control and periodic reviews of all aspects relating to vibrations and noise during the entire project and ship construction.
6. Implementation of a vibration, noise, and radiated noise measurement program during the sea trials to verify and, if necessary, certify compliance with established requirements.

Specific Requirements: Vibrations

Given the level of required comfort for these types of ships, a set of contractual limit values must be established for levels of structural vibration of the vessel, as defined in the **COMF-VIB grade 1 Regulations (Bureau Veritas)**, or similar, for vessels of lengths less than 65 meters, in the following areas (Table 1):

Table 1. Levels of structural vibration

Space	Curve Limit
Bridge	C3
Dining room and common spaces	C3
Cabins	C2
Works areas	C4
Laboratories	C3
Computer Center	C3

The vibration levels measured will be considered **acceptable** when they are below the curve defined for each location in Table 1.

Specific Requirements: Airborne

By considerations of comfort in the different locations of the ship for these types of vessels, contract limits are established, values for the noise level dB (A) depicted in the attached Table 2, which defines rules COMF - NOISE Ng = 1 (Bureau Veritas), or similar, for vessels less than 65 meters in length.

Table 2. Values for the noise level dB(A)

Spaces	dB (A)
Deck 1 measurement of fans	70
Crew space	60
Cabins	55
Galley	70
Corridors	65
Government bridge	63
Laboratories	60
Fishing park	65
Laundry	65
Locker rooms	65
Engine rooms	110
Engine cabin control	74
Workshops	74
Unspecified spaces	90

The noise level db (A), measured at different locations of the vessel, shall be considered **acceptable** when it is below the values defined in the attached table.

In general, the measuring procedure must comply with that specified by **Bureau Veritas Regulations (Pt F, Ch.6, Sec. 2 ADDITIONAL**

REQUIREMENTS FOR NOTATION COMFNOISE), or similar applicable, and will run through calibrated sound level meters.

Specific requirements: Radiated noise

To date, research and observations have shown that noise generated by a ship has the potential to contaminate the sampling of populations or fishing banks, which confirms the need to build ships with low radiated noise levels. In this regard, research vessels must comply with the recommendations set forth in document **ICES COOPERATIVE RESEARCH REPORT No.209 "Underwater Noise of Research Vessels Review and Recommendations"**.

In particular, the Level of Radiated Noise Lp (1-Hz bandwidth), expressed in dB (referring to 1 micro Pascal) standardized 1 meter from the hull, whereas a spherical propagation and free running speed, must comply or be below for the two specified frequency ranges of values of the lines of the graphic attached (figure), whose laws of variation are as follows:

LP = 135 - 1.66 x log f (Hz) for the range of Hz to 1 kHz.
LP = 130 - 22 x log f (KHz) for the range of 1 KHz to 100 KHz.

While there are experiences that demonstrate the complete and final acceptance of the capacity of the ship to avoid potential problems of radiated noise it is required to execute measurements from more than one form and under different conditions, such as:

- **Trawling vessel condition with the codend at medium depth.**
- **Trawling vessel condition with the codend in the background.**

However, for contractual purposes of acceptance of ship, the **Levels of Radiated Noise** must comply, on both sides of the ship, with the **ICES-209 criteria**, specified above and included in the figure above, in free running condition.

Fig. 19. Levels of radiated noise

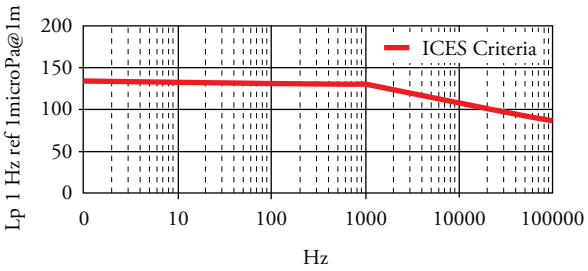

Deck Equipment

Deck machinery, make used for scientific research task, is described in this section.

To drive the different components of deck equipment, electric systems, instead of hydraulic, are more convenient. Election of this driving type represents the following advantages:

- Normally, Oceanographic ships are vessels with diesel-electric propulsion, this means that power generation capacity onboard is big and it can be managed optimally.
- The hydraulic solution would require an additional transformation of energy, with consequent losses resulting.
- Electrical machinery solution eliminates numerous pipelines, working under high pressure, of the hydraulic circuit, so this option reduces weight, as well as the disadvantages arising from leaking pipes.
- Electrical driving solution prevents many pipelines working under high pressure of the hydraulic circuit, so this option reduces weight, as well as the disadvantages arising from leaking pipes.
- Eliminating hydraulic pipelines and hydraulic pumps significantly reduces noise and vibration levels.
- Repair and maintenance costs are lower for electric winches.

Winch Equipment

Trawl winches. Two winches are usually mounted, one each band, with a spindle capacity of at least

1500 meters. The winches should be compact, robust and with three speeds (Fig. 20).

Net drum. A double-net drum is assembled with a capacity of 2 m^3 on each drum. One of the drums incorporates a sweep winch barrel on one side, while the other independent barrel is only for sweep (Fig.21).

Fig. 20. Trawl Winch

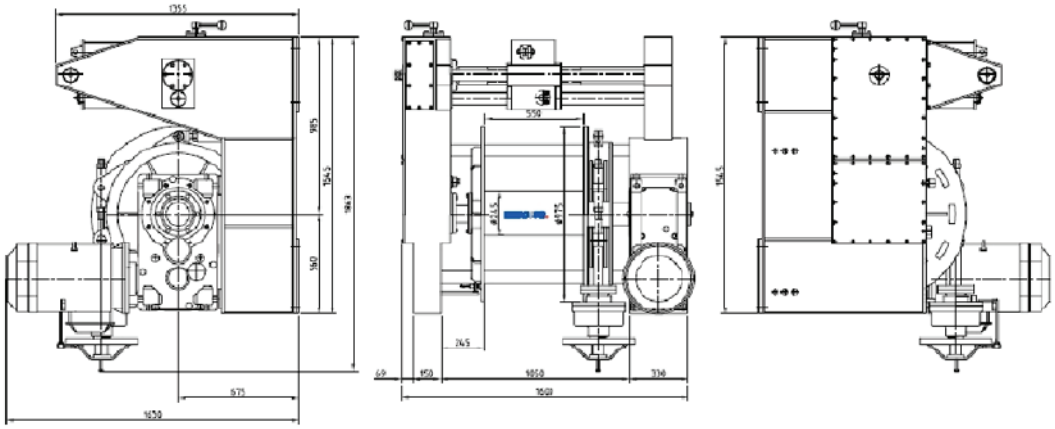

Fig. 21. Net Drum

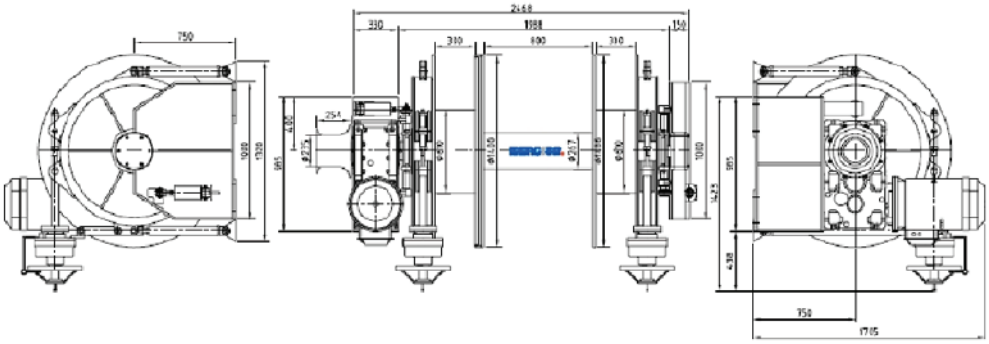

Oceanographic Winch. This winch is ready for handling different oceanographic equipments, as rossete, Niskin bottle, etc. The winch accommodates a 6,000-m long cable 8 mm in diameter (Fig. 22).

A command and control system by variable frequency drive is included. On the bridge, a control console is located, including: joystick twist control, potentiometer for traction regulation, indicators in meters shooted and dynamic traction on the wire.

To operate with the CTD, it has a special Oceanographic winch, incorporating a manual control and two remotes, one on the government bridge and one wet laboratory. (Fig. 23).

Sonar net cable winch. This winch will be placed on the cover Castle, looking aft
(Fig. 24).

Other Deck Equipment

These vessels are generally below the deck equipment:

A collapsible davit is aft for fishing operations, oceanographic research, and to manipulate the ROV. It consists of a single foot structure made up of two main elements that allow 360-degree rotation. This upper arm has a perpendicular arm 3 m in length. The maximum rotation of the intermediate support is 45 ° forward and 75 ° backwards.

- A crane for loading and unloading located in the spar deck. It is 16 m long and has a 5-ton capacity at 16 m and with a winch of equal strength. This equipment allows total autonomy to develop any operation without crane ports, transport trucks or other equipment. Enjoying a considerable interest in the actions of loading and unloading of the

Fig. 22. Oceanographic Winch

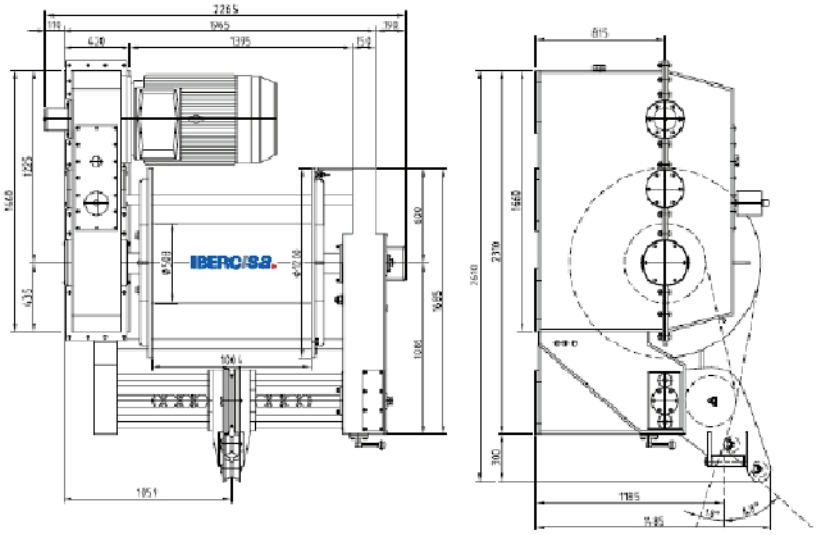

Fig. 23. CTD Winch

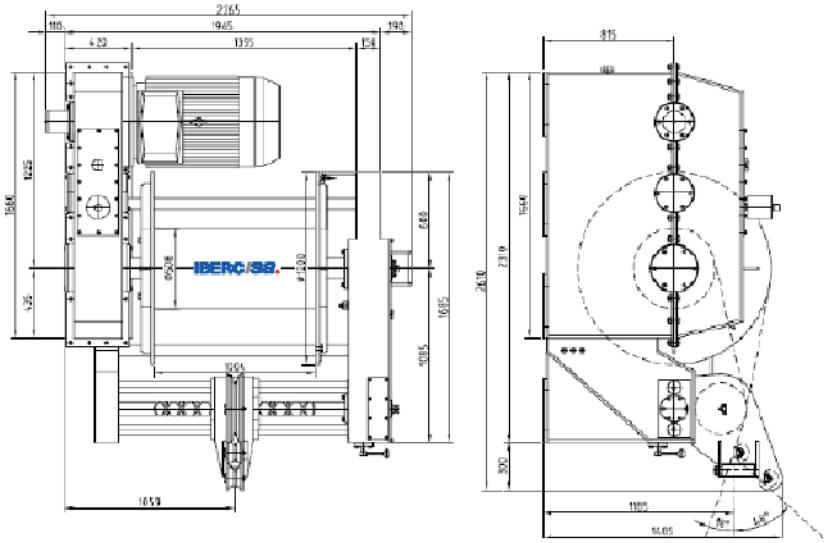

Fig. 24. Sonar Net Cable Winch

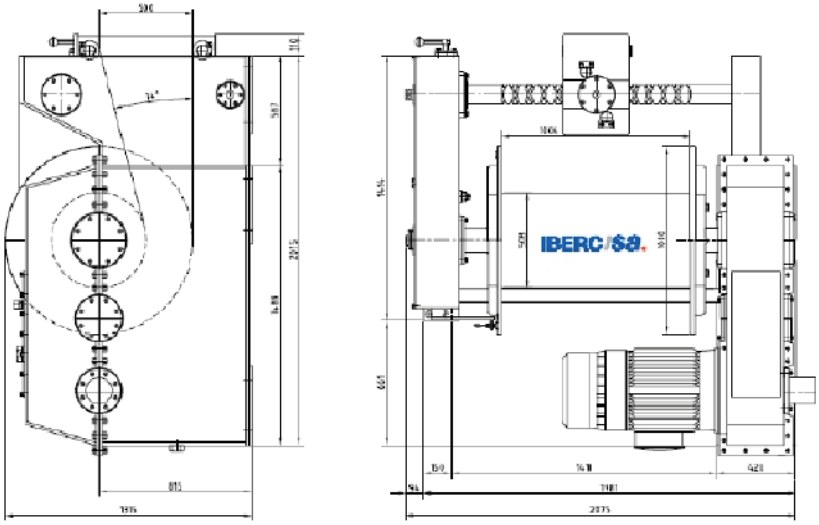

ship, container and underwater equipment for research management.

- A crane for manipulation of the rosette.

Photos in Fig. 25 present B/O MIGUEL OLIVER deck equipment.

Fig. 25. B/O MIGUEL OLIVER Deck Equipment

Laboratories

Oceanographic vessels are outfitted with a series of laboratories, which will be staffed by the scientific staff embarked to carry out research campaigns. Normally, the laboratories are referred to as "dry" and "damp", but from the scientific point of view, they could be grouped together into only three: "Oceanography laboratory", "Biology and Fishery Research Laboratory", and "Underwater Acoustics Laboratory".

Oceanography Laboratory

Its main functions include analyzing and quantifying the information gathered on the practices affecting the previously mentioned missions, in areas of Geology and Physical Oceanography with the equipment mentioned.

Control of winches, fishing machines (with digital output of the operating parameters) and gantry crane will be centralized with remote information, if necessary, on the bridge of government and main laboratories. At the same time, centralization and access to the “NMEA-box” type data were gathered in the dry laboratory system.

Biological Laboratory

It will be designed for environmental measurement, copy collection and analysis process. In this area, we can conduct analyses of marine biotoxins, proteins, pathologies of marine species, quality of water control, discharges and waste control, etc.

These laboratories are often divided into sections:

Microbiology section. Composed of the following elements:

- Biosafety cabinets
- Stoves and incubators
- Optical microscopes
- Account colonies
- Photometer
- Centrifuge
- Autoclave
- Personal computers

Biochemistry section. Composed of the following elements:

- Gas and liquid chromatograph
- Spectrophotometer
- Luminometer
- Thermocycler
- Personal computer

Many of the tools of analysis may be shared with the Oceanographic Laboratory. The most important are the following:

- Flow cytometry
- Spectrofluorimeter
- Fluorometer,
- Salinemeter,
- Titroprocesser,
- Liquid Scintillation counter.

Underwater Acoustics Laboratory

Equipped with systems to monitor and control the principal acoustic systems. It includes GPS repeater and repeater navigation plotters. The central systems of computer network and the telephone network of the boat connections are installed in this laboratory.

Normally located under fishing park, it includes:

- Specific equipment to conduct geology campaigns to study the morphology, reflectivity, and classification of the nature of the seabed.
- Specific equipment for biology of fish and plankton species identification, estimation and distribution campaigns.
- Specific equipment related in Paragraph 3.

Conclusions

- The possibility of determining the exact characteristics of the seabed, develop maps of fishing stocks of interest, or the opportunity to know the state of the marine resources are commitments that enable the respect and sustainable development of species, as well as cooperation among States.

- Ocean vessels must be technological and

Fig. 26. Biological Laboratory Equipment

Biosafety Cabinet

Cultivation Stove

GNO by volume

Microscope

Gas Chromatograph

Fluorometer

Autoclave

Spectrophotometer

innovation challenges for the national industry, not only in the naval construction industry, but also in the auxiliary industry; thus, allowing oceanography and fishing equipment to be of increasing national production.

- Leading European fishing countries have begun to design high-performance vessels with lengths over 100 meters. France, Norway, Great Britain, Germany, and France are the five countries that, currently, set the course of oceanographic and fishery research and have fleets of ships with worldwide capacity action, even allowing to delve into polar zones.

- The necessary renewal of the National Oceanographic Fleet must be targeted to advanced platforms, extremely quiet with greater energy efficiency, including the use of new fuels and scrupulous and advanced monitoring of environmental regulations. New construction designs based on Small-waterplane area twin hull (SWATH) or Trimaran technology; introduction of new alternative energy sources and monitoring techniques; and remote diagnosis of onboard equipment should be the points to aim at.

- The use of diesel electric propulsion (CRP)

provides considerable savings to shipping companies due to the reduction of fuel consumption, lower maintenance costs, and increased flexibility during boat design. Another important advantage is that pollution is reduced. This factor will gain in importance as environmental legislation is getting stricter by the day.

- The Integral Management of Vibration and Noise has been revealed as an effective tool that requires outsourcing and collaboration with different suppliers. "Acoustic dynamic design of the vessel commands".

- Oceanographic vessels use winches and gantry cranes to enable more efficient deployment of scientific equipment. These infrastructures are important parts of the ship's equipment and need constant innovation.

- Integration of bridge equipment and communications with scientific systems should be encouraged to allow working on the ship from land laboratories in real time.

References

BELTRÁN, PUBLIO; PÉREZ, ÁLVARO Y GALINDO, Carlos: "Buque Oceanográfico Miguel Oliver. Se ha logrado la excelencia en ruidos y vibraciones a bordo de un buque". Revista Ingeniería Naval. Madrid. Mayo 2007.

CARRASCO, VICENTE: "Buque Oceanográfico Miguel Oliver. Un reto tecnológico de Simrad Spain". Revista Ingeniería Naval. Madrid. Mayo 2007.

DÍEZ, JOSÉ IGNACIO: "La renovación de flota del IEO. Retos tecnológicos". 47 Congreso de Ingeniería Naval. Palma de Mallorca. Octubre 2008.

HERNÁNDEZ, JERÓNIMO: "Emma Bardán, Buque Oceanográfico construido para la Secretaría General de Pesca Marítima". Revista Ingeniería Naval. Madrid. Febrero 2006.

HERNÁNDEZ, JERÓNIMO: "Los buques de investigación pesquera y oceanográficos de la Secretaría General de Pesca Marítima". 47 Congreso de Ingeniería Naval. Palma de Mallorca. Octubre 2008.

NÚÑEZ, JOSÉ FERNANDO; PÉREZ, LUIS: "El buque de cooperación pesquera, una iniciativa de la administración para la pesca responsable y sostenible". 47 Congreso de Ingeniería Naval. Palma de Mallorca. Octubre 2008.

SIMRAD SPAIN: "Sonar de Red FS70, Discriminación de especies mediante ecosonda científica EK60". Revista Técnica A Fondo. Madrid.

Annex 1: Modern spanish Oceanographic & Research Vessels

B/O VIZCONDE DE EZA

It is the first ship built in modern times by the General Secretariat of the Sea (MARM). From April 2001 to February 2010, the "Vizconde de Eza" participated in 75 research campaigns and offered cooperation in eight countries: Gabon, Guinea-Bissau, Angola, Algeria, Morocco, Namibia, Mozambique, and Mauritania.

This Oceanographic ship is considered a large floating laboratory with six specialized laboratories (chemistry, biology, physics, acoustics, moist, and computer) equipped with advanced scientific instrumentation. Its hull, reinforced on the bow, allows sailing through floating ice. It also performs uprisings of the seabed of up to 5,000 m in depth.

General Characteristics

Overall length	53 meters
Molded Beam	13 meters
Maximum depth	7.55 meters
Molded draught	4.50 meters
Power	2448 H.P.
Maximum Speedy	13 knots
Tonnage	1400 GTs
Ship owner	MARM

B/O EMMA BARDÁN

The EMMA BARDÁN Oceanographic and Fisheries Research Ship, built by the General Secretariat of the Sea, entered into service in January 2006.

The Ministry of Environment, Rural and Marine aims, with this vessel, to obtain accurate and reliable data to evaluate the state of Spanish fisheries and marine resources, as well as to prepare maps of the Spanish continental shelf fishing.

The ship has adequate resources for semi-pelagic and bottom fishing by means of a towing system through the stern ramp and incorporates appropriate equipment for the classification and investigation of the fish caught.

General Characteristics

Overall length	29 meters
Molded Beam	7.5 meters
Maximum depth	3.9 meters
Molded draught	2.6 meters
Power	900 H.P.
Maximum Speedy	12 knots
Tonnage	200 GTs
Ship owner	MARM

B/O MIGUEL OLIVER

It was officially presented in Vigo on 6 July 2007; the ship is named after Marine Biologist and Secretary General of Sea Fisheries, between 1982 and 1986, Miguel Oliver.

B/O MIGUEL OLIVER is one of the five internationally leading scientific ships. The vessel is qualified as an ecologic and quiet ship and it is the first Spanish ship to meet the ICES 209 rule on emission of noise and vibration onto the water.

It is a multidisciplinary ship with advanced technological equipment for navigation, oceanography, and fisheries research. It can be considered the Spanish fleet's flagship in the search for fishing grounds.

General Characteristics

Overall length	70 meters
Molded Beam	14.4 meters
Maximum depth	8.5 meters
Molded draught	5.0 meters
Power	2720 H.P.
Maximum Speedy	15 knots
Tonnage	2495 GTs
Ship owner	MARM

B/O HESPÉRIDES (A-33)

This oceanographic research ship was delivered to the Spanish Navy in 1991. The military crew on the ship is responsible for maintaining the platform and the navigation and support requirement for on-board research.

Although it organically depends on the Navy, the responsibility for the maintenance of the scientific equipment of the ship lies on the *"Unidad de Tecnología Marina" (UTM) of the "Consejo Superior de Investigaciones Científicas"* (CSIC) in Barcelona, which provides the technical support staff in the oceanographic campaign.

With its commissioning, the Spanish Scientific Community featured a first-level ship, equipped with comparable last generation technologies of the best international research vessels. The start of operations was a qualitative and quantitative leap in scientific production.

General Characteristics

Overall length	82.5 meters
Molded Beam	14.3 meters
Maximum depth	7.35 meters
Molded draught	4.5 meters
Power	3800 H.P.
Maximum Speedy	15 knots
Tonnage	2710 GTs
Ship owner	IEO-CESIC

B/O SARMIENTO DE GAMBOA

The building of the ship "Sarmiento de Gamboa" was funded by the Ministry of Education and Science through the European Fund for Regional Development (FEDER), the Consejo Superior de Investigaciones Científicas (CSIC), and the Government of Galicia.

Although it organically depends on the Spanish Institute of Oceanography (IEO), the responsibility for the maintenance of the scientific equipment of the ship lies on the Unit of Marine Technology (UTM) of the (CSIC) in Barcelona, which provides the technical support staff in oceanography.

It is the most modern research vessel of the Spanish fleet. Launched in 2006, it entered into service in 2008, once all planned equipment were installed and tested.

The ship is intended for research in waters of the Atlantic Ocean. Focused on the study of global ocean circulation, marine biodiversity, fishery resources, and climate change, it has a wide variety of scientific and technical equipment for Oceanography, Biology and Marine Geochemistry, as well as complete laboratory and auxiliary equipment.

General Characteristics

Overall length	70.5 meters
Molded Beam	15.5 meters
Maximum depth	7.35 meters
Molded draught	4.6 meters
Power	3265 H.P.
Maximum Speedy	15 knots
Tonnage	2630 GTs
Ship owner	IEO-CESIC

Analysis and Prediction of Welding Distortion in complex Structures Using Elastic Finite Element Method

Análisis y Predicción de Distorsiones en Estructuras Soldadas por medio de un Análisis Elástico de Elementos Finitos

Adán Vega Sáenz [1]
Carlos Plazaola [2]
Ilka Banfield [2]
Sherif Rashed [3]
Hidekazu Murakawa [3]

Abstract

The Elastic Finite Element Method based on the inherent strain theory is used to predict the welding distortion of ship structures. In addition, a method to predict welding distortion of complex structures by using elastic FEM is presented. To evaluate the effectiveness of the proposed method, a typical case of a ship's structure is examined and the resulting welding distortion is compared to that obtained by using thermal elastic-plastic finite element method.

Key words: Complex Ship Structures, Elastic Analysis, Finite Element Analysis, Inherent Strain, Welding Distortion.

Resumen

Un análisis elástico de elementos finitos basado en la teoría de la deformación unitaria inherente es utilizado para predecir la distorsión causada por la soldadura en estructuras de barcos. Adicionalmente, se propone un nuevo método para predecir la distorsión de estructuras complejas. Los resultados obtenidos son luego comparados con aquellos obtenidos por medio de análisis termo-plástico de elementos finitos.

Palabras claves: Análisis de Elementos Finitos, Análisis Elástico, Deformación Unitaria Inherente, Distorsión de Juntas Soldadas, Estructuras de Barcos complejas.

Date Received: November 9th, 2010 - *Fecha de recepción: 9 de Noviembre de 2010*
Date Accepted: January 16th, 2012 - *Fecha de aceptación: 16 de Enero de 2012*

[1] Miembro del Sistema Nacional de Investigación SNI (SENACYT). Laboratorio Especializado en Procesos de Union y Manufactura (LEPUM), School of Mechanical Engineering, Technological University of Panama. Panamá City, Panamá. e-mail: adan.vega@utp.ac.pa
[2] Laboratorio Especializado en Procesos de Union y Manufactura (LEPUM), School of Mechanical Engineering, Technological University of Panama, 0819-07289, Panamá City, Panamá. e-mails: carlos.plazaola@utp.ac.pa, ilka.banfield@utp.ac.pa
[3] Joining and Welding Research Institute, Osaka University, 11-1, Mihogaoka, Ibaraki, Osaka, Japan. e-mails: sherif-rashed@hcc5.bai.ne.jp murakawa@jwri.osaka-u.ac.jp

Introduction

Welding deformation is a common and important problem in industry. In recent decades, researchers have made efforts to predict and control welding deformation. There are usually three ways to determine the welding deformation: 1) experiential formulas, 2) Thermal elastic-plastic Finite Element Method (FEM), 3) Inherent strain method based on FEM (*Liu, C and Zhang, X. 2009*), (*Wahab, M. et al., 2006*).

Experiential formulas are only fit for simple shape structures. The current thermal elastic-plastic method is usually simulated in either small or simple structures like butt-jointed plates, or focuses on the local weld zones of large structures without considering the surrounding structure. For three-dimensional large structures, predicting the welding deformation by using this method is almost impossible given the requirements of calculating time and large capacity computer memory.

Compared to the thermal elastic-plastic method, the inherent strain method is an economic and simple method in the prediction of large structure welding deformation. It only requires elastic FEM analysis to predict welding deformation (*Deng, D. et al., 2007*). Inherent strains are the residual plastic strains caused in welding processes. They always exist in the welds and nearby where structures undergo large thermal cycles and are considered a source causing the welding deformations. The key to using this method lies in knowing the inherent strains in advance during welding deformation analysis (*Liang, W. 2007*).

In this paper, the inherent strains method is used to predict the welding deformation of large complex ship structures. At first, a simple example on the welding deformation of a T-joint with two fillet welds is given, and then the inherent strain method is applied to the welding deformation analysis of the large complex ship structure. After that, and based on a new method to predict welding distortion by using the inherent strain method, the welding distortion of large complex ship structures is predicted. The analysis method and results can be taken as references not only for the choices of weld sequence, welding parameters, and location of fixture, but also for prediction of welding deformation of other ship structures.

Definition of Inherent Strain

Let us consider a continuous body in different states, as shown in Fig. 1 (a), (b), and (c), respectively (*Nishikawa, H. et al., 2004*). State (a) is the initial stress-free state in which neither external forces nor internal stresses exist. This state is regarded as the standard state. State (b) is a residual stress state. State (c) is the stress released state in which the body is cut into small elements. From state (b) to state (c), each element deforms elastically as much as necessary to completely release the residual stress. Now, denoting the distance between two close particles in the body in the initial state (a) by ds_0, and this distance in residual stress state (b) and in residual stress released state (c) by ds and ds^*, respectively, the strain in state (b) and (c) can be defined by the small deformation theory as follows (*Murakawa, H. 2007*):

$$\varepsilon = (ds - ds_0) / ds_0 \tag{1}$$

$$\varepsilon^* = (ds^* - ds_0) / ds_0 \tag{2}$$

Likewise, the strain increment between state (b) and (c) can be defined as follows:

$$\varepsilon^e = (ds - ds^*) / ds_0 \tag{3}$$

The strain in Equation 1 is usually called total strain and it satisfies compatibility conditions. The strain in Equation 2 is the inherent strain, which is incompatible. The strain in Equation 3 is elastic strain. From these equations, it may be seen that the total strain is composed of elastic and inherent strains, shown as follows:

$$\varepsilon = \varepsilon^e + \varepsilon^* \tag{4}$$

Given that the total strain ε corresponds to the deformation and the elastic strain ε^e corresponds to

Fig 1. Definition of inherent strain

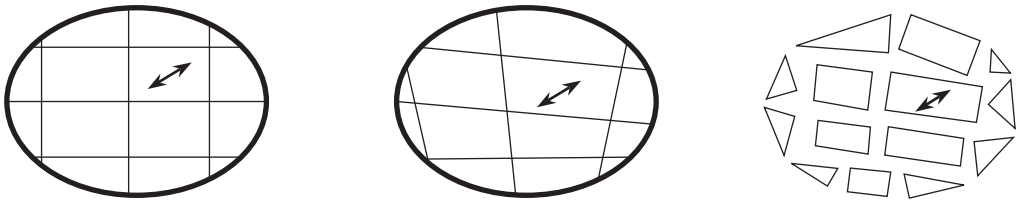

(a) Standard state (a) Stressed state (a) Stressed related state

the stress, the above equation can be written as follows:

$$\varepsilon^*(\text{Inherent strain}) = \varepsilon\,(\text{deformation}) + \varepsilon^e(\text{residual stress}) \quad (5)$$

Here, it is seen that the inherent strain produces both the deformation (inherent deformation) and the residual stress.

Inherent strain due to welding

The process under which the inherent strain is produced can be modeled by using an elastically restraint bar under thermal cycle, as shown in Fig. 2 (*Nishikawa, H. et al., 2004*). The heating region in welding, where the inherent strain occurs, can be modeled as a bar and the adjacent region, which resists deformations, can be modeled as a spring. The bar typically experiences thermal history according to the temperature change, while the spring experiences little change in temperature, but rather acts as a restraint on the bar.

The evolution of the inherent strain according to the temperature change of the bar is explained as follows: when the bar is heated to T_{max} from room temperature (zero degree) and then cooled to room temperature, compressive thermal stress is first produced in the heating process, as shown in Fig. 3. The phenomenon changes with the value of the maximum temperature, T_{max}, relative to T_1 and T_2, which are defined as:

$$T_1 = \sigma_Y / \beta\alpha E \quad (6)$$

Where, $T_2 = 2T^1$, E is Young's modulus, σ_Y is the yield stress, α is the thermal expansion coefficient, and β is the constraint parameter defined by using the stiffness of the bar and the stiffness of the spring as follows:

$$\beta = k^* / (k + k^*) \quad (7)$$

Where, $k = AE/L$ (stiffness of bar), k^* is the stiffness of spring, A is the cross-sectional area of the bar, and L is the length of the bar.

When $T_{max} < T_1$, the thermal stress does not reach the compressive yield stress in the heating process. Thus, no plastic strain (inherent strain) is produced. Because there is no inherent strain, no residual stress nor residual deformation is produced (route 0-A-0 in Fig. 3).

Fig 2. Simplified elastic-plastic analysis model

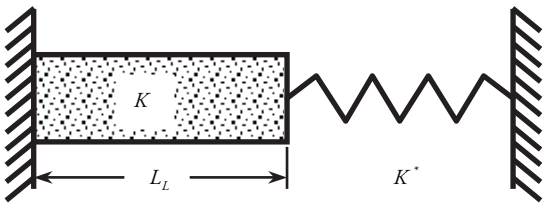

Fig 3. Thermal history

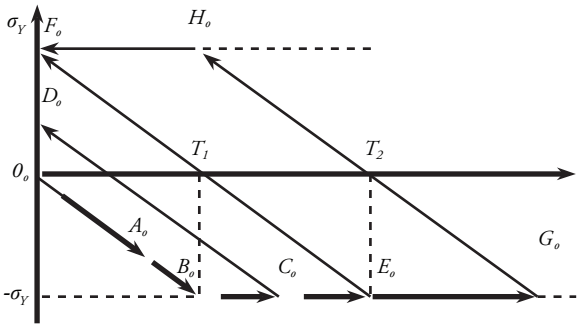

When $T_1 < T_{max} < T_2$, the thermal stress reaches the yield stress and compressive inherent strain is produced. However, the behavior of the bar is elastic in the cooling process (route 0-B-C-D in Fig. 3.

The inherent strain ε^*, residual stress σ_R and the residual deformation δ_R in this case are:

$$\varepsilon^* = -T_{max}\,\alpha + \varepsilon_Y/\beta = -T_{max}\,\alpha + \sigma_Y/E\beta \quad (8)$$

$$\sigma_R = \beta E\varepsilon^* = \beta T_{max}\,\alpha E - \sigma_Y \quad (9)$$

$$\delta_R = (\varepsilon^* + \varepsilon^e)L = (1-\beta)(-T_{max}\alpha + \sigma_Y/E\beta)L \quad (10)$$

When $T_{max} > T_2$, plastic deformation takes place in both the heating and the cooling processes (route 0-B-G-H-F in Fig. 3). In this case,

$$\varepsilon^* = -\varepsilon_Y/\beta = -\sigma_Y/E\beta \quad (11)$$

$$\sigma_R = \sigma_Y \quad (12)$$

$$\delta_R = (\varepsilon^* + \varepsilon^e)L = (1-1/\beta)\,\varepsilon_Y L \quad (13)$$

It may be seen that the inherent strain, residual stress, and the residual deformation are strongly influenced by both the highest temperature, T_{max}, and the constraint parameter β.

Prediction of welding distortion using Inherent Strain Method

An in-house 3-D thermal-elastic-plastic solid finite element code (*Serizawa, H. et al., 2007*) is employed to study the relation between the inherent strain and the final distortion of the structure. Figure 4 shows an example of the FE model and the area in which the inherent strains are introduced. The simulation procedure consists of two steps:

First, the components of inherent strain produced by single pass welding are obtained through thermal-elastic-plastic finite element analysis.

Second, these inherent strain components are introduced into the elastic FEM as initial strains and the welding distortion is estimated through elastic FE analysis. To simplify the analysis, uniform distribution of inherent strains is assumed at the central region of the plate; while at both edges, average values of inherent strains are used.

Fig 4. Schematic of elastic FEM model (a) Top surface, (b) Distribution through the plate thickness, and (c) Area in which the inherent strains are introduced

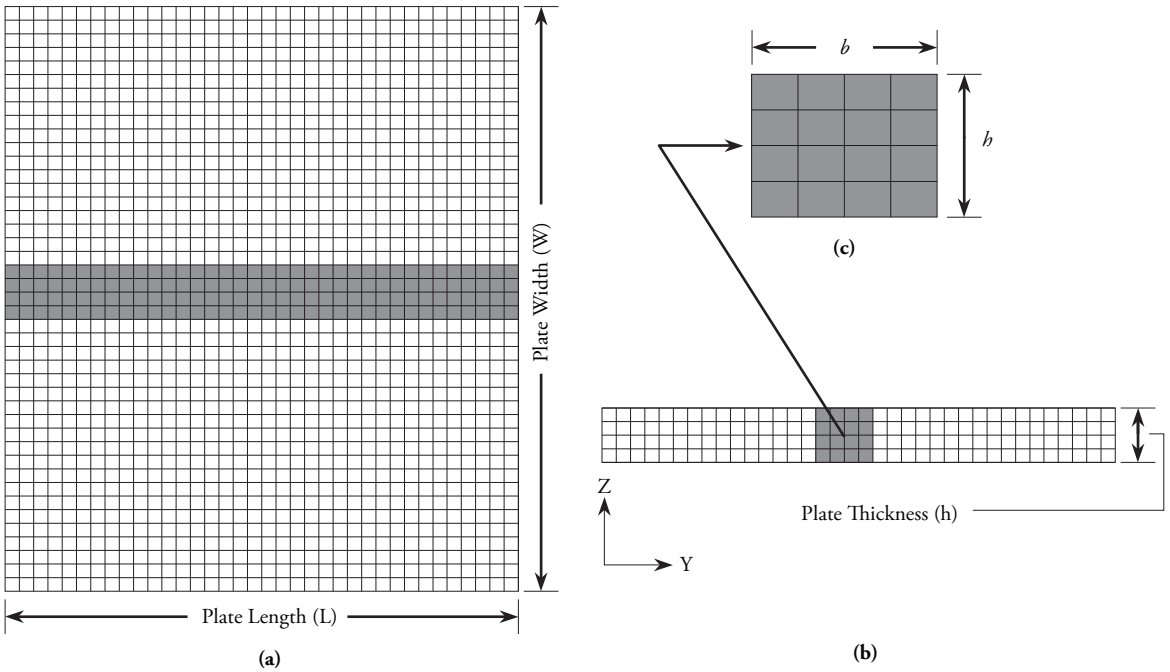

The deflections computed by the thermal-elastic-plastic FEM and the elastic FEM are compared in Fig. 5. The deflection along the transverse section at the center and that along the heating line are shown in these figures. As it may be observed from these figures, the welding distortion computed by the thermal-elastic-plastic analysis is accurately reproduced by the elastic analysis. This suggests that the elastic FEM can be employed to predict the welding distortion if the inherent deformation is know in advance.

Fig 5. Deflection distributions in the middle section produced by a single heating line (left) Transverse to the heating line and (right) Along the heating line

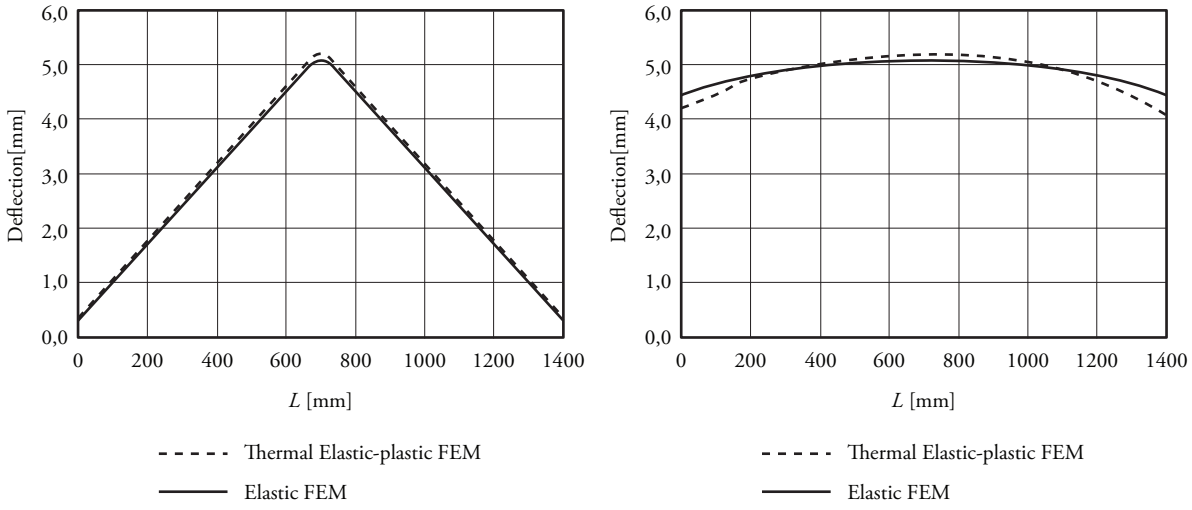

Improved method to predict welding distortion of complex ship structures by using elastic FEM

In the previous section, it was demonstrated that welding distortion can be accurately predicted by elastic FEM if the inherent strains are known. However, in shipbuilding, complex welded structures are usually found. In those cases, the welding distortion is difficult to obtain even with elastic analysis because of the influence of previous welding pass on further pass and other effects. In order to consider these influences in the analysis of plate distortion, the following procedure is proposed:

Step 1: Predict the four components of inherent strain at the central region of the plate.

Step 2: Predict the four components of inherent strain at plate edges.

Step 3: Correct the values obtained in Steps-1 and 2 for location of welding and plate size.

Step 4: Based on the sequence of welding, identify if multi-passes, parallel welding, and/or crossed welding are needed. Then, obtain the correction values from databases.

Step 5: Introduce the correction values obtained in Step-4 into the values of inherent strain predicted in Step-1 to Step-3.

Step 6: Introduce the inherent strain obtained in Step-5 into the elastic FE model. n

Step 7: Repeat Steps-1 to 6 for each additional welding pass.

Step 8: Perform elastic FE analysis.

Application of proposed method to predict welding distortion of complex ship structures

To evaluate the effectiveness of the proposed method, two cases were evaluated. First, a typical transversal section of a Car Carrier ship is taken as an example. Fig. 6 shows the general arraignment of the structure. Fig. 7 shows the FE mesh model used to evaluate the welding distortion. In order to apply the procedure explained in the previous section to this case, the welding inherent strain is

obtained through thermal elastic plastic analysis. The mesh model used is shown in Fig. 8. By using this model, an inherent strain database wass developed (for more details see *Liang, W. et al., 2004 and Murakawa, H. et al., 2005*). Later, the inherent strain from the database was introduced in the welding areas of the target structure (Fig. 7) and elastic FEM was performed.

Fig 6. Typical cross section of a car carrier ship

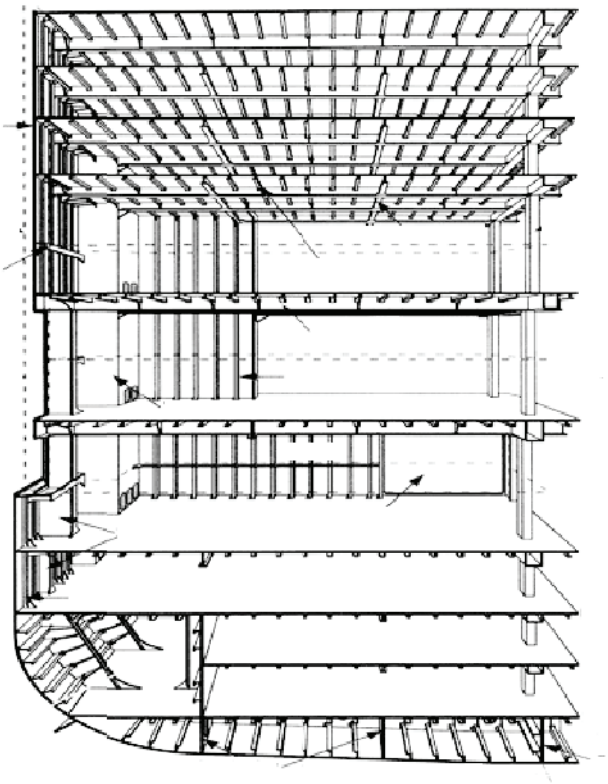

Fig 7. Finite element mesh of the full model of a car carrier

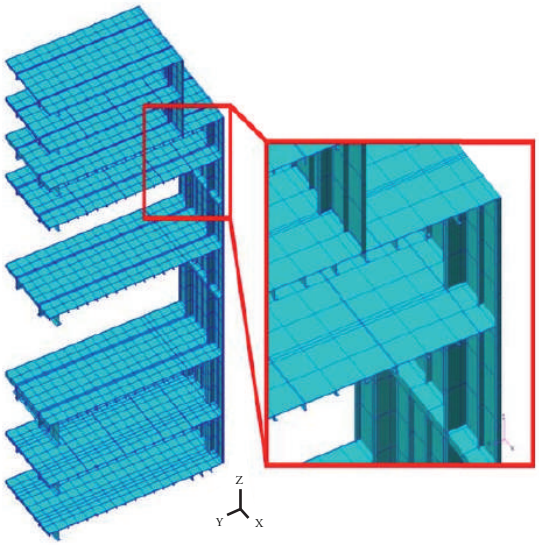

Fig 8. Typical finite element mesh model used to obtain the inherent strain

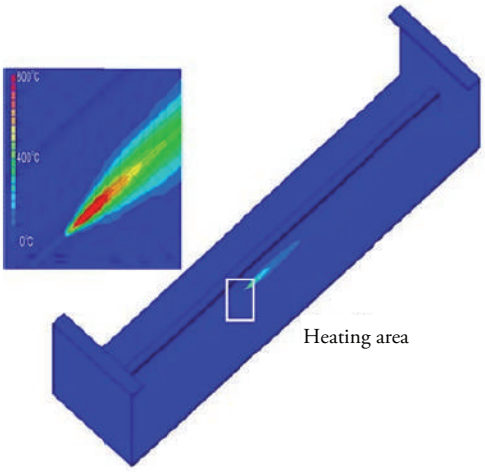

Fig. 9 shows an example of the predicted welding distortion of an 8-m length of deck section after welding and after straightening the deformed plate. In this case, the model consists of nine longitudinal fillet welds and six transverse fillet welds. Using thermal elastic plastic FE simulation, even with the faster computer, the computational time necessary to obtain similar results, is too long. Actually, not commercial software is designed to simulate such structure due to the fact that the advantage of FEM over other methods tends to disappear, once computational requirement and time exceeds designer's plans.

As seen in Fig. 9, both welding distortion and the straightened plate can be easily obtained through this elastic FEM. The comparison with thermal elastic plastic FEM and with the experiment will be presented in future papers; however, it was

Fig 9. Welding deflection of an 8-meter length ship deck (large heat input) obtained by using the proposed elastic FE (up) after welding, (down) after straightening

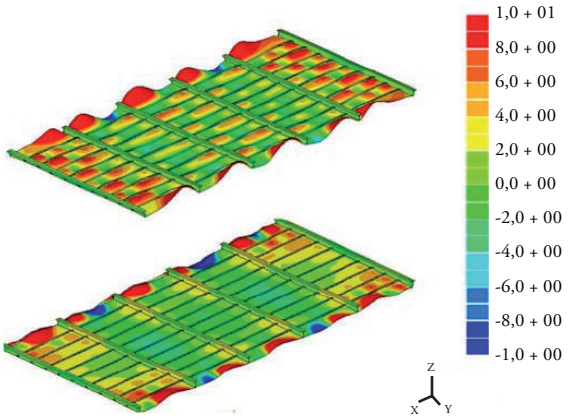

Fig 10. Side shell welding deflections of a bulk carrier

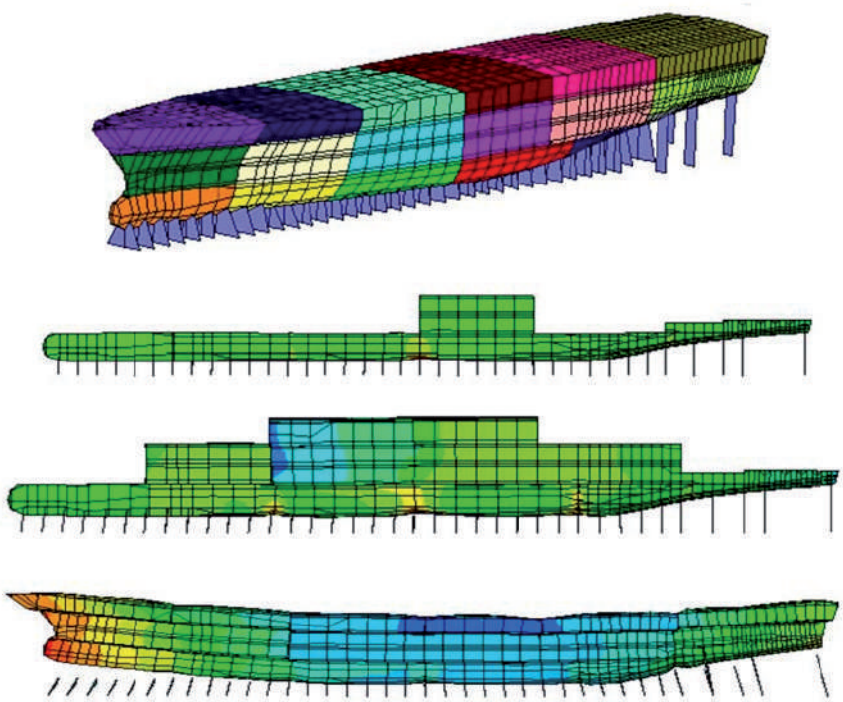

found that the deviation from the experiment is less than 8%.

The second case represents the ship block assembly process. In this case, the welding distortion produced is predicted through the same elastic FEM proposed herein. The objective of this study was to obtain the best welding sequence to be used in assembling the blocks. This is because during block assembly, welding distortion appears in decks due to existing residual stress produced by previous welding.

Fig. 10 shows the results of welding distortion predicted by this method. As seen in the figure, it is possible to predict the welding distortion of a large structure like the ship block assembly process.

Conclusions

A method to predict welding distortion of complex welded structures on ships has been developed. In this method, the inherent strain of single welding pass is first predicted based on the given heating condition and plate thickness. Then, by using the inherent strain databases of influential factors, corrections necessary for the inherent strain are made. The same procedure is followed for each welding pass, according to the welding sequence. Through numerical analysis, it has been demonstrated that this method can be used to easily and accurately predict welding distortion of complex ship structures.

In addition, the computational time is much shorter than that used in the thermo-elastic-plastic FEM. In the present study, the total computational time of both the thermal analysis and the thermo-mechanical analysis is approximately 36 hours for the thermo-elastic-plastic FE model (Case 1); whereas, the computational time of the elastic FE model is shorter than one hour (including pre-processing). For more complex ship structures (Case 2), the computation time required for thermo-elastic-plastic FEM proportionally increases with the number of welding passes, while that required in elastic FEM is approximately the same as in the first case.

Acknowledgement

Authors greatly appreciate the support of the National Secretary of Science and technology of Panama (SENACYT) through their program of grants for research and development. Also author would like to thanks to Isthmus Bureau of Shipping (CLASS IBS) for all their support in this research.

References

DENG, D. A.; MURAKAWA, H. AND LIANG, W. Comput. Methods Appl. Mech. Engrg. 196: 4613- 4627, 2007.

LIANG, W.; DENG, D. AND MURAKAWA, H. J. MATER. Process. Tech. 183: 219-255, 2007. Liang, W. et al., Transactions of JWRI. 33(1): 45-51, 2004.

LIU, C AND ZHANG, X. Sci. Technol. Weld. Join. 2009, 14 (1), 26-31. Murakawa, H. Mater. Sci. Forum. 539-543: 181-186, 2007.

MURAKAWA, H; LIANG, W. AND DENG, D. Transactions of JWRI. 34(1). 113-123, 2005.

NISHIKAWA, H. et al., H. Proc. Int. Soc. Offshore Polar Eng. Conf. Toulon, France. May 2004, ISOPE, 126-132.

SERIZAWA, H.; NISHIKAWA, H. AND MURAKAWA; H. Sci. technol. Weld. Join. 1282): 147-152, 2007. Wahab, M. et al., 2006, 85 (22), 35 - 43.

Study of the weld ability of Aluminum Alloy 5083 H116 with Pulsed Arc GMAW (GMAW-P)

Estudio de soldabilidad de aleación de aluminio 5083 H116 con arco pulsado GMAW (GMAW-P)

F. Cueca [1] E. Solano [1]
A. Patarroyo [1] A. Morales [2]
F. Rojas [1] R. Muñoz [3]

Abstract

This research was based on the analysis of the weldability of aluminum joints, Alloy GL AW 5083 H116, with filler AWS 5.10 ER 5183 by GMAW-P process to determine the conditions of the heat-affected zone in the base material, depending on the heat input for the GMAW-P process with different pulsed technologies available in Colombia. The variables considered within this study were: welding positions (horizontal, vertical up, and overhead), type of welded joints (butt and fillet), and parameters for welding equipment (voltage, current, speed, power supply, speed development), and protective gas used (Argon, 100%). Non-destructive and destructive testing techniques were used to characterize the discontinuities found and the criteria to accept or reject the AWS D1.2 code (STRUCTURAL WELDING CODE - ALUMINUM by the AMERICAN WELDING SOCIETY). As a result, the investigation yielded the conditions for the application of filler material (ER 5183) on base material (alloy AW5083 GL H116), supported by Welding Procedure Specifications Documents (WPS) and Procedure Qualification Record (PQR) to implement in aluminum welding at the COTECMAR shipyard.
Key words: Welding, Pulsed arc. Pulsed MIG, HAZ, Discontinuities, Synergic Curves.

Resumen

Esta investigación se basó en el análisis de la soldabilidad de las uniones de aluminio, Aleación GL AW 5083 H116, con relleno AWS 5.10 ER 5183 mediante proceso de soldadura por arco metálico con gas (GMAW-P) para determinar las condiciones de la zona afectada por calor en el material base, dependiendo de la entrada de calor para el proceso GMAW-P con diferentes tecnologías de impulsos disponibles en Colombia. Las variables consideradas dentro de este estudio fueron: posiciones de soldadura (horizontal, vertical hacia arriba y por encima), tipos de uniones de soldadura (a tope y filete) y parámetros para equipo de soldadura (voltaje, corriente, velocidad, suministro de potencia, velocidad de desarrollo) y gas de protección utilizado (Argón, 100%). Se utilizaron técnicas de pruebas destructivos y no destructivas para caracterizar las discontinuidades halladas y los criterios para aceptar o rechazar el código AWS D1.2 (CÓDIGO DE SOLDADURA ESTRUCTURAL - ALUMINIO de la SOCIEDAD AMÉRICANA DE SOLDADURA). Como resultado, la investigación arrojó las condiciones para la aplicación del material de relleno (ER 5183) sobre material base (aleación AW5083 GL H116), apoyado por los documentos de Especificaciones de Procedimientos de Soldadura (WPS, por el término en inglés) y Registro de Calificación del Procedimiento (PQR, por el término en inglés) para implementar en soldadura en aluminio en el astillero de COTECMAR.
Palabras claves: Soldadura, arco pulsado. MIG pulsado, HAZ, Discontinuidades, Curvas Sinérgicas.

Date Received: October 22th, 2010 - *Fecha de recepción: 22 de Octubre de 2010*
Date Accepted: January 16th, 2012 - *Fecha de aceptación: 16 de Enero de 2012*

[1] Servicio Nacional de Aprendizaje SENA. e-mails: apatarroyo@misena.edu.co; elsomon7@misena.edu.co; facum64@hotmail.com; hfrojas@misena.edu.co
[2] Corporación de Ciencia y Tecnología para el Desarrollo de la Industria Naval, Marítima y Fluvial COTECMAR. e-mail: amorales@cotecmar.com
[3] Universidad Nacional de Colombia, Faculty of Mechanical Engineering. Bogotá, Colombia. e-mail: rmuñoz@unal.edu.co

Problem

The heat-affected zone (HAZ) is the section in the base material in which the mechanical properties are affected by the arc during the welding process in any metallic material. Depending on the amount of heat input, the magnitude of the HAZ increases or decreases as temperature on the material increases or decreases.

In aluminum alloys, the mechanical properties are seriously diminished by the effect of heat introduced by the welding process. It is more critical for the 5083 series alloys, which are heat-treatable alloys commonly used in the maritime industry and whose mechanical properties are assigned to their main alloying element, magnesium, and the residual stresses generated by a given hardening by cold work.

Documentation of the process of gas metal arc welding (GMAW) and pulsed-spray transfer is limited by these types of aluminum alloys in marine applications. The generation of pores and discontinuities can be attributed to the use of gas mixtures, lack of qualified technical welding personnel in this type of material, and non-updating of standard skills for applications with GMAW and pulsed technology.

Introduction

Aluminum is a material with excellent mechanical properties and corrosion resistance; with its implementation in the shipbuilding industry, there is a decrease in fuel consumption and investment in vessel maintenance.

The GMAW process is a semi-automatic or automatic process, where an electric arc is maintained between a solid wire electrode that functions as continuous and the work piece. This process has different modes of mass transfer, *short circuit, globular, and spray*.

The shipbuilding industry is using Colombian high-strength materials like aluminum-magnesium alloys (GL AW Alloy 5083 H116) welded with filler 5183 AWSER 5.10 and shielding gas (100% argon (Ar)) that meet the requirements of tensile strength, as specified in codes.

State-of-the-art

Designation of alloys

The designation of aluminum and its alloys are based on the quality of forged or cast products (molded). Table 1 shows the system for designating wrought alloys.

Table 1. Designation of wrought aluminum alloys

Designation	Major Alloy Elements
1XXX	None, aluminum 99.00% min
2XXX	Copper (Cu)
3XXX	Manganese (Mn)
4XXX	Silicon (Si)
5XXX	Magnesium (Mg)
6XXX	Magnesium and silicon
7XXX	Zinc (Zn)
8XXX	Other components
9XXX	No uses

Source: Materials Science - selection and design, Pat L. Mangonon, Prentice Hall

Characteristics of the forged alloy 5083 H116

Chemical composition
The chemical composition of aluminum alloys must meet the requirements of the International Association of Classification Societies (IACS) Section W25 (Table 2).

Mechanical properties
The mechanical properties must meet the requirements furnished in Table 3.

Table 2. Requirements in the chemical composition of aluminum alloys for hull construction and marine structures

Grade	Si	Fe	Cu	Mn	Mg	Cr	Zn	Ti	Other Elements	
									Each	Total
5083	0,40	0,40	0,10	0,40-1,0	4,0-4,9	0,05-0,25	0,25	0,15	0,05	0,15
5383	0,25	0,25	0,20	0,7-1,0	4,0-5,2	0,25	0,40	0,15	0,05[5)]	0,15[5)]
5059	0,45	0,50	0,25	0,6-1,2	5,0-6,0	0,25	0,40-0,90	0,20	0,05[6)]	0,15[6)]
5086	0,40	0,50	0,10	0,20-0,7	3,5-4,5	0,05-0,25	0,25	0,15	0,05	0,15
5754	0,40	0,40	0,10	0,50[3)]	2,6-3,6	0,30[3)]	0,20	0,15	0,05	0,15
5456	0,25	0,40	0,10	0,5-1,0	4,7-5,5	0,05-0,20	0,25	0,20	0,05	0,15
6005A	0,50-0,9	0,35	0,30	0,5[4)]	0,40-0,7	0,30[4)]	0,20	0,10	0,05	0,15
6061	0,40-0,8	0,70	0,15-0,40	0,15	0,8-1,2	0,04-0,35	0,25	0,15	0,05	0,15
6082	0,7-1,3	0,50	0,10	0,40-1,0	0,6-1,2	0,25	0,20	0,10	0,05	0,15

Notes:
[1)] Composition in percentage mass by mass maximum unless shown as a range or as a minimum.
[2)] Includes Ni, Ga, V and listed elements for which no specific limit is shown. Regular analysis need not to be made.
[3)] Mn + Cr: 0,10 - 0,60
[4)] Mn + Cr: 0,12 - 0,50
[5)] Zr: maximum 0,20. The total for other elements does not include Zirconium
[6)] Zr: 0,05-0,25. The total for other elements does not include Zirconium

Source: IACS - Section W25

Table 3. Requirements of the mechanical properties of rolled aluminum products for the construction of hulls and marine structures

Grade	Temper condition	Thickness, t	Yield Strenght R_{p02} min. N/mm²	Tensile Strenght R_m min. or range N/mm²	Elongation, % min.	
					A_{50mm}	A_{5d}
5083	O	3 ≤ t ≤ 50 mm	125	275 - 350	16	14
	H112	3 ≤ t ≤ 50 mm	125	275	12	10
	H116	3 ≤ t ≤ 50 mm	215	305	10	10
	H321	3 ≤ t ≤ 50 mm	215 - 295	305 - 385	12	10

Notes:
1) Elongation in 50 mm apply for thicknesses up to including 12.5 mm and in 5d for thicknesses over 12.5 mm.
2) 8% for thickness up to including 6.3 mm.

Source: IACS - Section W25

Requirements regarding materials and welds according to IACS - STANDARD W25

These requirements apply to aluminum alloys with thicknesses between 3 and 50 mm. The numerical designation (grade) of aluminum alloys and the description of basic statements are based on the designation of the Aluminum Association (AA), as shown in Table 4.

Table 4. Requirements of aluminum products for the construction of hull and marine structures

Rolled products (plates, strips, and panels)	Extruded Products (sections, plates, rods, and closed profiles)
5083, 5086, 5383, 5059, 5754, 5456 With the following statements: O/H112, H116, H321	Aluminum Alloys: 5083, 5383, 5059, 5086 With the following statements: O/H111, H112 And alloys 6005A, 6061, 6082 with statements T5 or T6

Source: IACS - Section W25

Recommended filler materials to weld aluminum alloys

Table 5 shows the input materials recommended by the American Bureau of Shipping (ABS) to weld aluminum alloys; remember that the solder joints in this investigation consist of 5083 H116 alloy plates 6.7 mm thick.

Table 5. Recommended filler materials to weld aluminum alloys

Base Metal Alloys	5083	5086	5454[1)]	5456
5083	5183	5356	5356	5183
5086	5356	5356	5356	5356
5454[1)]	5356	5356	5554[1)]	5356
5456	5183	5356	5356	5556
6061	5356	5356	5554[2)]	5356

Notes:
[1)] 5454 aluminum alloy welded with 5554 filler metal is generally recommended for above 65ºC (150ºF) such as for smoke stacks and engine rooms enclosures.
[2)] 5183 or equivalents may be used.

Source: IACS - Section W25

Required filler materials to weld aluminum alloy 5083 H116

The properties of consumables or filler material used to weld aluminum alloy 5083H116 comply with ABS code requirements and are characterized in the Metal Handbook, Volume 6, according to Table 6.

Table 6. Requirements in the chemical composition of aluminum welding consumables

Composition in percent maximum, unless shown as a range or specified												
Alloy	Silicon	Iron	Silicon and Iron	Copper	Manganese	Magnesium	Chromium	Zinc	Titanium	Other Elements		Aluminum
										Each	Total	
4043	4,5-6,0	0,8	0,5	0,3	0,05	0,05		0,1	0,2	0,05	0,15	Remainder
5183	0,4	0,4	0,4	0,1	0,5-1,0	4,3-5,2	0,05-0,25	0,25	0,15	0,05	0,15	Remainder
5356			0,4	0,1	0,05-0,20	4,5-5,5	0,05-0,20	0,1	0,60-0,20	0,05	0,15	Remainder
5554				0,1	0,50-1,0	2,4-3,0	0,05-0,20	0,25	0,05-0,20	0,05	0,15	Remainder

* The maximum Beryllium content of all tiller wires is to be 0,008 %

Source: ABS (American Bureau of Shipping) - Part 2 Appendix 2/E

Required mechanical properties of aluminum welding consumables

The mechanical properties of aluminum welding consumables are shown in Table 7.

Table 7. Required mechanical properties of aluminum welding consumables

Filler Alloy	Shear Strength			
	Longitudinal		Transverse	
	MPA	KSI	MPA	KSI
5183	128	18,5	193	28,0

Source: ASM Metals HandBook Volume 6 - Welding, Brazing, and Soldering - Pag. 1801

Requirements regarding materials and welds according to IACS - STANDARD W25

Within the development process used, different variables are presented below.

Essential variables of the process

These are the numerical values of the parameters that directly affect the geometry of the weld deposit and its quality. Knowledge and control of these parameters is essential for quality welds because these variables are not independent given that a change in one of them produces or involves changes in some of the others. Key parameters to become part of the characteristics of welding and, therefore, the quality of the weld are: welding current, arc voltage, electrode free length (Stick-out), polarity, forward speed, electrode diameter, electrode orientation and shielding gases, whose requirements are shown in Table 8.

Types of forces acting on the process

Surface tension
Gravitational force
Electromagnetic force

Transfer of metal

Short Circuit
Globular transfer
Spray
Pulsed Spray

Advantages and disadvantages of the welding process transfer by pulsed Spray

Table 9 shows the advantages and disadvantages of the welding process of transfer by PULSED SPRAY.

Table 9. Advantages and disadvantages of the welding process transfer by pulsed spray

Advantages	Disadvantages
• It allows implementations in all positions without splash 3 to 50mm • Versatile and productive programmable. • Allows welding filler materials greater than 0.9mm.	• High initial equipment cost • Acceptance of welder and process knowledge • Difficulty to adjust the parameters. • Limited application in open meetings and poor fit

Source: PROCESS OF PULSED WELDING - EXSA- Juan Guardia G. - OERLIKON

Table 8.Protection requirements in aluminum welding gas

Base Metal	Protection Gas	Beneficts
Aluminum	100 % Ar	Penetration of 0 to 25 mm, better transfer and arc stability, less sizzle.
	35% Ar – 65% He	Penetration of 25 to 76 mm; most induced heat than with pure argon, best features of fusion with the series Al-Mg alloys 5XXX series.
	25% Ar – 75% He	More than 76 mm of penetration, the maximum introduced heat and minimal porosity.

Source: PROTECTIVE GAS WELDING - Publication Abello Linde

ER 5183 wire features

Welding ER 5183 are very good fluidity, low melting point (eutectoid point) and widely used in the shipbuilding industry.

Table 10. ER 5183 Wire features

Alambre de Aluminio ER5183		
Composición	Si	0,40%
	Fe	0,40%
	Cu	0,10%
	Manganeso	0,50-1,0%
	Magnesio	4,3-5,2%
	Cr	0,05%-0,25%
	Zn	0,25%
	Ti	0,15%
	Otros elementos	0,05%
	La suma de los elementos	0,05%
	Al	Resto
Caracterización del metal depositado	σs: 140 MPa σb: 300 MPa δ: el 20%	
Temperatura de fusión	574/638ºC	
Metales bajos preferidos	AlMg4,5Mn; AlMg4Mn; AlMg5Si; AlZnMgCu1,5; AlZnMgCu0,5 Protegido por el Argón de la pureza elevada, y utilizado para la aleación de aluminio de alta resistencia de la soldadura: AlMg4,5Mn; AlMg5Si; AlZnMgCu1,5; AlZnMgCu0,5	

Source: http://spanish.alibaba.com/product-gs/aluminum-wire-er5183-356630685.html

Shielding gases (Argon, Ar, 100%)

In gas-shielded arc welding, the shielding gas can have a great influence on the properties of the weld metal. It is, therefore, necessary to check the solder in a controlled atmosphere. In welding with covered electrodes, the gases surrounding the arc come from the combustion of certain substances contained in the electrode coating. In the Metal Inner Gas process a protective atmosphere is achieved around the arc with a jet of gas, supplied through a nozzle, and from an external power source.

This gas has been used for many years as a means of protection in fusion welding. Argon is used in welding generally has a purity of 99.995%. When greater purity is required, the gas may be chemically purged at concentrations of 99.999%. One of the main qualities of argon is its low ionization potential. This means more stable arches, quiet, with few projections. It also reduces the arc voltage and, consequently, reduces the power of penetration. These properties make it highly recommended for small thickness welding. Pure Argon gas is rarely used as a safe protection in welding metals like aluminum, copper, nickel, and titanium.

Aluminum welded joints have been extensively studied for years. Many researchers have focused on the metallurgical melt or weld phenomenon (*Hermann et al., 1996; Hepples et al., 1992*), others have characterized the mechanical properties (*Debbouz and Navaï, 1997; Bloem et al., 2000*) and, however, there are few studies on the evolution of the heat affected zone in these HAZ13 alloys.
Fig. 1 shows the base-metal interface weld, increasing the energy of dissolution of the shielding

Fig. 1. Diagram Evolution of energy and temperature of dissolutions of Shielding Gases in distance function

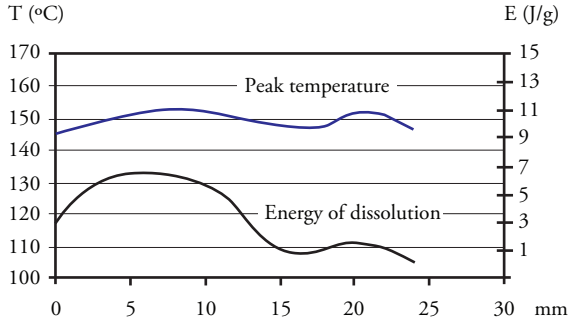

Source: http://erevistas.saber.ula.ve/index.php/cienciaeingenieria/article/viewFile/

gases, indicating a higher level of these changes on the aluminum matrix.

Experimental Design

The present study considered a type comparative experiment of setting up such parameters welding process used such as: gas type, number of joints, and number of specimens, joint design and base material.

Methodology

The methodology carried out during the investigation was as follows:

Search and selection of power supplies for welding with GMAW-P., obtaining samples for chemical and mechanical characterization of the base material, chemical and mechanical characterization of the base material , joint design according to the AWS D1.2 code , consolidation of boards and equipment as selected variables, development of the encoding matrix, assurance process traceability of materials, preparation and machined seals, welding joints, test-granting ticket, verification stamp discontinuities through visual inspection techniques and NDT Penetrating, determining the number of samples to obtain welded joints AWS D1.2 code, Court stamp, Specimen preparation and machining, Mechanical testing, collection and analysis of results.

Results

Spectrometric analysis performed on the base material in the laboratory results from the study genre similar to those referenced by the IACS-W25; Mg decreased and Cr content could not be recorded by the computer (Table 11).

The results of the mechanical properties of the filler are shown in Tables 12 and 13 and in Figs. 2 and 3 for technology Y and Z, respectively; the values were greater than the efforts established by IACS-W25, registered in Table 7.

Table 11. Chemical Composition Laboratory

Chemical Composition Laboratory	
Element	**% Weight**
Si	0,556
Fe	0,283
Cu	0,0312
Mn	0,5322
Mg	C,001
Cr	---
Zn	0,001
Ti	0,0138
Al	99,077
Other elements	0,0037

Source: Spectrometry Laboratory - Materials and Testing Center - SENA

Table 12. Mechanical Characteristics of Base Material

Mechanical Characteristics	
Yield strength (Mpa)	213,745
Breaking strength (Mpa)	303,38

Fig. 2. Diagram Curve formation efforts of filler material by using technology Y for butt-weld joint

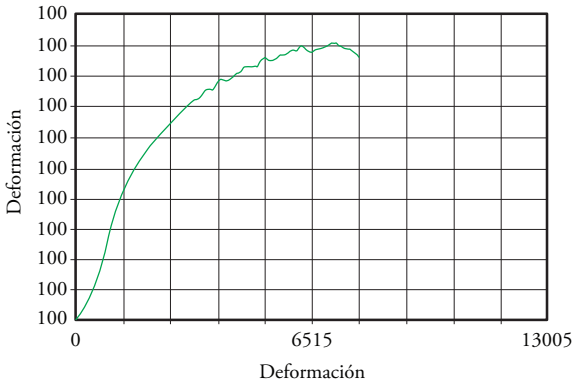

Source: Materials Laboratory - Universidad Los Libertadores

Table 13. Mechanical characteristics of filler material by using technology Y for butt-weld joint

Mechanical Characteristics	
Yield strength (Mpa)	166,85
Breaking strength (Mpa)	243,815

Fig. 3. Diagram Curve formation efforts of filler material by using technology Z for butt-weld joint

Source: Materials Laboratory - Universidad Los Libertadores

For the designs of butt joints and fillet is served in accordance with the parameters set in Figs. 4 and 5.

Fig. 4. Scheme Joint design butt

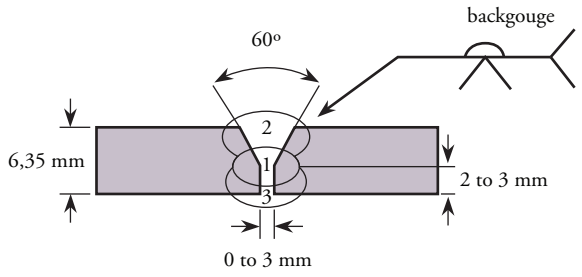

Source: Project authors

The acceptance and rejection criteria applied in Non Destructive Testing inspection techniques and visual inspection and penetrating liquid were according to AWS D1.2, which evaluated surface discontinuities, Figs. 6 and 7 show the designs of the stamps to obtain the specimens and subsequent machining and bending test for both butt joints, and fracture for fillet joints.

Fig. 5. Scheme Joint design for fillet

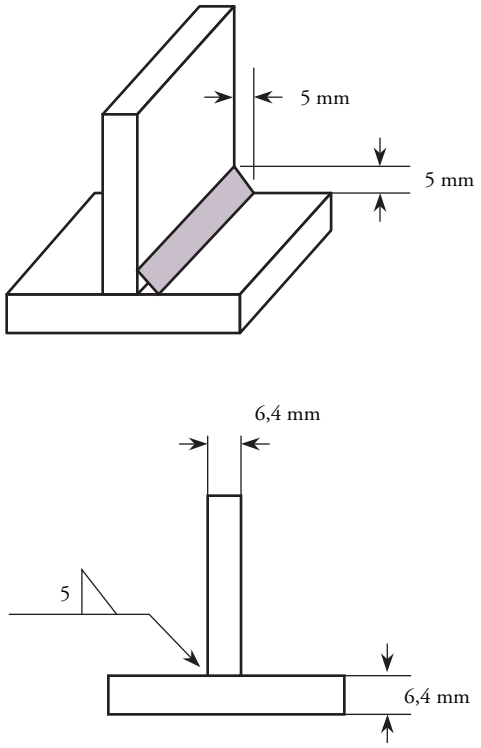

Source: Project authors

Fig. 6. Scheme Sizing for specimens - Butt joints

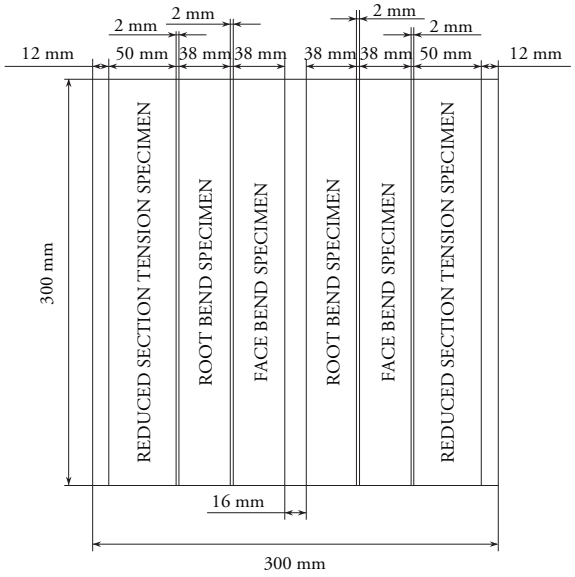

Source: AWS - D1.2

Fig. 7. Scheme Sizing for specimens - Fillet joint

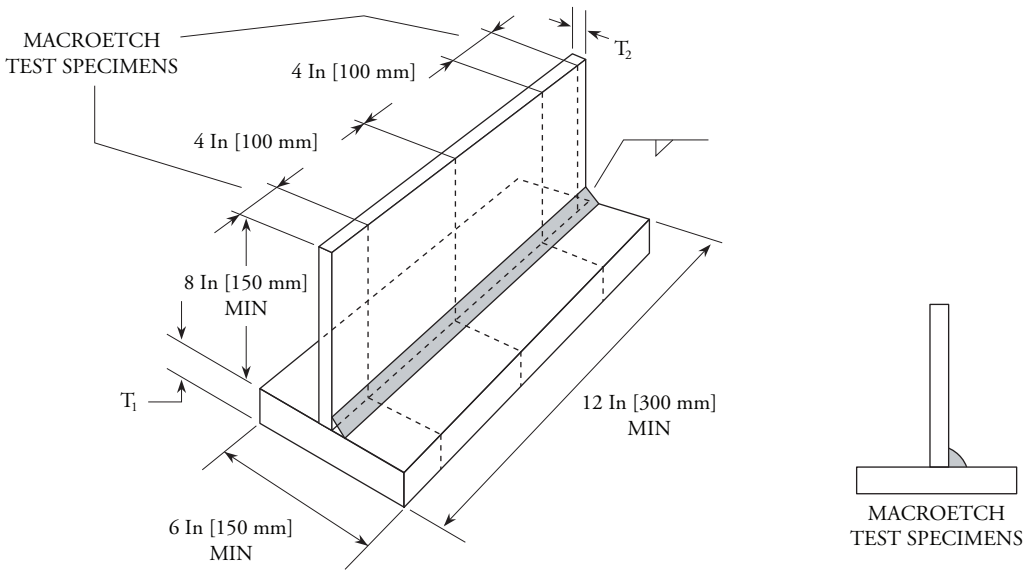

Source: AWS - D1.2

Macrography

Figs. 8, 9 and 10 show macrographies with the observation points of the specimens obtained from the joint for **Z** technology, there is the base material, the heat affected zone (HAZ) and weld material; sections of macro-attack are also noted as indicated by the design.

Fig. 8. Macrography code F2G2

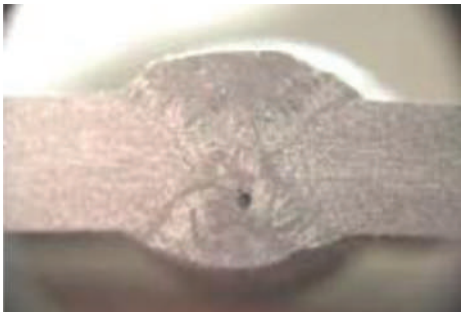

Fig. 9. Macrography code F3G2

Fig. 10. Macrography code F4G2

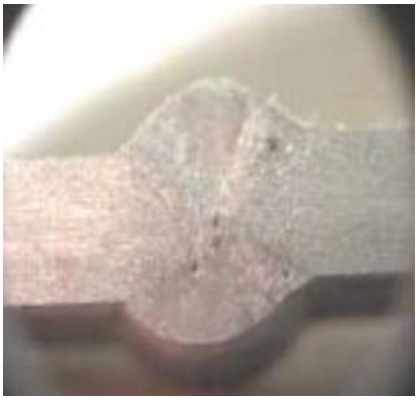

Source: Project authors

Figs. 11, 12, and 13 show macrographies correspond to the **Y** technology with the same features listed above.

It should be noted that for all the specimens macro-attack solution was used 200cc HNO3 and 50cc

HF at room temperature for 1 min to establish the dissolution of the precipitates and the recognition of discontinuities like rust, cracks, and inclusions.

Fig. 11. Macrography code M2G2

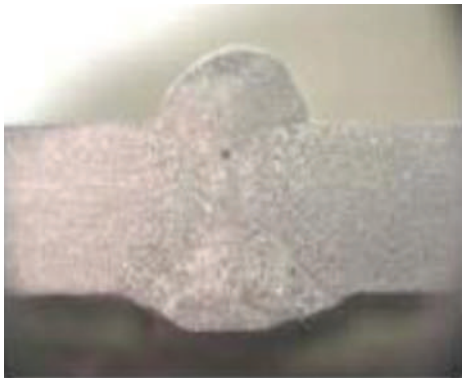

Fig. 12. Macrography code M3G2

Fig. 13. Macrography code M4G2

Source: Project authors

Bending test

The bend test for butt joints was made after verification of these macroscopic conditions and showed a brittle fracture behavior of welded specimens in all the **Z** technology with almost complete breakdown, as shown in Fig. 14, while as for **Y** technology applications and the Fig. 15 shows the generation of transverse cracks through on the side of the root.

Fig. 14. Macrography – Z technology

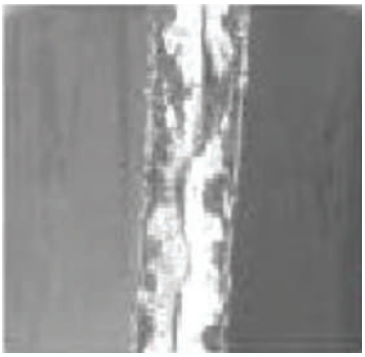

Fig. 15. Macrography – Y technology

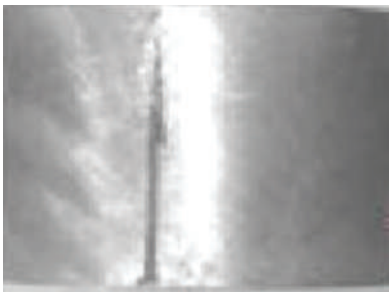

Source: Project authors

Fracture test

The fracture test was performed to fillet welded joints, whose behavior for the entire application with **Z** technology was the generation of pores and the lack of significant fusion, as seen in Figs. 16, 17 and 18. The **Y** technology shows in Figs. 19, 20 and 21 a better condition in the generation of pores and lack of fusion.

Fig. 16. Macrography – Z technology

Fig. 17. Macrography – Z technology

Fig. 18. Macrography – Z technology

Fig. 19. Macrography – Y technology

Fig. 20. Macrography – Y technology

Fig. 21. Macrography – Y technology

Source: Project authors

Metallographic tests

Fig. 22 shows microstructures with the results of metallographic test for the design of butt joints and Fig. 23 presents the results for fillet joints. Items designated as "a" and "c" in the design correspond to the HAZ, point "a" is evaluated at the top of this area and point "c" at the bottom. "b" is valued in the filler and point "d" in the base material.

Hardness tests

Fig.s 24 and 25 correspond to the hardness profiles for the designs of butt joints with **Z** and **Y** Technologies respectively, showing an asymmetry in the profiles for the **Z** Technology, while for the **Y** Technology and the tendency of these is to be symmetrical. The same behavior can be seen in Figs. 26 and 27 for the hardness profiles of the butt and fillet joints.

Fig. 22. Metallography Butt Joint M4G2 at 100X

a. b.

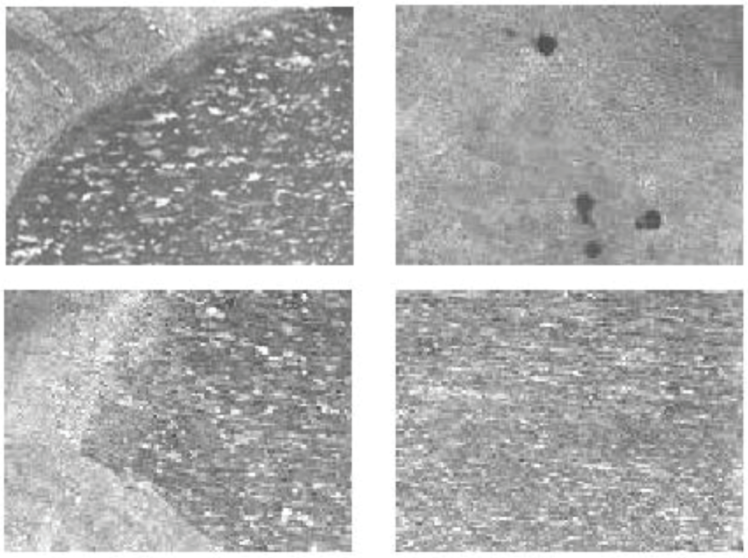

c. d.

Fig. 23. Metallography Butt Joint M4G2 at 100X

a. b.

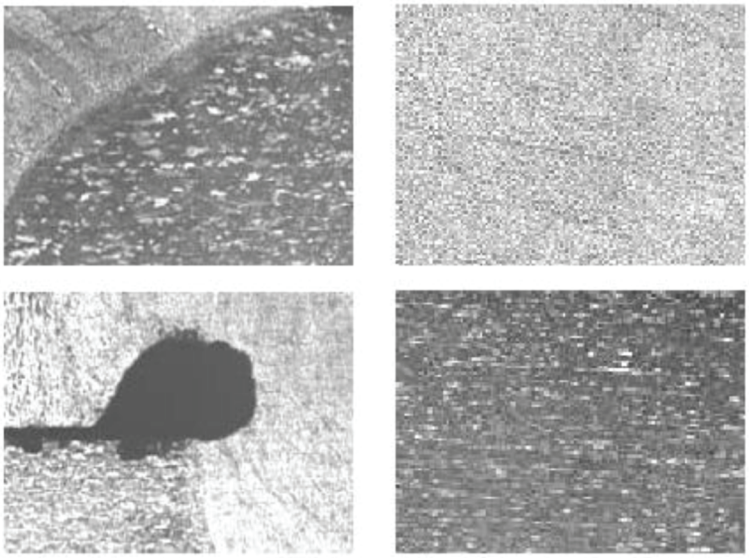

c. d.

Fig. 24. Diagram Hardness Profile Z Technology – Butt Joint

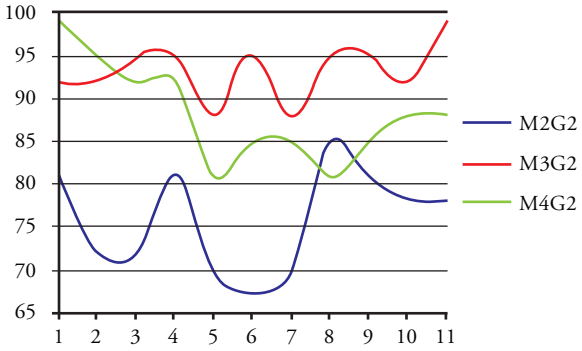

Fig. 25. Diagram Hardness Profile Y Technology – Butt Joint

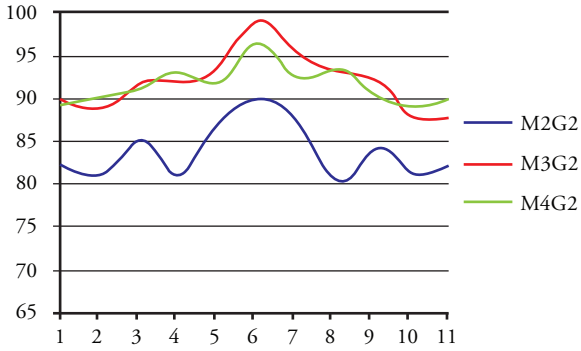

Fig. 24. Diagram Hardness Profile Z Technology – Fillet Joint

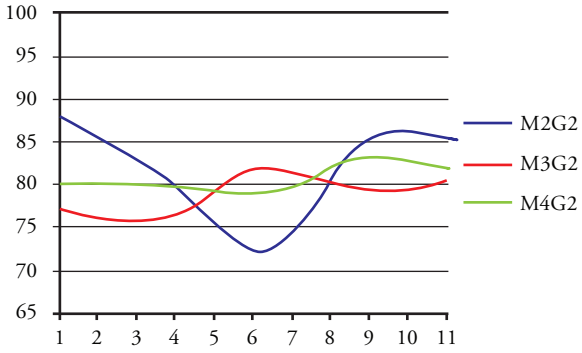

Fig. 25. Diagram Hardness Profile Y Technology – Fillet Joint

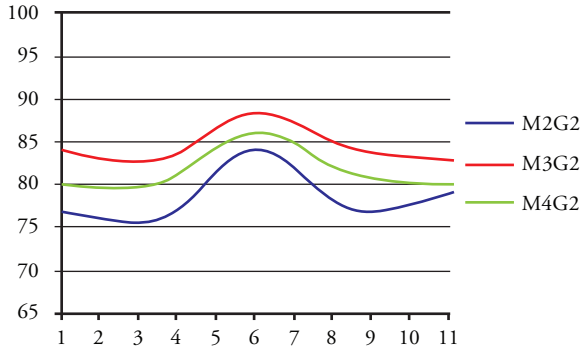

Source: Project authors

Conclusions

We selected two applications of GMAW-P technologies, which were designated as **Y** and **Z**, respectively, and these designs were applied to butt joints and fillet, with welding positions 2G, 3G, and 4G to stop and 2F, 3F, and 4F for fillet.

The preliminary characterization of the base material and filler with spectroscopy and mechanical tests allowed establishing comparisons with the theoretical references considered. The values of the mechanical tests for tensile test of butt joints show an increase of 28.1% in the yield stress and 24.5% for breaking strength on the welded joints with **Z** technology.

The visual analysis showed the weld areas of the base material, heat affected zone (HAZ) and weld material. The fracture testing of fillet joints shows better behavior mechanical with **Z** technology than the **Y** technology.

The metallographic analysis showed in more detail the microstructure of the zones of welded joints and discontinuities such as pores and confirms lack of fusion. This procedure was performed with a metallographic optical microscope connected to an image analyzer with a 100x magnification of gray levels because the interests of the investigation was to determine the overall condition of filler material in front of the base, in the micrographs is reached to appreciate dendritic areas (white points) in the HAZ with anisotropic orientations because of the possible phases present as Si, Mg 2 Si, and Fe3SiAl12 Fe2Si2Al9 within a matrix of aluminum-rich solid solution based on the results of chemical analysis.

A hardness profile in the symmetry of the points it has the **Y** technology, while technology **Z** shows irregularity in their profiles. The magnitude of higher hardness presents the welded joints with **Y** technology with nominations F3G2 with 95, HB and F3F2 with 82 in the filler, while for the appointments M3G2 and M3F2 were 99HB and 88 HB respectively.

References

Ingeniería de soldadura - Efraín Tabares A. - Profesor asociado a la Universidad Nacional de Colombia - Abril 5 del 2001 - Departamento de ingeniería mecánica - Universidad Nacional de Colombia.

Journal of Achievements in Materials and Manufacturing Engineering - Arc voltage behavior of one drop per pulse mode in GMAW-P - VOLUME 17- ISSUE 1-2 -July-August - 2006.

SUNARC - Tecnología en soldadura- www.sunarc.com

GASES DE PROTECCIÓN PARA LA SOLDADURA - Publicación Abello Linde.

PROCESOS DE SOLDADURA POR ARCO PULSADO - EXSA- Juan Guardia G. - OERLIKON.

MANUAL DEL SOLDADOR - Germán Hernández Riesco - Asociación española de soldadura y Tecnología de unión.

EL LIBRO DEL ALUMINIO, INDUSTRIA Y ARQUITECTURA - Alu-stock S.A.- capitulo 10 - información técnica.

MANUAL DE SOLDADURA MODERNA - Tomo 1 - segunda edición - Howard B. Cary - Prentice Hall Hispanoamericana S.A.

AMERICAN BUREAU OF SHIPPING - Requirements for Materials and Welding - PART 2 - Aluminum.

HUEHL, ROBERT O. Diseño de experimentos 2ª edición Thomson Learning.

AWS D1.2 - Structural Welding Code - Aluminum

Shooting Simulator for Fluvial Combat Training

Sistema de simulación de tiro para entrenamiento de combate fluvial

Carlos F. Rodríguez [1]
José Tiberio Hernández [2]
Pablo Figueroa [3]

Abstract

Virtual shooting training has become very attractive because of possible cost reductions and precise evaluation. This article describes the development of a shooting simulator to train soldiers in fluvial combat. This simulator combines the motion of a mechanical platform with virtual imagery and sound to produce an immersive scenario for training purposes. Our prototype, which is in its last phase of construction, has four training tasks with three levels of difficulty. Initially, each task is defined in terms of a virtual trajectory, used by our custom-based motion platform to produce realistic movements, based on a simple dynamic model from real measurements. Our visualization, sound effects, and metrics are implemented on the Torque game engine. Finally, a postprocessor system computes a metrics report.

Key words: Motion simulation platform, virtual training, virtual reality.

Resumen

El entrenamiento de tiro virtual se ha vuelto muy atractivo debido a las posibles reducciones de costos y a la evaluación precisa. Este artículo describe el desarrollo de un simulador para entrenamiento de soldados en combate fluvial. El simulador combina el movimiento de una plataforma mecánica con imágenes virtuales y sonido para producir un escenario de inmersión con propósitos de formación. Nuestro prototipo, que se encuentra en su última fase de construcción, tiene cuatro tareas con tres niveles de dificultad. Inicialmente, cada tarea es definida en términos de una trayectoria virtual usada por nuestra plataforma de movimiento personalizado para reproducir movimientos reales, basado en un modelo de dinámica simple a partir de mediciones reales. Nuestra visualización, efectos de sonido, y métricas son implementados en el motor de juegos Torque. Finalmente, un sistema de post-procesamiento calcula un informe de medidas.

Palabras claves: Plataforma de simulación de movimiento, entrenamiento virtual, realidad virtual.

Date Received: October 24th, 2010 - *Fecha de recepción: 24 de Octubre de 2010*
Date Accepted: January 16th, 2012 - *Fecha de aceptación: 16 de Enero de 2012*

[1] Facultad de Ingeniería, Universidad de los Andes. Bogotá, Colombia. e-mail: crodrigu@uniandes.edu.co
[2] Facultad de Ingeniería, Universidad de los Andes. Bogotá, Colombia. e-mail: jhernand@uniandes.edu.co
[3] Facultad de Ingeniería, Universidad de los Andes. Bogotá, Colombia. e-mail: pfiguero@uniandes.edu.co

Introduction

The recent armed conflict situation in Colombia has forced the National Naval Force (*Armada Nacional de la República de Colombia, ARC*) to develop special abilities to battle in rivers. Almost half of the Colombian territory is jungle and most of this vast area can be cruised by rivers. Jungle areas are used by guerrillas and illegal drug producers. Therefore, ARC is very motivated to develop tactics, equipment, and training for its troops in fluvial combat. As a result, ARC has become a worldwide leader in fluvial combat.

The basic ability of a soldier is to shoot different guns with precision. The use of virtual tools for shooting training has advantages in cost reduction (less ammunition used) and in evaluation metrics (many conditions can be controlled and monitored). There are many commercial products available for shooting training, although most of them are not adequate for shooting training from a moving vehicle.

Moreover, motion simulation platforms are nowadays widely used to replicate the dynamics of a given vehicle to train different users with lower costs and risks than real training. This is the case of combat boats in which users must train to get used to the unanticipated motions of the boat while ensuring good performance in their combat tasks.

This paper presents the development of a shooting simulator for fluvial combat. The simulator combines the motion of a mechanical platform with virtual imagery and sound to produce an immersive scenario for training. The general conception of the simulator is explained first. The following three sections describe the mechanical platform, the simulation software and the postprocessor.

General Concepts of the Simulator

The simulator is based on the use of a dynamic simulator in a virtual reality environment. The dynamic simulator is a custom-built robotized platform with three degrees of freedom that reproduces the motion of the boat (Fig. 1).

Fig 1. Robotized mechanical platform

The shooting training site is installed over this platform. It is composed of a section of the hull of the boat, the back part of the gun (including the trigger), and a 55-inch monitor where virtual images are displayed (Fig. 2). The system is complemented with virtual audio effects. This site is adaptable for two types of guns and shooter poses: an M2 rifle (0.50) for a standing shooter and an M60 rifle for a seated shooter. The gun mockup is instrumented; thus enabling the measurement of events like shooting (trigger), aiming direction (one encoder for elevation and one for orientation), unlocking (micro switch), gun reloading (micro switch) and relative position of the gun and the shooter (photocell).

The simulator is programmed for a set of training tasks: preparation, flank changing, target identification, target shooting and gun reloading. Each task can be run in three difficulty levels: tutorial, normal, and combat. Several parameters can be selected for each training session such as daytime, weather, location, number of enemies, and behavior.

The core of our simulator development is the feedback on the user's progress. A postprocessor identifies the user's actions from events in a training task. Evaluation criteria for task fulfillment are efficiency (use of resources), adherence to military doctrine, discipline under attack, along with rules of engagement and safety. The metrics associated to

Fig 2. Shooting training site

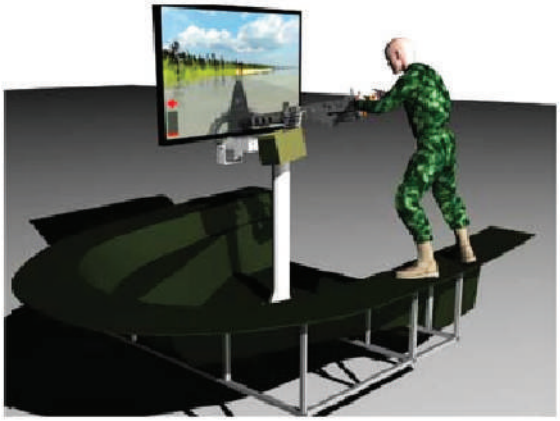

each criterion are computed by the postprocessor. Examples of these measured variables are: time to perform an action (reload the gun, aim at the target, etc.), number of bullets used, variation of aiming with boat in motion, and adherence to a predefined sequence of actions.

Mechanical Platform

To resemble a boat's typical maneuvers, a 3-DOF parallel robot with a passive mass compensator (3UPS+PU) was developed (Fig. 3).

Fig 3. 3 UPS + PU platform

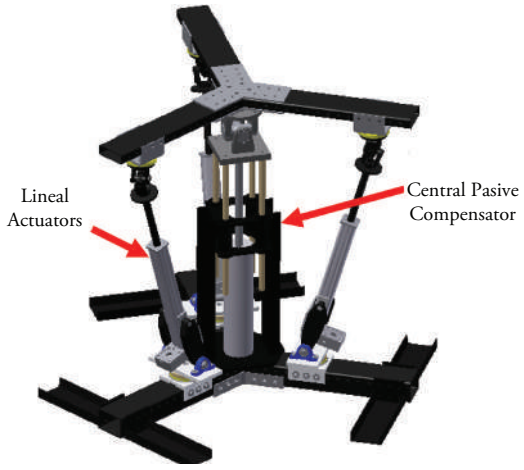

This robot permits three uncoupled degrees of freedom of the upper platform: roll, pitch, and vertical displacement (heave). It is driven by three electrically actuated prismatic limbs. The passive mass compensator consists of a pneumatic actuator that keeps a constant vertical force and restrains the other DOF's by an additional prismatic structure. The compensator is fixed to the lower platform and coupled to the upper platform by a universal joint.

After an optimization procedure, the configuration of the limbs and the position of the shooting training site were selected. This procedure minimizes the average force of each actuator during a training session. Fig. 4 shows the final mechanical configuration of the simulator.

Fig 4. Mechanical configuration of the simulator

Three Yaskawa, 800-watt servomotors with Exlar actuators were used for the robotized platform. The motion control is performed with a Yaskawa controller SMC-4000. This controller allows

communication via Ethernet with the simulation computer for synchronization purposes.

Simulation Software

The game engine Torque was used to develop the virtual scenario and to process events of a training session. This engine enables the definition of training terrain, the definition of the boat's path, the definition of behavior for objects in the scenario (enemies, civilians, other boats, etc.), the simulation of events (shooting, impact, tracer bullets, enemy bullets, etc.), the simulation of light and weather conditions, and the visualization from different points of view (user, boat, etc).

Our procedure for terrain definition is as follows (Fig. 5). It begins with a rough specification of the geography of the river and its surroundings. Then the sky and details of the river basins are added. Finally, the vegetation (grass, trees, etc.) complete the terrain.

Once the terrain is generated, the next step is to define possible training tasks on it. This process is similar to the specification of a storyboard. Fig. 6 shows a terrain and a schematic definition of a task sequence, in terms of a boat's path. This definition was made by ARC officers with broad experience in combat and training. It is translated into a sequence and saved in the simulation data base. This operation needs the definition of the boat´s

Fig 5. Procedure of terrain definition

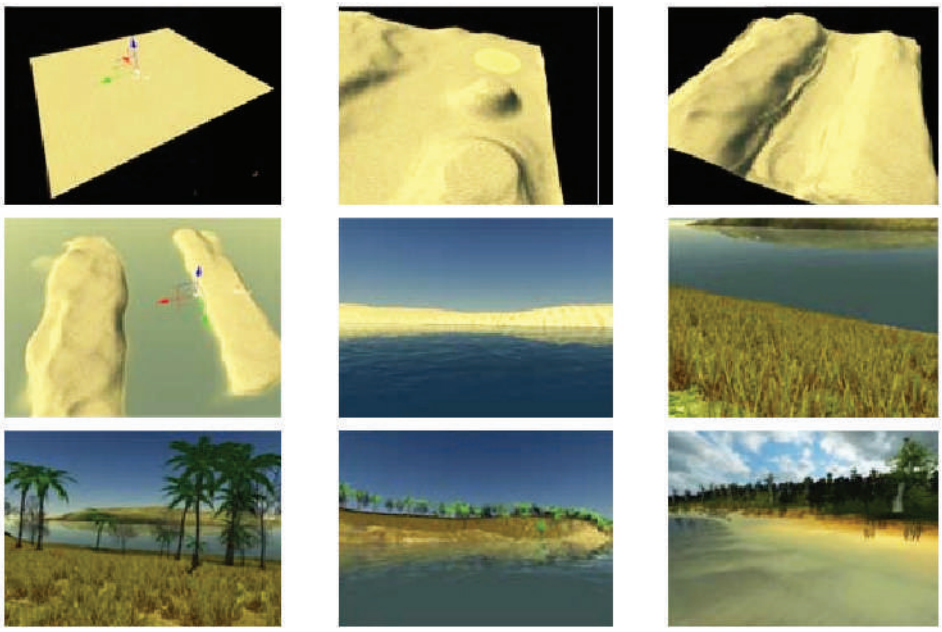

Fig 6. Task sequence and boat´s path definition

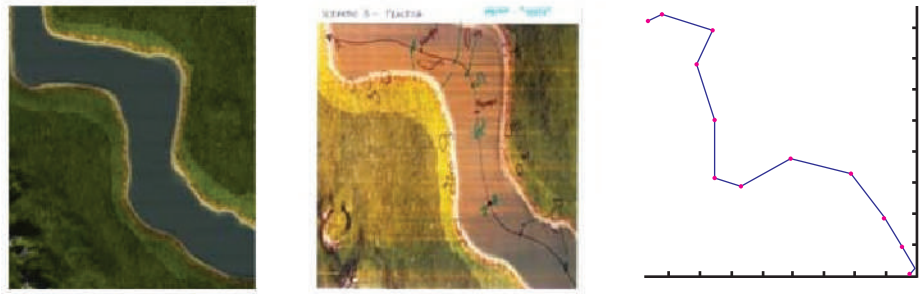

path and the association of tasks to each path's segment.

Two more elements are required to complete a simulation scenario for a training session: a context and a set of dynamic objects. The context is defined by the following set of variables: daytime, weather, type of gun, training level (tutorial, normal, combat), and mean velocity of the boat. Dynamic objects are entities with a body and a behavior. These include enemies, civilians, groups of people, other boats, etc. The behavior includes autonomous actions like moving and shooting, and the specification of triggers for the action (for example, hide if a bullet hits near the object, shooting back, etc.).

This software is complemented with communications with peripherals via Virtual Reality Peripheral Network (VRPN: 10.1145/505008.505019). By means of VRPN we defined a communication protocol with our mechanical platform and our gun. We also add sound in order to create a more immersive experience.

Finally, a trajectory generator based on a simplified dynamic model of the boat's motion completes the simulator software. It receives as input the path and the the boat's mean velocity and it produces a number of variations of the trajectories of the boat. The trajectories differ in few random parameters, introducing variety in case of repetition of the training sessions.

The dynamic model was uncoupled by planes. Fig. 7 shows some degrees of freedom of the boat's motion and the coordinate systems used for the model derivation.

Fig 7. Coordinate systems for model derivation

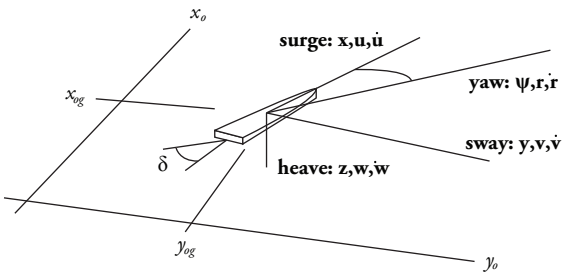

The horizontal plane model considers the surge, sway, and yaw and it is a linearized model of the Newton equations applied to the boat:

$$X = m\dot{u} \tag{1}$$

$$Y = m(\dot{v} + ur) \tag{2}$$

$$N = I_z \dot{r} \tag{3}$$

where X, Y and N are force in the x direction, force in the y direction, and torque around z direction, respectively, u is the forward velocity, v is the lateral velocity, and r is the angular velocity of the boat. Rewriting the equations with respect to the mid-ship point, we have:

$$X = m\dot{u} \tag{4}$$

$$Y = m(v + ur + x_g r) \tag{5}$$

$$N = I_z \dot{r} + mx_g \dot{u} \tag{6}$$

In general, $Y = Y(u, v, r, \dot{u}, \dot{v}, \dot{r})$ and the same is true for X and N. So using a first-order approximation

$$Y = \Delta u \frac{\partial Y}{\partial u} + \Delta v \frac{\partial Y}{\partial v} + \Delta r \frac{\partial Y}{\partial r} + \Delta \dot{u} \frac{\partial Y}{\partial \dot{u}} + \Delta \dot{v} \frac{\partial Y}{\partial \dot{v}} + \Delta \dot{r} \frac{\partial Y}{\partial \dot{r}} \tag{7}$$

Due to the symmetry of the boat, the terms $\partial Y/\partial u$ and $\partial Y/\partial \dot{u}$ are null. Using the short notation $\partial Y/\partial v = Y_v$ the equation becomes

$$Y = vY_v + \dot{v}Y_{\dot{v}} + rY_r + \dot{r}Y_{\dot{r}} \tag{8}$$

Similarly, for the torque N

$$N = vN_v + \dot{v}N_{\dot{v}} + rN_r + \dot{r}N_{\dot{r}} \tag{9}$$

The partial derivatives (Y_v, Y_r, etc.,) in the preceding equations are called *hydrodynamic derivatives, stability coefficients* or *hydrodynamic coefficients*.

The following is the set of linearized dynamic equations of motion:

$$
\begin{aligned}
&X_u\ (u-u_1)+(m-X_{\dot{x}g})\,\dot{u}=P\ \mathrm{Cos}\ \delta\\
&-Y_v v+(m-Y_{\dot{v}})\,\dot{v}-(Y_r-mu_1)\,r-(Y_{\dot{r}}-mx_g)\,\dot{r}=P\ \mathrm{Sin}\ \delta\\
&-N_v v+(N_{\dot{v}}-mx_g)\,\dot{v}-(N_r-mx_g u_1)\,r+(I_z-N_{\dot{r}})\,\dot{r}=L_p P\ \mathrm{Sin}\ \delta
\end{aligned}
\tag{10}
$$

where P is the propulsion force, δ is the angle between this force and the x axis of the boat and L_p is the length from the origin of the coordinate system fixed in the boat and the point of application of the propulsion force. The hydrodynamic coefficients were taken from literature and Computational Fluid Dynamics (CFD) simulations and verified experimentally.

The description of the vertical motion is approximated by a series of harmonics that resemble the spectrum of frequencies of the boat's motion. We used measurements on a real boat, during a set of typical maneuvers. Both models were implemented in MATLAB/SIMULINK for the computation of trajectories.

Postprocessor

Log data of training sessions is downloaded to a data base for post processing. Three main routines were implemented for the evaluation of user performance: a collision detector, a metrics calculator, and a report generator.

The collision detector allows the identification of an impact point of every shot during the training session. If the session includes tasks of target identification (without shooting), this routine also computes the line of action of potential shots. Fig. 8 shows the concept of this routine. Large circles represent constructions, while the small circles represent people. The medium circle represents another boat.

In order to compute the aiming direction and the objects reachable by shots, the historical log of the session is revisited. Each object in the scene is surrounded by a sphere and a ray is projected departing from the gun for each instant of time in the training session. This information is then used to compute the metrics related to the task.

Fig 8. Collision detector computing in a given time instant

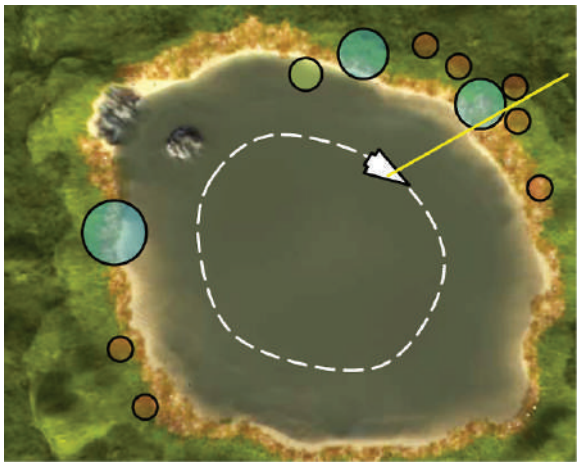

The next post-processing step is taken to segment the whole session into defined tasks. Each task of the training session should have occurred in a given portion of the path traveled by the boat. The log file contains the information of every event that occurred while traveling that portion of the path, so events are segmented and associated to the task under execution during that time.

By using the definition of metrics for each task, the corresponding variables are then quantified: number of actions, time until a given event, sequence of actions, etc. The measurement of these variables constitutes the basis for the evaluation of the user's performance.

Finally, a report for the session is automatically produced. The routine puts together user´s identification information, historical data on his/her training, and values of the metrics for the tasks in the training session.

An example of the report is shown in Fig. 9. The first section is the user and session identification data. Then, the percentage in time of each task during the session is presented, followed by the appropriate

sequence of execution. Computed values of the variables for metrics are then included, and the percentage of success in each task is depicted.

Fig 9. Example of the report generated for a training session

REPORTE sesión entrenamiento 001

15/12/2010
Información de la sesión

INFORMACIÓN DEL INFANTE

Castro Martínez, David
Sargento Mayor de Comando
Brigada Fluvial No.1

Documento: 192782
Fecha de inicio: 01/01/2010
Horas de Entrenamiento: 2 Horas
Nivel de Entrenamiento: Tutorial

INFORMACIÓN DEL ESCENARIO

Zona: Putumayo
Condiciones de Luz
Hora: 19:00
Neblina: 10%
Clima: Soleado
Recorrido: Velocidad: Media
Intensidad de Entrenamiento: 4
Dificultad del entrenamiento: 4

INFORMACIÓN DE LA SESIÓN

Fecha: 15/12/2010
Duración: 00:04:25
Objetivos: Mejorar el empleo de la doctrina y la seguridad en la ejecucion de la tarea e identificacion de blancos.
Modo de Entrenamiento: Tutorial
Número de Repeticiones: 0

Entrenador: Ruiz Caballero, Felipe
Documento entrenador: 19852963

COMPOSICION DE LA SESIÓN

Composición de la sesión según tareas y repeticiones de cada tarea *ACIBRA

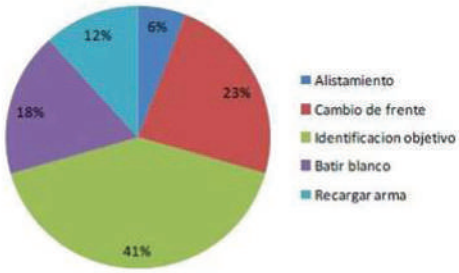

OPERACIÓN - SECUENCIA DE TAREAS

Las tareas programadas para cada sesión de entrenamiento asociadas a los segmentos de la trayectoria del bote.

TIPOS DE TAREAS (*ACIBRA)

A - Alistamiento (*1)
C - Cambio de frente (*3)
I - Identificación de objetivo (*7)
B - Batir blanco (*3)
RA - Recargar arma (*2)

Orden de las tareas:

1. Alistamiento
2. Cambio de frente
3. Identificación de objetivo
4. Identificación de objetivo
5. Cambio de frente
6. Identificación de objetivo
7. Batir blanco
8. Recargar arma
9. Cambio de frente
10. Identificación de objetivo
11. Batir blanco
12. Identificación de objetivo
13. Batir blanco
14. Identificación de objetivo
15. Identificación de objetivo
16. Recargar arma

REPORTE 001
sesión entrenamiento

15/12/2010
Ejecución de la sesión

DETALLE DE LA EJECUCIÓN DE LAS TAREAS

1. Alistamiento (00:00:01)					
EFI_101	EFI_102	DOC_101	DIS_101	SEG_101	SEG_102
20 segundos	OK	OK	0 disparos	OK	20%

2. Cambio de frente (00:00:50)							
EFI_201	EFI_202	EFI_203	DOC_201	DOC_202	DIS_201	SEG_201	SEG_202
0.3 segundos	2 segundos	OK	OK	OK	0 disparos	OK	0%

3. Identificación de objetivo (00:00:55)					
EFI_301	DOC_301	DOC_302	DIS_301	REG_301	SEG_301
5 segundos	3 segundos	true	0 disparos	0.5 segundos	3 segundos

4. Identificación de objetivo (00:01:00)					
EFI_303	DOC_301	DOC_302	DIS_301	REG_301	SEG_301
20 segundos	0.1 segundos	false	0 disparos	0 segundos	0.1 segundos

REPORTE 001
sesión entrenamiento

15/12/2010
Ejecución de la sesión

EVALUACIÓN

Porcentaje de éxito en la ejecución de las tareas

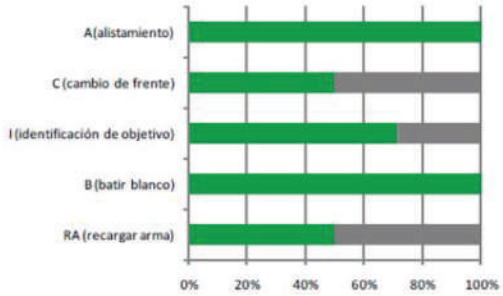

Secuencia:
s = {A,C,I,I,C,I,B,RA,C,I,B,I,B,I,I,RA}

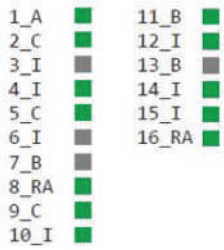

Conclusions

The conception and development of a shooting simulator for training in fluvial combat have been described. Starting from the definition of the set of combat tasks, a mechanical platform and simulation software have been combined to produce an immersive scenario for training.

The prototype permits training individual users by recreating the motion, view, and sound of the real boat. As the training scenario is fully controlled, a set of metrics to measure user progress is computed.

Acknowledgements

Once the prototype is finished, training tests will be conducted to test the level of realism of the experience and its effectiveness for developing the user's combat abilities.

The authors acknowledge the support given by the Research Division of the National Naval Force of Colombia (ARC) and the work by the project research team: Sergio Ordoñez, Juan Camilo Blanco, Luis Felipe Ramirez, Diana Fernandez, Raul Oses, Camilo Cortes, David Castro, Mauricio Parra, and Nicanor Quijano.

References

BERTRAM, V. "Practical Ship Hydrodynamics". s.l. : Butterworth, Heineman.

BLANCO J.C., RODRIGUEZ C.F. "Configuration Optimization of a Boat Simulation Platform for a Mobile User", Proceedings of the ASME 2010 International Mechanical Engineering Congress & Exposition, IMECE2010 November 2010, Vancouver, British Columbia, Canada.

CLARK J., KENDIR T., SHECHTER M., ROSA S., "Firearm Laser Training System And Method Employing An Actuable Target Assembly", Patent 6575753, USA, June 2003.

FALTINSEN, O. "Hydrodynamics of High-Speed Marine Vehicles". s.l. : Cambridge University Press, 2005.

GAO, F., LI, W., ZHAO, X., ZHENLIN, J., and HUI, Z., 2002, "New Kinematic Structures for 2-, 3-, 4-, and 5- DOF Parallel Manipulator Designs", Mechanism and machine theory, 37, pp. 1395-1411.

LVOVSKIY M., "Training Simulator For Sharp Shooting", Patent 6942486, USA, September 2005.

MASTINU, G., GOBBI, M., AND MIANO, C., 2006, Optimal Design of Complex Mechanical Systems. Springer-Verlag, Berlin, pp. 57-67. [8] Merlet, J. -P. 2006, Parallel Robots, Springer, Netherlands, pp. 19-93.

MONONEN K., VIITASALO J.T., ERA P., KONTTINEN N. "Optoelectronic Measures in the Analysis of Running Target Shooting", Scandinavian Journal of Medicine & Science in Sports, Vol. 13, No. 3, 2003.

MORRISON G.B., "Police and Correctional Department Firearm Training Frameworks in Washington State", Police Quarterly, Vol. 6, No. 2, 2003.

PEREZ, T. "Ship motion control". London: Springer-Verlag, 2005.

POOR, CR. "Simulink Modeling of a Marine Autopilot for TSSE Shiip Designs". Master´s Thesis, Naval Postgraduate School. Monterey, California: s.n., a996.

QUEVEDO L., SOLÉI J., "Visual Training Program Applied to Precision Shooting", Ophthalmic and Physiological Optics, Vol. 15, No. 5, September 1995.

SAUS E., JOHNSEN B.H., EID., RIISEM P.K., ANDERSEN R., THAYER.F., "The Effect of Brief Situational Awareness Training in a Police Shooting Simulator: An Experimental Study", Military Psychology, Vol. 18, No. 3, 2006.

STAN, S.-D., MĂTIEŞ, V., AND BĂLAN, R., 2008, "Optimal Design of Parallel Kinematics Machines with 2 Degrees of Freedom", Parallel manipulators towards new applications, Wu, H., ed., I-Tech Education and Publishing, Vienna, pp. 295-320. n

SUZUKI K., "Shooting Game Machine", Patent 5366229, USA, November 1994. e

The Math Works, Inc. Genetic algorithm and direct search toolbox for use with MATLAB: user's g de (Version 1.0.1. ed.). The gui Math Works, c2004.

TSAI, L.-W. , 1999. Robot Analysis: The mechanics of Serial and Parallel Manipulators, John Wiley & Sons, Inc, New York, Chap. 1.

WANG, Z.G; HU, Y.; XIE, F., "Optical Fiber Simulator for Shooting and Aiming Practices", Proc. SPIE VOL. 2895, The International Society for Optical Engineering, 1996.

ZAENGLEIN, JR. W.G., "Shooting Simulating Process and Training Device Using a Virtual Reality Display Screen", Patent 5641288, USA, June 1997.

Side-boat tow to Test the Influence of Flaps in a 2-meter Planing Craft Model

Remolque lateral de embarcación para comprobar la influencia de dispositivos sustentadores (flaps) sobre un modelo de embarcación de planeo de 2 metros

José R. Marín [1]
Daniela A. Benites [2]

Abstract

A small craft is considered in the planing regime when its Froude number is higher than 1.2, and under that condition its weight is mainly supported by hydrodynamic pressure acting on the bottom of the hull. It is also known that installing stern flaps at a certain angle from the bottom line will alter the trim angle and, as a consequence, the resistance exerted by the water. In this work, using the classical work from Savitsky, the resistance on a planing craft is estimated, including the effect of flaps, and then the influence of those appendages on the hydrodynamic behavior of a craft of local design was experimentally verified. The wooden model was 2.0 meters long and was side towed from an outboard powered boat, with a 3.2-m arm, in a small artificial lake. The tests were run between 5 and 12 knots, with uneven intervals due to the outboard control; the model was towed without and with flaps at 5 and 10°. Finally, experimental and empirical results for towing force and trim angle were plotted. In some of the experimental curves the presence of humps may be identified, but less pronounced than with the theoretical results. Experimental resistance values are lower than those obtained from Savistky's formulation for no flaps; in the case of flaps at 5°, the agreement in trim angle was very good. Finally, the benefit of flaps on the performance of the planing model was corroborated, but it should be emphasized that this improvement is only valid for a certain velocity range.

Key words: Planing boat, model test.

Resumen

Se considera que un bote opera en el régimen de planeo cuando su número de Froude es mayor a 1.2, y en esa condición su peso es soportado principalmente por la presión hidrodinámica que actúa en el fondo del casco. También se sabe que el instalar flaps en la popa, a un cierto ángulo de la línea del fondo, alterará el ángulo de trimado y, como una consecuencia, la resistencia ejercida por el agua. En este trabajo, usando el método clásico de Savitsky, la resistencia sobre un bote planeador es estimada, incluyendo los efectos de flaps, y se verificó experimentalmente la influencia de esos apéndices sobre el comportamiento hidrodinámico de un bote de diseño local. El modelo de madera tenía 2.0 metros de eslora, y fue halado por el costado de un bote impulsado por un motor fueraborda, con un brazo de 3.2 m, en un pequeño lago artificial. Las pruebas fueron desarrolladas entre 5 y 12 nudos con intervalos no uniformes debido al control del fueraborda; el modelo fue arrastrado sin y con flaps a 5 y 10°. Finalmente, los resultados empíricos y experimentales para la fuerza de halado y ángulo de asiento fueron graficados. En algunas curvas experimentales se puede identificar la presencia de máximos, pero menos pronunciados que con los valores teóricos. Los valores experimentales de resistencia son inferiores a los obtenidos con la formulación de Savitsky, para el caso sin flaps; en el caso con flaps a 5°, la concordancia en ángulo de trimado fue muy buena. Finalmente, el beneficio de flaps sobre el desempeño de un bote planeador fue comprobado, pero debe enfatizarse que esta mejora es sólo válida en un cierto rango de velocidad.

Palabras claves: Bote planeador, prueba de modelos.

Date Received: October 24th, 2010 - *Fecha de recepción: 24 de Octubre de 2010*
Date Accepted: January 17th, 2012 - *Fecha de aceptación: 17 de Enero de 2012*

[1] Faculty of Maritime Engineering, ESPOL. Guayaquil, Ecuador. e-mail: jrmarin@espol.edu.ec
[2] Naval Engineer, Guayaquil, Ecuador, e-mail: dbenites@espol.edu.ec

Introduction

According to Brown (Brown and Savitsky, 1976), a boat enters the planing regime when its relative velocity, or velocity coefficient, is > 1.5; this parameter is equivalent to the Froude number, taking the beam at the chine as the representative length. Under this condition, the hydrodynamic pressure acting on the bottom lifts the hull, producing a significant change in draft, trim angle, and resistance (*Faltinsen*, 2005). It is also well known that installing a flap on the transom of the hull may help to reduce resistance; those devices having an angle with respect to the bottom develop a local hydrodynamic force, producing a change in trim and altering the longitudinal component of the normal force acting on the bottom of the boat.

Precisely installing flaps in the transom of planing boats has been an option that was locally considered, but due to lack of experience on their sizing, could not be implemented. That is the reason for this work.

Not many tests on planing boats with flaps installed on the stern of their hulls have been conducted, especially with the characteristics of local designs. Also, those tests are quite expensive and the size of the projects cannot justify their costs. Within this context, one option is to develop ship model tests towing them from a boat by using an adequate side arm. In this work, an experimental set to test a model of a planing boat was developed, including flaps at the transom (*Benites*, 2012). The model does not correspond exactly to the original boat, but to one with an increased deadrise angle.

Description of the prototype boat

The prototype boat is 11 meters long and it is intended for patrol duties in the port of Guayaquil, Ecuador; Table 1 presents main dimensions of the boat. It has prismatic shape from Midships, with a deadrise angle of 13°, and with a 32-knot design speed, powered by two 493-hp diesel engines impelling corresponding waterjets. Hull and superstructure were built with 5086 aluminum alloy.

Table 1. Main dimensions of prototype

Overall length	11.00	m
Beam	3.80	m
Beam at chine	2.40	m
Depth	1.70	m
Deadriseangle	13.0	o

According to Brown (*Brown and Savitsky*, 1976), a boat is in the planing regime when the velocity coefficient reaches a value of about 1.5. This nondimensional parameter is defined as:

$$C_V = \frac{v}{\sqrt{gb}} \tag{1}$$

where v is the boat velocity, g is the gravitational acceleration, and b is the beam at chine. In the present case, the boat's planning would start at a velocity of 18 knots. Given that the design speed is 32 knots, this craft is classified as a planing boat.

For the experimental development, an aluminum boat was available powered with a 40-hp outboard engine, reaching around 14 knots. Thus, equaling Froude numbers of the prototype, with 11 m and 32 knots, and the model, with the velocity of the boat to tow the model, a 2-meter length was obtained.

The final ship lines of the model are presented in Fig. 1. The main difference with the prototype considered is the deadrise angle, increased to 16.7°, and a change in the profile on the forward zone.

Once the model enters the planing regime, this part of the hull emerges completely out of the water; thereby, this geometric difference does not need to be further mentioned. Savitsky's calculations for comparison were developed with the model's deadrise angle.

At the transom of the model, flaps were installed on each side, completely covering the bottom. The chord of the appendages (dimension in the longitudinal direction) was 13 cm. To change the

Fig 1. Ship lines plan of the model

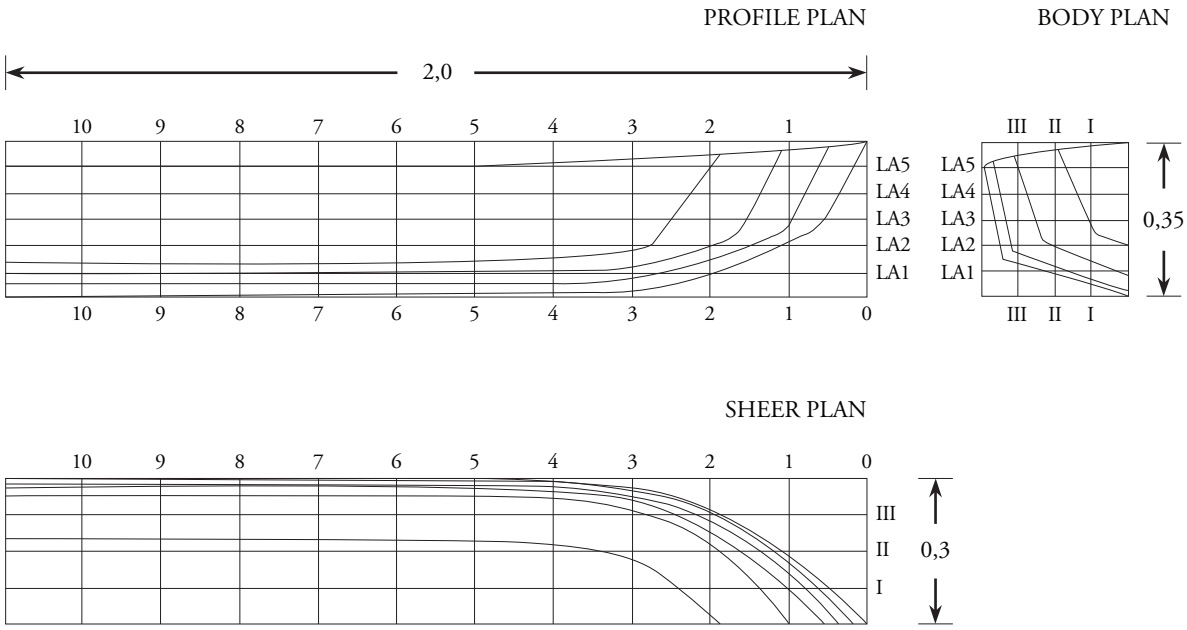

angle of the flaps, hinges and tensors were installed on each side, see Fig. 2.

Fig 2. Flaps at the transom of the model

Estimation of resistance by using Savitsky's method

In spite of its age, Savitsky's method, (*Savitsky*, 1964), is probably the first option to estimate the resistance of a planing boat at a preliminary stage. In the present calculation, the influence of flaps was included, by following another Savitsky work, (*Brown and Savitsky*, 1976). Table 2 presents the two load conditions considered for the calculations, representing real ship situations.

Table 2. Load conditions for tests

	Cond. 1	Cond. 2	
Weight	70.1	91.9	kg
LCG, from trans.	72	75	cm

To develop Savitsky's calculations, the following information was used for both conditions, see Table 3. Water density was measured and the kinematic viscosity was taken from table 10 in Principles of Naval Architecture (*Van Manen*, 1988), for fresh water at 25°C:

Table 3. Parameters for Savitsky's calculations

Beam at chine	58.4	cm
VCG (scaledfromprot.)	16	cm
ε, thrust line angle	4.31	°
f, distance of thrust to G	0.28	m
ρ (measured)	1000	kg/m^3
υ, kinematicvelocity	0.939E-6	m^2/s

For all calculations, as recommended by Savitsky, the Frictional component of the resistance was estimated with the formula for C_f from the American Towing Tank Conference (*Van Manen*, 1988). This is adequate for this close to 2D flow, produced when water flows on the flat bottom of the planing boat. In Table 4, trim angle and resistance force are reported for the model with no flaps in the two analyzed load conditions:

Table 4. Model resistance results with no flaps

v [kn]	C_v	Condition 1		Condition 2	
		Trim [deg]	Res. [kg]	Trim [deg]	Res. [kg]
5.00	1.07	7.89	12.02	8.98	17.04
6.00	1.29	8.97	14.91	10.33	22.08
7.00	1.50	9.29	15.44	10.89	23.38
8.00	1.72	8.91	14.68	10.59	22.29
9.00	1.93	8.24	13.64	9.85	20.46
10.00	2.15	7.49	12.73	8.99	18.73
11.00	2.36	6.78	12.07	8.16	17.35
12.00	2.58	6.14	11.65	7.39	16.34
13.00	2.79	5.58	11.45	6.71	15.65

To calculate resistance with flaps, two angles were considered, 5 and 10°, see results in Tables 5 and 6:

Table 5. Model resistance results with flaps at 5°

v [kn]	C_v	Condition 1		Condition 2	
		Trim [deg]	Res. [kg]	Trim [deg]	Res. [kg]
5.00	1.07	6.17	9.77	7.39	14.37
6.00	1.29	6.34	10.95	7.81	16.90
7.00	1.50	6.06	10.61	7.70	16.69
8.00	1.72	5.39	9.73	7.10	15.22
9.00	1.93	4.56	8.97	6.23	13.58
10.00	2.15	3.71	8.58	5.30	12.30
11.00	2.36	2.91	8.67	4.40	11.52
12.00	2.58	2.18	9.33	3.57	11.28
13.00	2.79	1.52	10.79	2.83	11.60

Table 6. Model resistance results with flaps at 10°

v [kn]	C_v	Condition 1		Condition 2	
		Trim [deg]	Res. [kg]	Trim [deg]	Res. [kg]
5.00	1.07	4.75	8.39	6.04	12.52
6.00	1.29	4.26	8.74	5.75	13.54
7.00	1.50	3.45	8.32	5.08	12.68
8.00	1.72	2.46	8.16	4.13	11.48
9.00	1.93	1.48	8.94	3.06	10.80
10.00	2.15	0.66	11.58	2.02	11.16
11.00	2.36	0.15	19.08	1.10	13.15
12.00	2.58	0.00	62.09	0.41	18.47
13.00	2.79	-	-	0.07	33.36

Notice that with 10° flap angle, in load condition 1 at 12.0 knots, the trim angle is null, and for 13.0, the iterative process could not reach a solution.

Side tow test of the model

To experimentally determine the behavior of the prototype, a 2.0-m wooden model was built and it was towed by using an aluminum arm, 3.20 m long, installed on the side of the boat. The arm could be lifted with a cable through a pulley at the top of a vertical rod, so the tension on the model could be exerted in the direction of the propulsion force, as closely as possible, as recommended by the International Towing Tank Conference for High Speed Vessels (ITTC, 2002).

To register the results, a load cell and a 2-axis inclinometer were installed on the model, so milivoltages corresponding to pulling force and trim and heel angles could be stored in a portable

computer via a data acquisition card. The scan rate employed was 120 scans/sec. Also, a stream velocity meter was used for the boat/model speed, and a hand anemometer for wind velocity. The appendix shows a scheme of the equipment used for the tests.

The tests were carried out on July 2012 in a small artificial lake at the ESPOL Prosperina campus in Guayaquil. The water was considered fresh, at an average temperature of 25 °C, with a measured density of 1.00 gr/cm3. Because of the length of the lake, the model could not be towed more than 40 seconds on each test (at a 10-knot speed).

With Average and Standard deviation from the recordings, the Variation Coefficient was calculated (ratio of Standard Deviation/Mean*100), showing values below 10% (see graph in the Appendix). Also, wind and model velocity show a similar behavior, allowing us to discard any negative influence from that parameter (see Figure in the Appendix).

Experimental results: Condition 1 (70.1 kg)

These tests included the model without flaps and with them at 5 and 10°. The initial conditions are presented in Table 7. Also, Fig. 3 presents photographs taken during some tests, including overall length and scaled values for mean wetted length.

Table 7. Initial conditions for test in load condition 1

	No flaps	Flaps at 5°	Flaps at 10°
Trim, [°, +by stern]:	3.69	0.56	0.56
Heel [°]:	-0.52	-0.42	-0.52

Experimental results: Condition 2 (91.9 kg)

Table 8 presents the initial conditions and Fig. 4 shows photographs taken during the tests for the load condition 2.

Fig. 3. Tests with no flaps in load condition 1

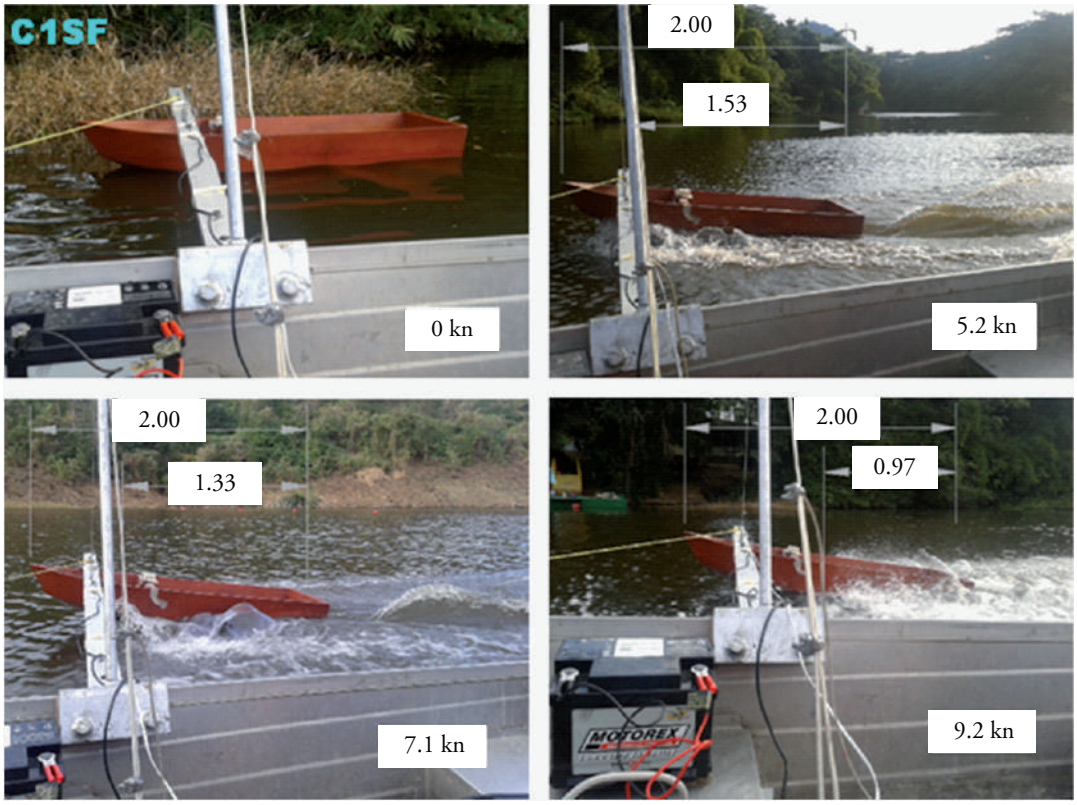

Table 8. Initial conditions for test in load condition 2

	No flaps	Flaps at 5°	Flaps at 10°
Trim, [°, +by stern]:	4.74	0.13	0.03
Heel [°]:	0.10	-0.69	-0.69

Analysis of Results

In Figs. 5 and 6, towing force and heel angle with respect to the initial value are presented for the two load conditions for different speeds. The results by using Savitsky's method are also included. In the test with high flap angle, the bow wave from the towing boat collided with the wave from the model, producing some interaction and spray, wetting the interior of the model. Those results were considered unacceptable, and are not presented in the figures.

With no flaps, the coincidence in tendency for the trim angle can be noted, with a hump present at a slightly higher velocity; the experimental results present higher heel values. For flaps at 5°, the coincidence is very good in heel angles. For load condition 2, the results are similar to those in the first condition.

Experimental resistance results with no flaps show lower values than the theoretical ones, also with the presence of a hump. It is noticeable that, theoretically and experimentally, flaps tend to reduce the mentioned force, up to a certain velocity. After that, resistance increases, that is, flaps are useful only in a certain velocity range.

As part of the Savitsky's results, the ratio of mean wetted length to beam at chine, called λ, is calculated. Also, by using photographs from the tests with no flaps, see Figs. 3 and 4, the

Fig. 4. Tests with no flaps in load condition 2

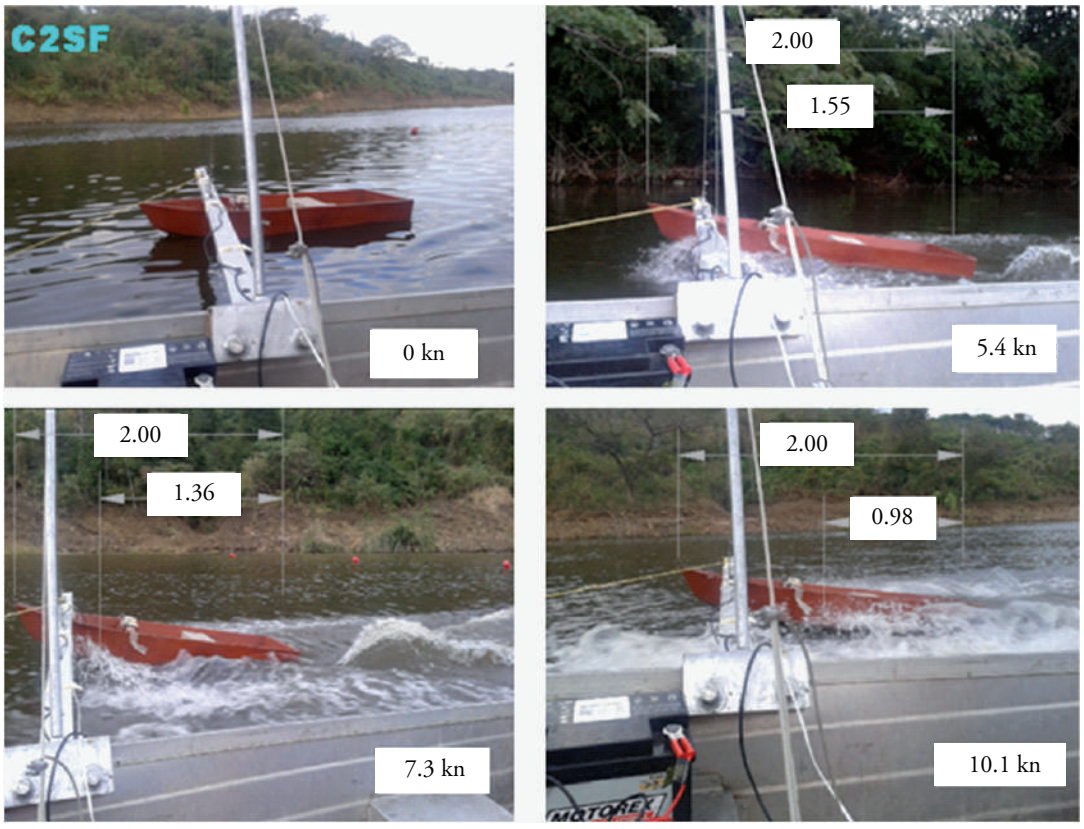

Fig. 5. Empirical and experimental results for load condition 1 (C1 SF SAV: Condition 1, No flaps, Savitsky's results; C1 SF E: Condition 1, No flaps, Experimental; C1 F5 SAV: Condition 1, Flaps at 5°, Savitsky's results; C1 F5 E: Condition 1, Flaps at 5o, Experimental)

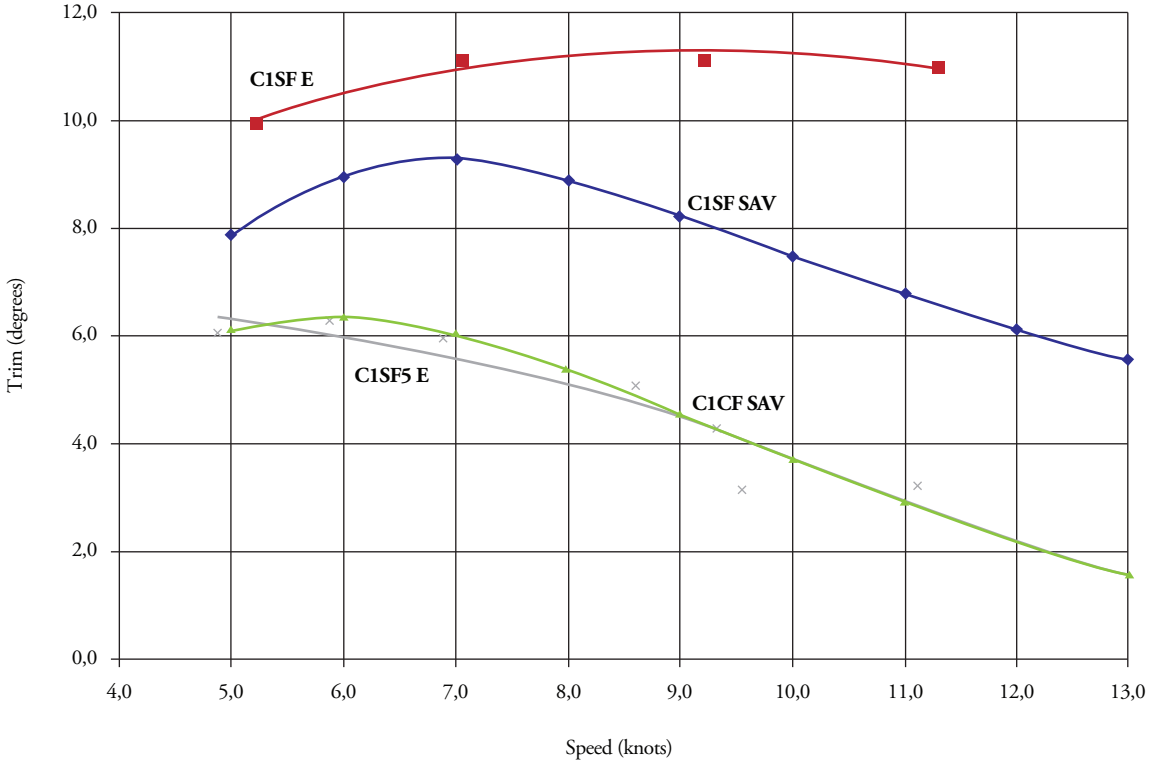

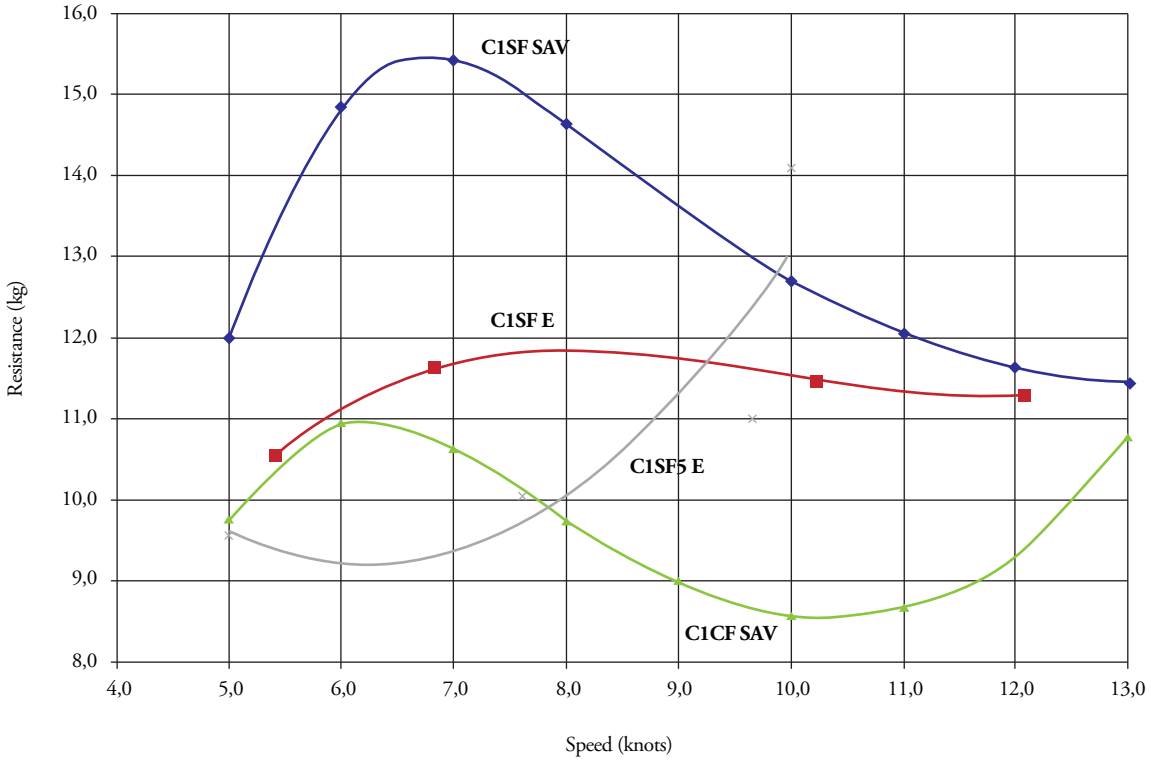

Fig. 6. Empirical and experimental results for load condition 1 (C2 SF SAV: Condition 1, No flaps, Savitsky's results; C2 SF E: Condition 1, No flaps, Experimental; C2 F5 SAV: Condition 1, Flaps at 5°, Savitsky's results; C2 F5 E: Condition 1, Flaps at 5o, Experimental)

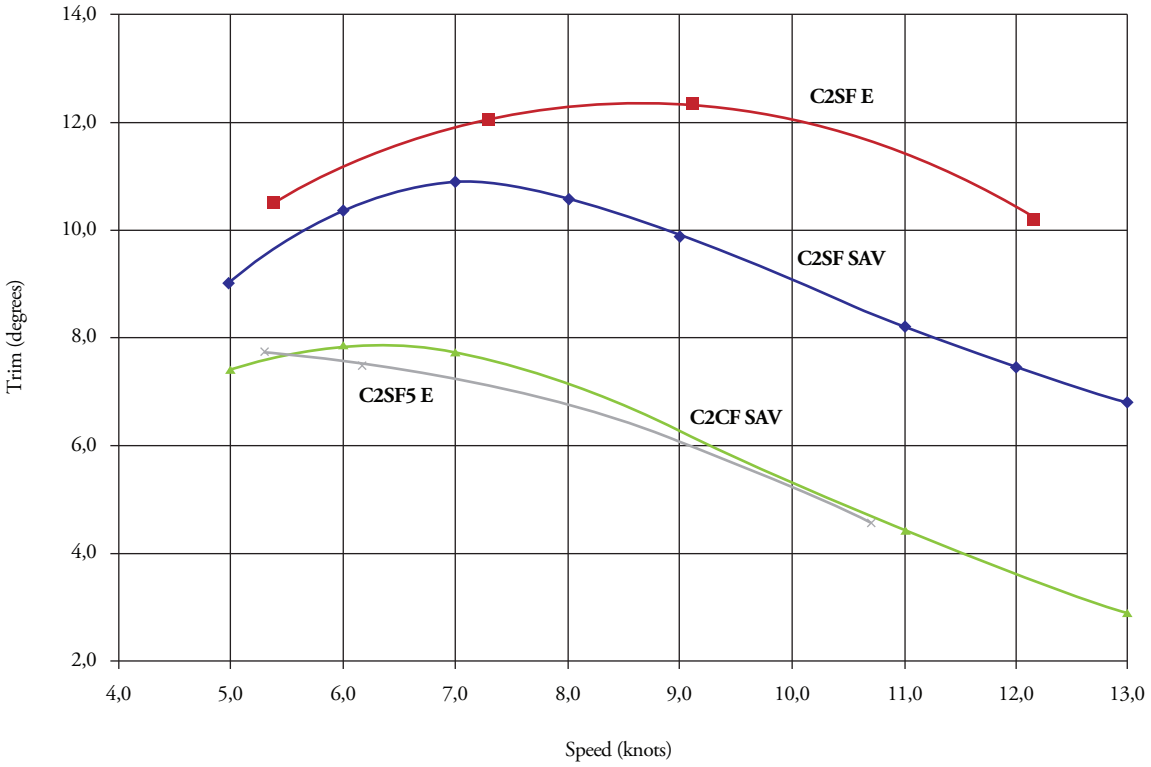

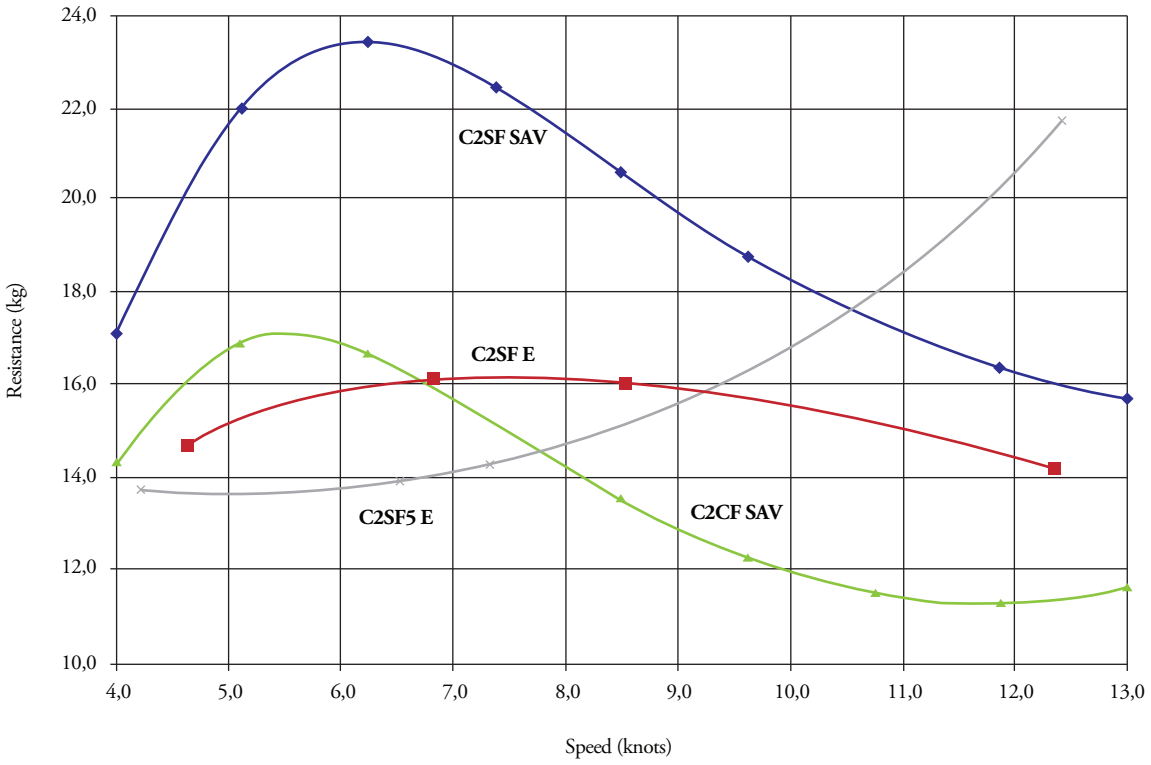

mean wetted length of the model was estimated. Following, in Fig. 7 theoretical and experimental values of the λ ratio, are presented. Good agreement may be noted for the case of no flaps. In the tests with flaps, it is very difficult to estimate the wetted length from photographs (see appendix).

Fig. 7. Mean wetted length from tests with no flaps

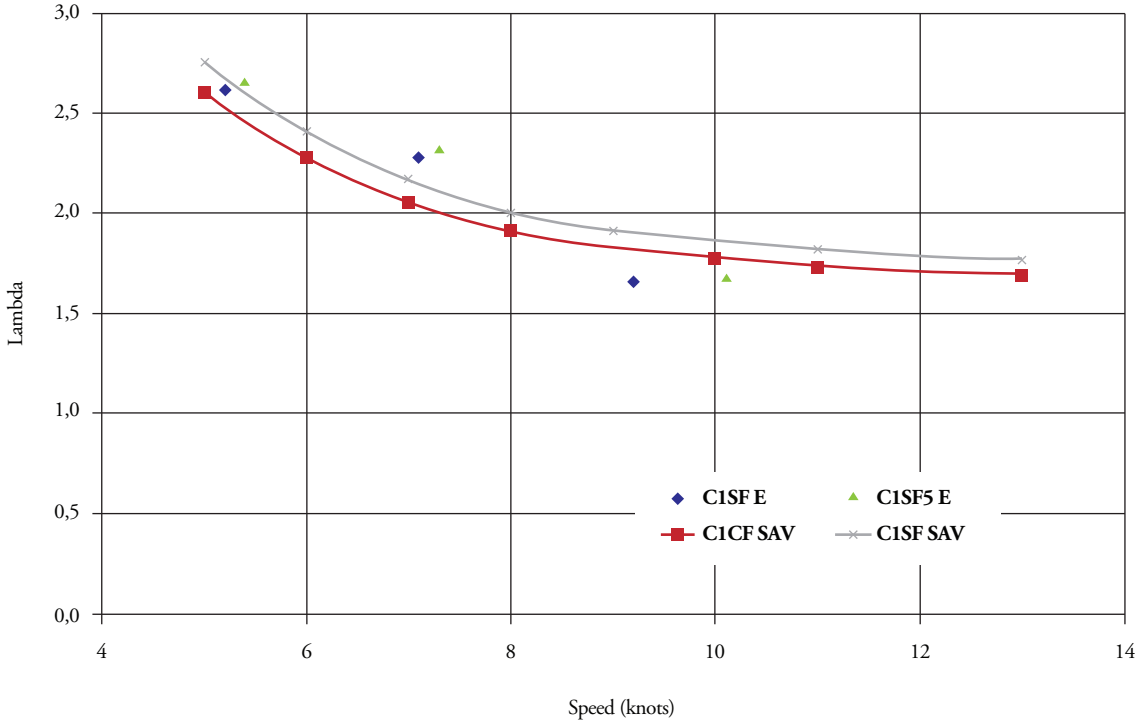

Conclusions and Recommendations

The experimental arrangement utilized for these tests is simple and inexpensive, but it presents several limitations, which we seek to minimize. These included controlling the presence of debris and obstacles in the trajectory of the towing boat and keeping boat velocity steady. The Variation coefficient shows values below 10%, denoting that in spite of the limitations, recorded values may be considered useful.

Flaps are appendages that reduce the trim angle of a planing craft and also reduce the resistance exerted on the hull. But this benefit is limited to a certain velocity range. A boat designer must be aware that outside this range, flaps will increase resistance. Even though Savitsky's process to estimate improved boat performance is simple, experimental confirmation of results is always recommended.

References

BENITES, D. A., Pruebas Experimentales para Determinar la Influencia de Flaps en la Resistencia al Avance de una Lancha Planeadora de 11 metros, Naval Engineer Thesis, Faculty of Maritime Engineering, ESPOL, Guayaquil, Ecuador, 2012

BROWN, W. AND SAVITSKY, D., Procedures for Hydrodynamic Evaluation of Planing Hulls in Smooth and Rough Water, Marine Technology, SNAME, Vol 13, No.4, 1976.

FALTINSEN, O., Hydrodynamics of High-Speed Marine Vehicles, Cambridge University, 2005.

ITTC, Recommended Procedures and Guidelines – Testing and Extrapolation Methods (Resistance Test for High Speed Marine Vehicles), 7.5-02-05-01, 2002.

SAVITSKY, D., Hydrodynamic Design of Planing Hulls, Marine Technology, SNAME, Vol. I, 1964.

VAN MANEN, Resistance, Ch. 5 in Principles of Naval Architecture Vol II, E. Lewis, Ed., SNAME, 1988.

Appendix

Arrangement of equipment on boat

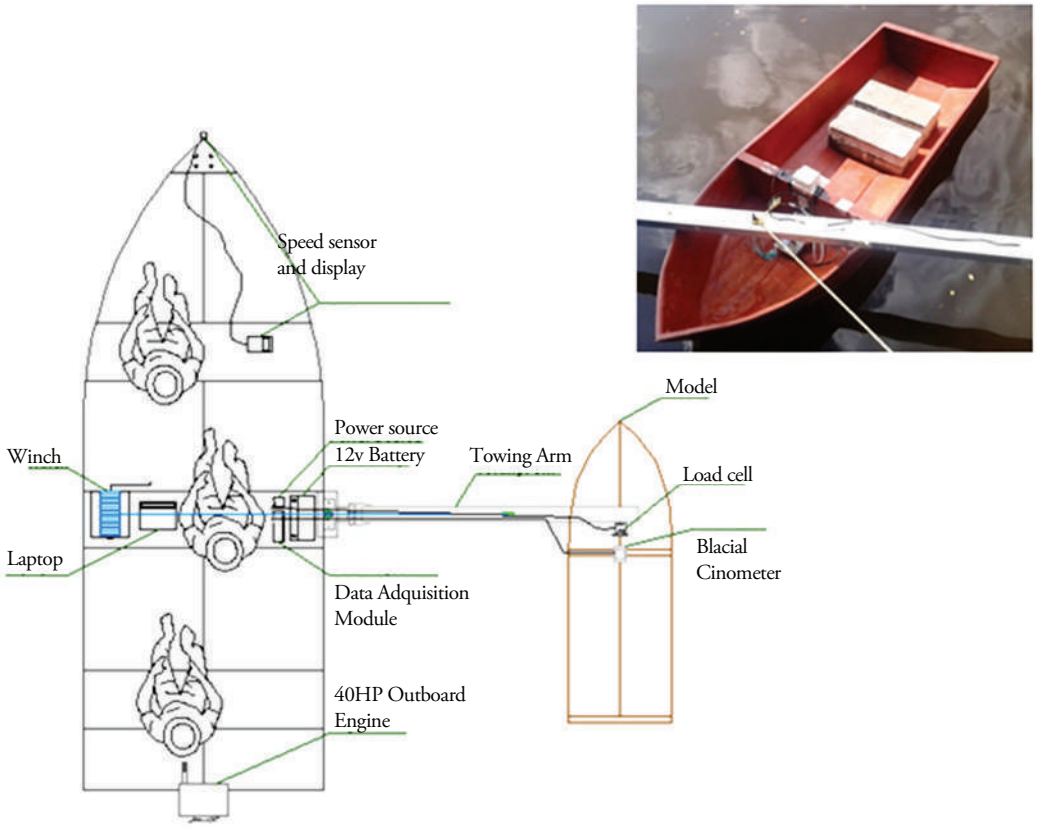

Variability of Test results

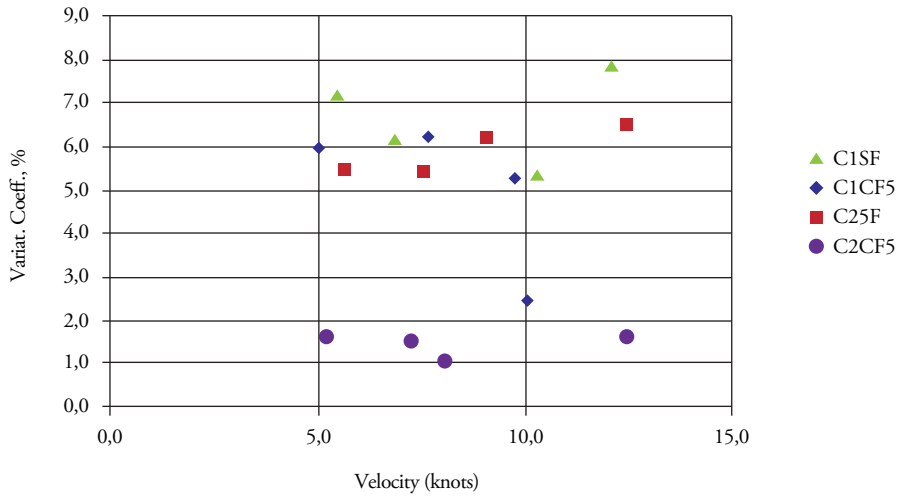

Wind velocity influence during tests

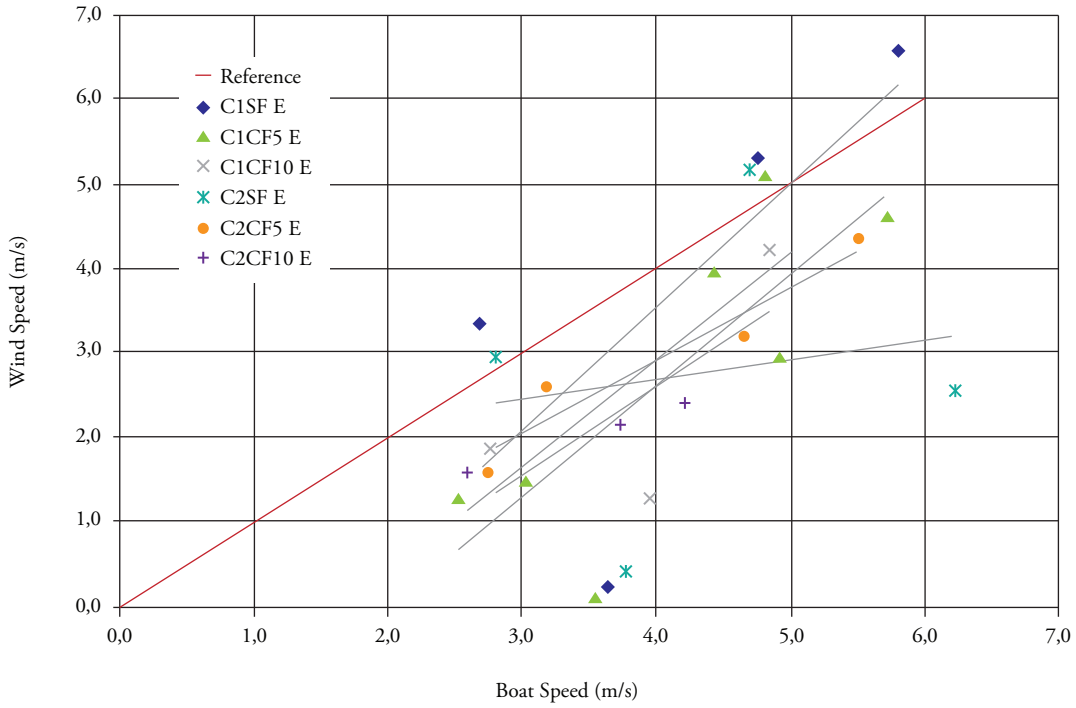

Tests with flaps at 5° in load condition 1

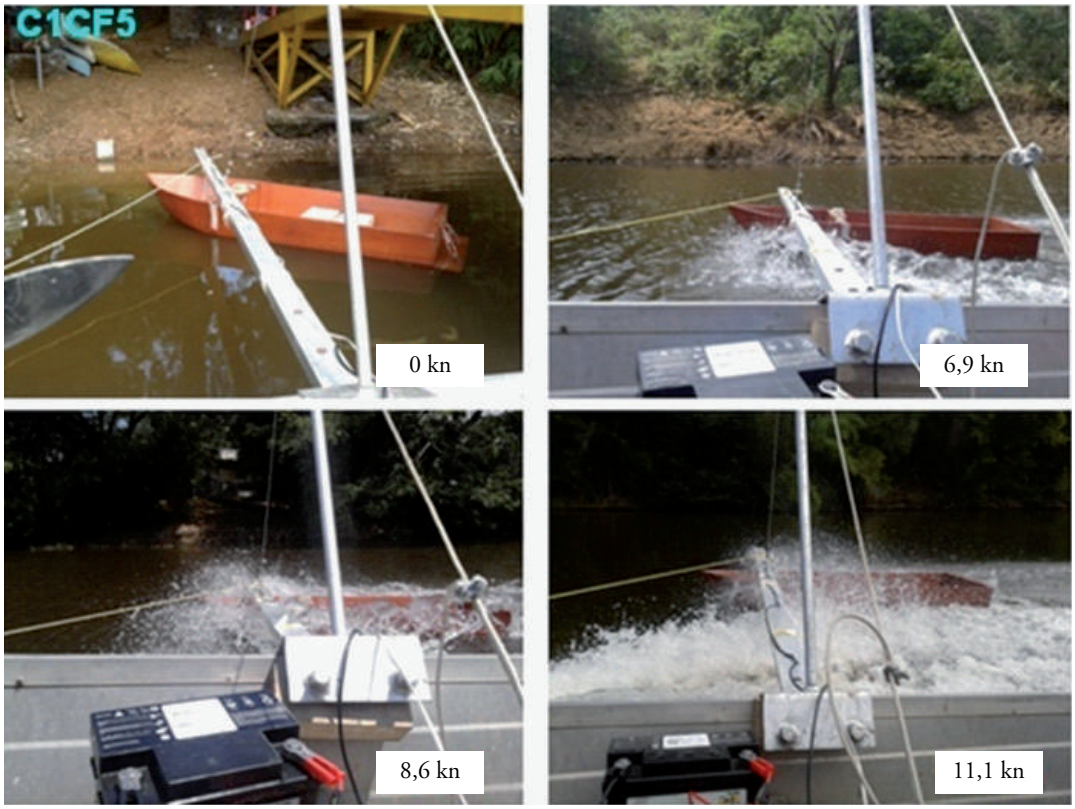

Tests with flaps at 5° in load condition 2

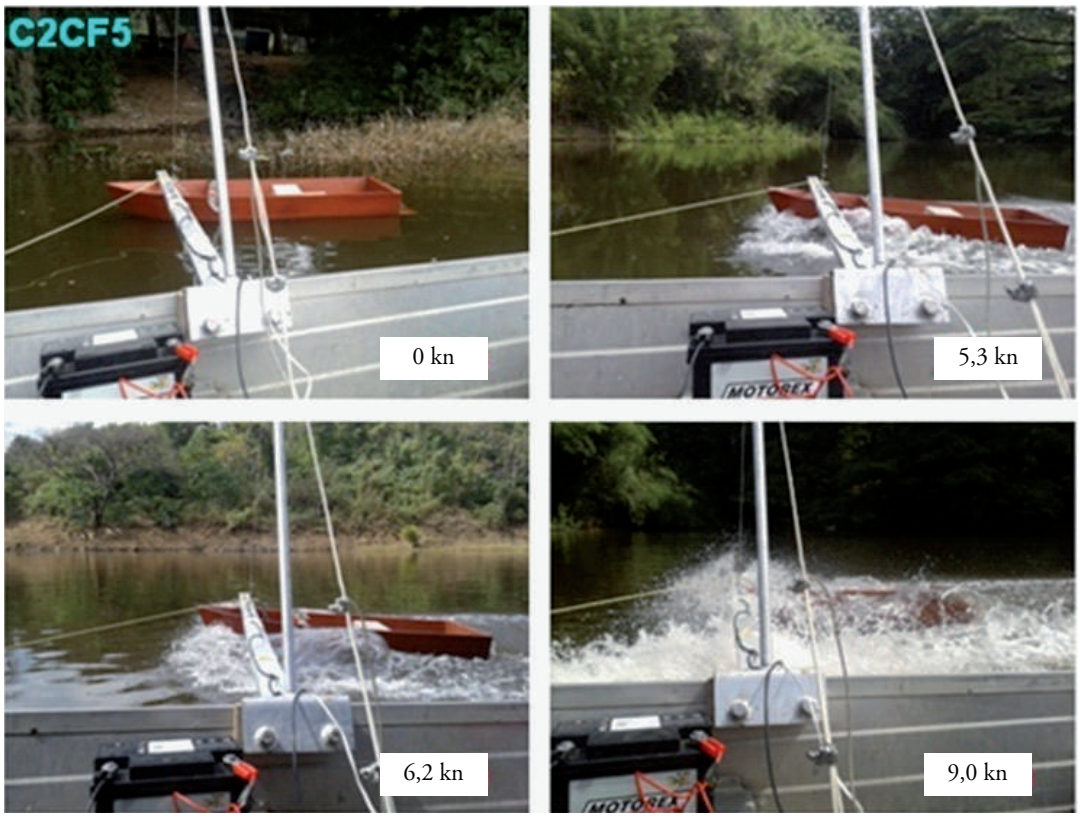

Dynamic modeling of trawl fishing gear components

Modelación Dinámica de componentes de Aparejos de Pesca de Arrastre

Jorge Freiria Pereira [1]

Abstract

A numerical model has been developed to calculate the resistance of the different components of a trawling gear, by deduction of the drag and lift components. For this purpose, mathematical models have been considered for all the elements, such as trawl cables, floats, doors, and the net itself.

The most important contribution of this numerical model is that the action of forces upon different elements permits modifying the geometric configuration of the complete set with a mutual accommodation of resistance and geometry, simulating the actual dynamics, where forces and geometry converge toward an equilibrium state. Some results obtained from actual fishing gear with data obtained from sensors during sea trials are used to compare the results of the simulator.

Key words: Nets, fishing, numeric model, net gear.

Resumen

El Grupo de Investigaciones Pesqueras del Instituto de Mecánica de los Fluidos e Ingeniería Ambiental (IMFIA) de la Facultad de Ingeniería en Uruguay ha desarrollado un modelo numérico que permite calcular la resistencia de los distintos componentes de un aparejo de pesca de arrastre, deduciendo las componentes que corresponden al arrastre (drag) y la sustentación (lift). Para ello, se han adoptado modelos matemáticos de todos los elementos tales como los cables de arrastre, flotadores, portones y la propia red. En este modelo numérico, la acción de las fuerzas sobre los distintos elementos modifican la configuración geométrica del conjunto con lo cual se produce un acomodamiento resistencia – geometría, reproduciendo la simulación del estado real, donde las fuerzas y la configuración convergen hacia una condición de equilibrio. Al final del trabajo, se presentan algunos resultados obtenidos en aparejos de pesca reales con datos obtenidos de sensores en pruebas de mar por medio de los cuales se pueden comparar los resultados del simulador.

Palabras claves: redes, pesca, modelación numérica, aparejo.

Date Received: October 24th, 2010 - *Fecha de recepción: 24 de Octubre de 2010*
Date Accepted: January 17th, 2012 - *Fecha de aceptación: 17 de Enero de 2012*

[1] Facultad de Ingeniería, CP 11300 Montevideo, Montevideo, Uruguay. e-mail: jfreiria@fing.edu.uy

Introduction

Trawl fishing is carried out by trawling a fishing gear of a certain complexity, comprised of numerous individual elements among which the fishing net stands out as the principal element, through which the water mass is filtered with the objective of capturing the fish contained in it.

The trawling device is generateslly a boat (trawler) or a couple of boats, which provide the necessary power to drag the fishing gear. Once the fishing session is completed, the gear is lifted by the trawler with the aid of winches.

The gear is constituted by a set of traction cables that drive the gear, hydrodynamic profiles (doors), floaters, and plummets that permit generatesting the horizontal and vertical openings necessary at the net mouth for its good operation, rigging cables, and the net itself with ist structural elements (bolt ropes). Each of these elements is subject to a set of demands of diverse nature: hydrostatic, hydrodynamic, gravitational, and friction. These requests generateste stress on the gear that result in deformations that permit adopting, in the equilibrium state and for stationary conditions, an adequate configuration for the purpose for which it was conceived.

The finality of estimating the resulting forces and configurations is to anticipate the system's performance, modify it, and obtain the best result for efficient fishing, both from the point of view of fishing personnel, as well as from the resourse.

The Trawl Fishing system

The complete system, developed from a trawl unit, is integrated on one side by a drag unit, comprised of one or two vessels, depending on the capture modality, and on the other side by the fishing gear that is dragged and is responsible for the capture.

Trawl unit

The trawl unit, as mentioned, is constituted by one or two vessels from whose winches the fishing gear is dragged. When using a single vessel, the gear must include devices that generateste the necessary lift to maintain the net mouth open. In case of two units being involved, the horizontal opening function is conducted by the separation between both boats. Trawl cables are fed the winch drum located on deck; each of these must withstand the effort necessary to move half the gear at the sustained speed of capture. The power necessary to carry out this force, added to that consumed by the hull, will have to be supplied by the boat's propeller plant, which must be dimensioned in function of these requirements for efficient system operation.

Fishing gear

The fishing gear is a flexible system comprised of cables that drag the lift hydrodynamic devices or doors, and through these, through another set of cables, the trawl net, which is the element where the capture takes place.

Trawl cable

Consists of a flexible cable normally made with stranded steel wires on a textile fiber core, relatively large, depending on the depth of the fishing zone. It is the element that ties the traction device located on the boat's deck and the rest of the elements that comprise the gear. It is connected at an end to the trawl winch and at the other to the door, laterally displaced with respect to the central plane due to its lift forces.

Doors

Doors are fundamental pieces in the gear, generatesting a lateral hydrodynamic force, normal to the forward direction, which produces a horizontal opening in the net mouth through the arrangement of the corresponding cables. These have diverse shapes and over the years their form of construction has been transformed, going from simple wooden structures to complex hydrodynamic structures made of laminated steel. The operating principle is the circulation of a fluid over a finite surface where differential pressure is generatested and, hence, a net force in the normal flow direction, thanks to the lack of

the device's symmetry in relation to current lines, a effect accomplished from the configuration of the latching system with trawl cables (anterior) and flanges (posterior). Also, other force components exist with the bottom trawls, which are associated to friction generatested by the displacement of the door's lower edge over the seabed.

Bridles or Patents / Flanges

Guiding the net from the upper end of the door is carried out through a set of cables, a first individual section denominated bridle o patente, which is continued, connected through a special piece to another pair of parallel cables denominated flanges that hold, respectively, the ends of the net's upper and lower bolt ropes. These cables practically work on a horizontal plane, forming a certain angle with the flow direction, an angle that will be determined by the lateral sliding action of the doors. Tension on the ends of these cables will correspond to the quota part of the resistance of the trawl net and accessories located upstream.

Trawl net

The net serves to filter water and small fish (young fish), keeping inside fish whose size corresponds to adult individuals. Meshings are designed in size to favor this distintion among sizes, an action that is denominated as "selectivity" of the art. The prior section whose shape can be modeled as a truncated cone, guides fish toward the upper part, whose essential form is a cylinder and which is denominated tunnel or copo. The upper end of the tunnel is the space where fish are finally captured. The neta consists of a structure formed by paños(layers) or sections woven of stranded wires forming regular meshings of rhomboidal shape (Fig. 1). These sections are joined among themselves, dimensioned in such a manner that once subjecting the whole to hydrodynamic and hydrostatic effort these end up adopting the configuration required; the shape it takes resembles the surface composed by a souped cone added to a cylinder, which is closed in its rear end. The front end of the cone is firmly fastened to cables that define structural aspects of the net and transmit the hydrodynamic efforts to the bridles. These are donominated upper and lower bolt ropes. To obtain the biggest base opening of the cone or mouth of the net, a series of floaters are placed on the upper bolt rope whose mission id to raise said cable, while placing plummets on the lower bolt rope to accomplish the contrary effect; that difference of vertical forces along with the hydrodynamic forces are responsible for the vertical opening.

Fig. 1. Weave of a polyethylene net

Mathematical Model

The analysis and representation of simple or complex physical systems requires the determination of models that can be evaluated through mathematical procedures. These models are a representation of realidad; they show via numbers the behavior of the system affected by particular environmental and physical conditions, and are developed from a set of mathematical equations.

The fishing gear constitute a complex physical system, affected by conditions related to the environment, temperature, type of bottom, and speed of the vessel. Response of the gear to these factors is unique and it is represented by a final equilibrium configuration. However, it is difficult to express this response from a simple mathematical model represented by a single algorithm where

eventually all the parameters and variables involved in the phenomenon could be integrated, and which would have a universality that would encompass the infinite modifications that could be introduced in each of the component elements.

Also, the individual components are susceptible to a mathematical modeling with greater or lesser degree of difficulty according to their structure, which permits, with appropriate idealization of the element, determining its behavior under the established operating conditions.

As of these idealizations or models, we may predict the individual configuration given by its spatial position and intervening forces, integrating these with those corresponding to each of the remaining components to determine the configuration of the whole.

This integration needs some work hypothesis, which are part of the global model: the forces and reactions that act in each individual element do not affect or are independent from the rest, maintaining continuity through the requests on the link elements among them, and symmetry exists in the arrangement of the gear with respect to the flow direction.

To calculate the hydrodynamic forces, we used Newton's model:

$$R = \frac{1}{2} C \cdot \gamma \cdot S \cdot V^2 \qquad (1)$$

Where:

R is the hydrodynamic force
C is the dimensionless resistance coefficient
γ is the specific weight of the fluid
S is the projected surface according to a plane normal to the flow direction
V is the flow rate or relative speed between the fluid and the moving element

The following describe the models adopted for each of the component elements of the bottom fishing trawl gear.

Mathematical Model for the Net

The following will present some concepts and definitions used in the development of the formulations of the drag coefficient in reference to Figs. 2 and 3:

Side of meshing: the distance between two consecutive knots over a filament of diameter d.
Knot: Union of two filaments that compose the section, an equivalent diameter, d_k, (sphere) is assigned.
Meshing opening: denominates the angle formed by two filaments joined at a knot, seen in longitudinal sense, θ.
Attack angle: is the angle formed by the meshing plane with the flow direction, α.
Filtering coefficient: is the ratio between the projected area of the wire composing a meshing and the meshing area, S.

Fig. 2. Elements of an individual net

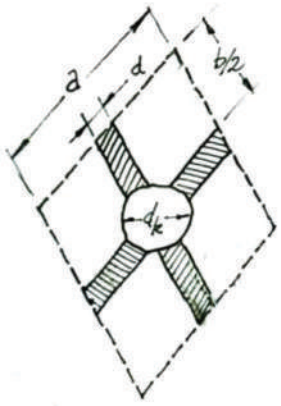

Fig. 3. Idealization of elements of the net

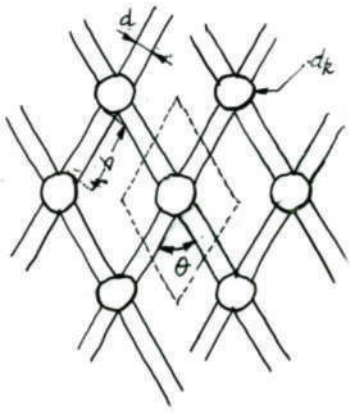

Filtering the water through the meshings generates a hydrodynamic resistance component on each wire segment forming the meshing (bar) and each knot joining these segments.

The model to be used is denominated *"sine squared"*; it is presented by Wileman and Hansen (*Wileman & Hansen, 1988*) and introduces a modification in the expressions of the drag coefficient posed by Ferro and Hou (*Ferro & Hou, 1984*), establishing that it is proportional to $sine^2\beta$ for a bar representing a wire from a net meshing. This ratio derived from experimental works, substituting that used until then with respect to $sine^3\beta$, improves the benefits of the model:

Better functional ratio between C_D and the opening angle θ
Dependency is corrected with relation to the attack angle α
Introduces a term to reduce the trawl prediction

The expression of this coefficient will be evaluated in different manner for the frontal zone or cone of the net, and for the rear part or tunnel; each of these portions is configured by bars that define the meshings and knots in the ends of said bars having expressions for the calculation of the individual resistance coefficients.

Resistance coefficient for the cone zone

Hydrodynamic coefficient for a bar

$$C_{D\,BARRA} = C_{D\,CYL} \cdot sin^2\beta \cdot (1 + 0{,}5 \cdot sin\alpha) \cdot \left(1 - \frac{d_k}{a}\right) \quad (2)$$

Where:

$C_{D\,CYL}$ is the resistance coefficient for a cylinder, with a suggested value of *1.1* (*Ferro & Hou, 1984*)
α is the angle formed by the bar in relation to the flow direction
β is the angle formed by the meshing in relation to the flow direction
a is the side of the meshing
d_k is the knot diameter

Friction coefficient for a bar

$$C_{f\,BARRA} = m \cdot C_{D\,CYL} \cdot (1 + 2 \cdot sin\beta - 3 \cdot sin^3\beta) \cdot \left(1 - \frac{d_k}{a}\right) \quad (3)$$

Where:

$m \cdot C_{D\,CYL}$ is the associated friction coefficient of the surface of the bars, with a suggested value of *0.0315* (*Ferro & Hou, 1984*)

Hydrodynamic coefficient for a knot

$$C_{D\,KNOT} = C_{D\,ESF} \cdot \frac{\pi}{4} \cdot d_k{}^2 \cdot \frac{1}{2 \cdot a \cdot d} \quad (4)$$

Where:

$C_{D\,ESF}$ is the drag coefficient for a sphere, with a value of *0.47*
d is the wire diameter or bar; assuming a d_k/d ratio between *3.16* and *3.64*

Resistance coefficient for the tunnel area

The meshings in the tunnel, unlike those in the cone, are arranged in the same direction as the flow.

Hydrodynamic coefficient for a bar

$$C_{D\,BAR\,0} = C_{D\,CYL\,0} \cdot \int sine^3 \frac{\theta}{2} \cdot \left(1 - \frac{d_k}{a}\right) \quad (5)$$

Where:

$C_{D\,BAR\,0}$ is the resistance coefficient of the bars in the tunnel
$C_{D\,CYL\,0}$ is the resistance coefficient for a cylinder, considering now a value of *1.0*

Friction coefficient for a bar

$$C_{D\,BAR\,0} = C_f \cdot cos^2 \frac{\theta}{2} \cdot \left(1 - \frac{d_k}{a}\right) \quad (6)$$

Where:

C_f is the friction coefficient of the surface of the bars, with a suggested value of *0.07* (*Ferro & Hou, 1984*)

Shadow effect

This case includes the effect produced on a wire that immediately in front, understanding that both are aligned in the flow direction, through a factor directly affecting the total resistance value:

$$C_{AP\,0} = \left(1 - C_S \left(\frac{d}{a \cdot cos\frac{\theta}{2}}\right)^{1/2}\right)^2 \quad (7)$$

Where:

C_s is an experimental coefficient whose value can be considered equal to *1.0*

Actuation areas

The previously detailed coefficients are applied to Newton's equation to calculate hydrodynamic resistance, where the fluid's actuation area should also be indicated.

The same coefficients are defined in function of a unitary meshing area, for which it simply remains to multiply them by the number of bars and knots according to what corresponds for each of the sections considered.

Mathematical Model for Floaters

Diverse types of floaters exist; however, currently, those made of plastic materials have extended use. The shape adopted is most often spherical, with different material thicknesses according to the depths and pressures that must be endured.

Their hydrodynamic resistance is calculated by Newton's formula, considering the sphere's projected area, the diametral circle, and a drag coefficient extracted from the graphic that shows their behavior in function of the associated Reynold's Number (*Re*) (Fig. 4).

For the normal velocities developed during fishing operations and the dimensions of the floaters used, the values of *Re* range within 5.10^5, which is why it is established in literature that the drag coefficient can be estimated in *0.47*.

$$R_{FLOT} = \frac{1}{2} \cdot C_{D\,ESF} \cdot \rho \cdot S \cdot V^2 \quad (8)$$

Where:

$C_{D\ ESF}$ is an experimental coefficient whose value is estimated at *0.47*

The vertical force represented by the net

Fig. 4. Hydrodynamic drag coefficient as a function of Re (Fridman A. L., 1969)

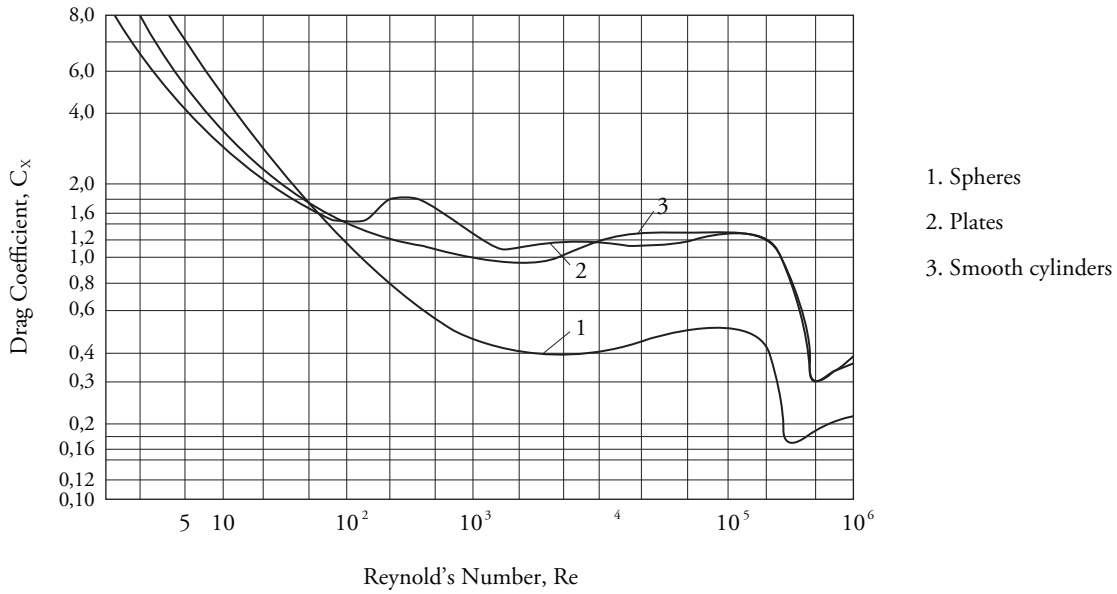

flotation should also be considered, calculated as the difference between absolute flotation and the unit weight.

Mathematical Model for Plummets

Dragging gear elements over the seabed, as with plummets, generates efforts derived from the friction appearing on the interfase. This force depends on the weight of the moving element, on the surface of actuation or friction, on the type of surface and on the type of relative movement (glide, rolling).

Fig. 5. Diagram of Forces during glide

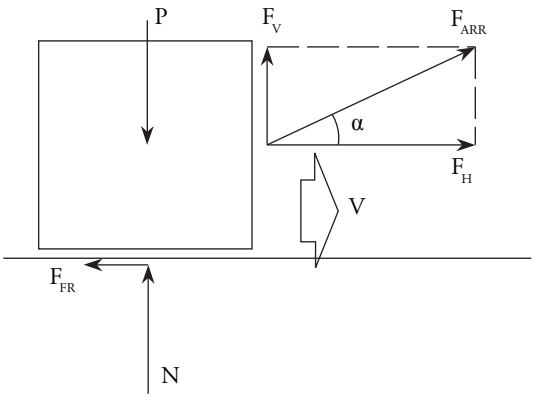

The diagram of forces of an element subjected to friction efforts is that described in Fig. 5, whose algebraic expression is given by the following system of equations:

$$F_{FR} - F_H = F_{FR} - F_{ARR} \cdot cos\ \alpha = 0 \quad (9)$$

$$N + F_V - P = N + F_{ARR} \cdot sin\ \alpha - P = 0 \quad (10)$$

$$F_{FR} = f \cdot N \quad (11)$$

Where

F_{FR} is the friction force
F_{ARR} is the external force acting on the element, with its components F_H and F_V
N is the reaction on the contact surface
P is the weight of the element
f is the friction coefficient on the element and the contact surface

The friction process has two operating regimes; while the actuation force does not manage to move the body, the system is at equilibrium and the friction factor is defined as static, f_s; once this resistance to movement is overcome, that is, when the action force is higher than the friction force, a regime is established associated to a friction factor of lower value than the previous, denominated dynamic friction factor, f_d. An alternative to define *fs* would be to experimentally determine the action force necessary to move a known weight, varying the materials of the bodies and the contact surface.

Some values of *f* are given in Table 1, understanding that said values correspond to the static friction coefficient:

Table 1. Friction coefficients according to type of material and glide surface

Material	Sand and stone	Fine sand
Iron	0.47	0.61
Wood	0.51	0.73
Stone (granite)	0.54	0.70
Lead	0.44	0.53
Sand (in sacks)	0.63	0.76
Strings (plant fibers)	0.70	0.80

Source: (Fridman A. L., 1969)

Model of Bolt Ropes

The hydrodynamic effort and of other nature on the net, floaters, and plummets is transmitted to the traction system through two steel cables that occupy ocupan una structural function, denominated upper and lower bolt ropes.

A hydrodynamic effort exists on the cable itself, which is added to the effort on the rest of the net. The shape of the bolt ropes ends up being defined by the numerous requests to which they are subjected: tension on the ends, representative of

the vessel's drag; tension from the net distributed throughout its whole length; tension from floaters in one case and from plummets in another.

Fig. 6. Flat representation of relinga

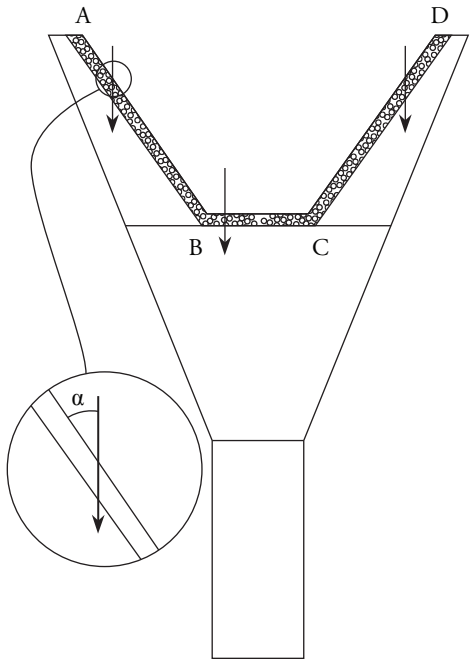

The catenary formed must be determined with precision to apply the drag coefficients point to point and integrate them in the longitudinal direction. However, in this fase of the model the bolt rope has been considered deployed on a single plane, considering different linear sections subjected to hydrodynamic efforts, using as representation of the cable that of an infinite cylinder (Fig. 6).

Each of these sections is considered individually with the corresponding angle of action in relation to the incident flux. This correspondence is necessary to bear in mind the effects of the calculation given that the resistance coefficient depends functionally on said magnitude.

In these hypotheses, the hydrodynamic resistance is the sum of components represented by the following expression:

$$R_{RELINGA} = \sum_i \left(\frac{1}{2} \cdot C_{D\,CIL}\,(\alpha_i) \cdot \rho \cdot S \cdot V^2\right) \qquad (12)$$

Where:

$C_{D\,CYL}$ is the resistance coefficient for a cylinder in function of the flow angle of incidence whose ratio is defined in Table 2.

α_i is the angle formed by sections of bolt rope on the net plane

Table 2. Resistance coefficients for a cylinder as functions of flow angle of incidence

α	$C_{D\,CYL}$	α	$C_{D\,CYL}$
0	0.12	50	0.70
10	0.20	60	0.90
20	0.32	70	1.12
30	0.41	80	1.25
40	0.56	90	1.3

Source: (Fridman A. L., 1969)

Model of Flanges and Bridles

The hydrodynamic force on these cables is calculated assuming the hypothesis that they form a straight line during fishing operations. Although the real representation should include a small catenary, the effect in this case is considered residual in relation to the total value.

Tension at its ends corresponds to half the total resistance of the net and accessories located upstream, which is transmitted to the doors.

Fig. 7. Angle of Flanges and Bridles in relation to flow direction

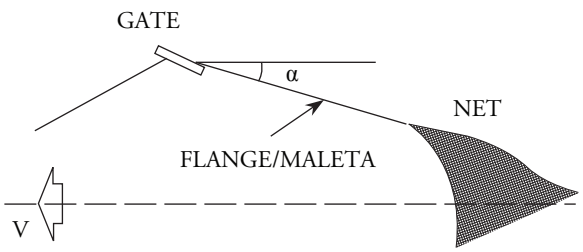

The calculation in this case can be reduced to that of a cylinder of known dimensions, which forms a given angle α with the incident flux. The incidence angle is deducted from the initial conditions imposed by the model and then from successive iterations until reaching the regime condition.

$$R_{BRIDAS/MALLETAS} = \sum_i \left(\frac{1}{2} \cdot C_{D\,CIL}\,(\alpha) \cdot \rho \cdot S \cdot V^2\right) \qquad (13)$$

Where:

$C_{D\,CYL}$ is the resistance coefficient for a cylinder in function of the incidence angle

α is the angle formed by the flange or bridle with the incident flux

Model of Doors

The door is an element inserted in the cable line linking the vessel and the net, and whose function is to generate a lateral force that permits expanding the distance between both trawl cables and permit the transversal opening of the mouth of the art. It consists of a vertical structure that generates a lift force (normal to the flow direction), which is responsible for the mentioned lateral expasion, besides a resistance to drag, like the rest of the gear elements.

The drag and lift forces have a direct link with the shapes of these devices. The most elemental and primitive consist of flat plates, with a very low lift/drag ratio, rates that have been improved through the current hydrodynamic designs. The values of these forces are calculated by using the coefficients provided by the manufacturers.

$$R_{PORTÓN} = \frac{1}{2} \cdot C_{D\,PORTÓN} \cdot \rho \cdot S \cdot V^2 \qquad (14)$$

$$S_{PORTÓN} = \frac{1}{2} \cdot C_{L\,PORTÓN} \cdot \rho \cdot S \cdot V^2 \qquad (15)$$

Where:

$C_{D\,DOOR}$ and $C_{L\,DOOR}$ with the drag and lift coefficients (according to manufacturer)

Doors, as well as plummets fastened to the lower bolt rope, work by dragging through the seabed for which a friction component exists that must be added to the resistances calculated. Said component, relatively smaller in comparative terms with the door resistance values, is calculated by using friction data established in Table 1, as seen previously.

Model of Trawl Cables

The trawl line consists of a very log cable with a very marked catenary, depending on its dimensions and weight, on the length and depth of the site. The vertical plane containing this catenary forms a working angle in relation to the flow direction.

Fig. 8. Relative position of the trawl cable

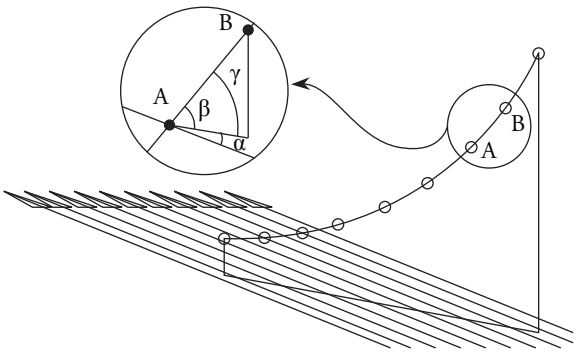

For effects of its calculation for the program, we considered a division in linear sections to approximate the shape to a polygonal, where each of the segments considered individually is subjected to the flow defined by the relative spatial angle, β, defined by the following expression:

$$\sin\beta = (1 - \cos^2\gamma \cdot \cos^2\alpha)^{1/2} \qquad (16)$$

Where:

α is the incidence angle formed by the flow and the catenary plane

β is the incidence angle formed by the flow and a catenary section

γ is the horizontal projection angle within the catenary plane

Onced defined angle β, the drag coefficient is calculated for that bar by using the ratio of drag coefficients for a bar in function of the angle (Table 2).

Initial conditions

The main dificulty in implementing a model is selecting a set of initial conditions with which we manage to establish a first spatial configuration of the gear, and on which mathematical models can be applied of the individual elements to then integrate them in the whole; as of this first configuration and through successive approximations, a geometric and dynamic conditon of equilibrium can be established.

Works carried out by Nomura and Yamazaki (*Nomura & Yamazaki, 1975*) permit conducting this approximation from the experimental formulation for trawl net resistance whose expression is the following:

$$R_{RED} = 8 \cdot g \cdot L_m \cdot L_n \cdot (\frac{D_t}{m_s}) \cdot V^2 \qquad (17)$$

Where:

R_{NET}, Net's resistance to drag (N)
L_m, extended perimeter of the mouth of the net (m)
L_n, length of the extended net (m)
D_t, mean diameter of the wire (mm)
m_s, length of the mean meshing (mm)
V, velocity (m/s)
g, gravity acceleration (m/s^2)

From this initial value corresponding to the net's resistance with its gear, without including the resistance of the doors, the first spatial configuration of the system is determined from the geometric-dynamic ratios presented by Fridman (*Fridman, 1986*), defined by the vertical and horizontal openings of the mouth of the net, and the openings of doors.

Modeling of Case Studies

Upon defining the gear's first spatial configuration, we calculated for each of the individual component elements the hydrodynamic forces and forces of other nature that act on these, by applying the expressions developed previously and which constitute the core of the mathematical model. Now, we include the forces developed by the trawl doors, which are not considered in the calculation according to Nomura's formula.

With the different components of forces resulting from the application of the different algorithms calculated, the gear configuration is again defined, which will present variants with respect to the initial configuration, as the value of the forces takes a different value than the initial value.

We can, therefore, visualize in these first steps the philosophy of the model, which represents in discrete manner a process that in nature occurs continuouslly, the interaction among the set of forces applied to a flexible complex system, and its spatial configuration as of the internal tensions.

Fig. 9. Convergence in the Net's Resistance Calculation

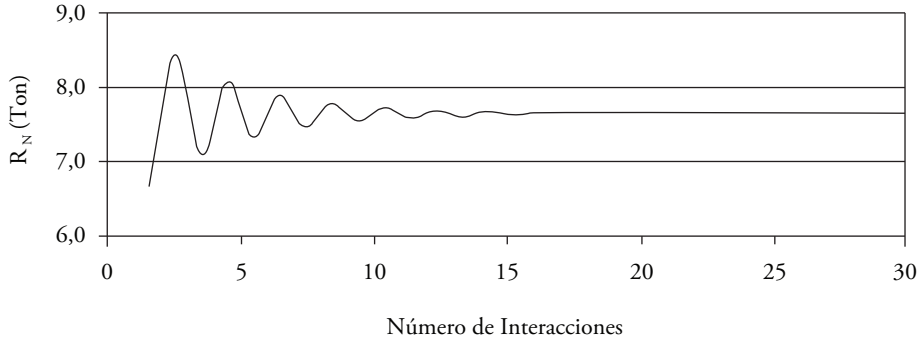

The calculation process in alternative and interactive manner between the forces and geometric configuration reflects the physical reality of this type of system. A mechanism is included to end the calculation stage having reached conditions of dynamic equilibrium, consisting in establishing a difference among the values obtained in two consecutive steps whose difference is transformed into a marginal value pre-established as a percentage of the calculated total.

Convergence is a fundamental condition for the viability of the model; in all fields defined it is rapidly accomplished. Fig. 9 shows the behavior of the Net resistance, R_N, variable.

This enhances the application in two senses: on the one hand the rapidity of the response to variations introduced, and on the other the robustness of the code.

Results

After ending the stage of constructing the logical structure and introducing the algorithms that represent each of the elements of the model, this was tested to visualize its convergence, an aspect mentioned before, and verify alignment of the results obtained with comparative data that will have a high level of operator confidence.

The data available to conduct the validation were provided by competent personnel directly involved in the determination of the measurements through ultrasound probes, which is why they are considered valid data for the effects of the current review.

The nets used in the comparison excercise have the general characteristics indicated ahead, establishing in Table 3 to Table 5 the corresponding comparative values.

Identification: HVT 536

Characteristics: Upper bolt rope, 51.0 m; Lower bolt rope, 60.0 m; Bridle, 205.0 m; Upper and lower flanges, 50.0 m each; Trawl cable, 540.0 m; Floaters, 90 units; Plummet, 2559 Kg (in water); Area of doors, 5.0 m^2 each; Length of body, 51.0 m.

Table 3. Comparative values sensor / simulator for the HVT 536 net

Magnitude	Sensors	Model
Velocity (Knots)	4.0	4.0
Resistance of Net (Kg)	-	6981
Resistance Doors (Kg)	-	2347
Height of mouth (m)	2.80	2.75
Distance between doors (m)	160	164
Opening of Wings (m)	-	32.2

Identification: HVT 630

Characteristics: Upper bolt rope, 61.0 m; Lower bolt rope, 66.5 m; Bridle, 320.0 m; Upper and lower flanges, 50.0 m each; Pie de gallo, 3.0 m; Trawl cable, 540.0 m; Floaters, 105 units; Plummet, 2559 Kg (in water); Area of doors, 7.5 m^2 each; Length of body, 63.0 m.

Table 4. Comparative values sensor / simulator for the HVT 630 net

Magnitude	Sensors	Model
Velocity (Knots)	4.0	4.0
Resistance of Net (Kg)	-	8573
Resistance Doors (Kg)	-	3520
Height of mouth (m)	3.30	2.85
Distance between doors (m)	218	228
Opening of Wings (m)	-	37.6

PescaPuerta

Characteristics: Upper bolt rope, 78.0 m; Lower bolt rope, 100.0 m; Bridle, 265.0 m; Upper and lower flanges, 30.0 m each; Pie de gallo, 2.8 m; Trawl

cable, 960.0 m; Floaters, 60 units; Plummet, 12933 Kg (in water); Area of doors, 6.2 m^2 each; Length of body, 66.4 m.

Table 5. Comparative values sensor / simulator for the PescaPuerta net

Magnitude	Sensors	TrawlSim 3d
Velocity (Knots)	4.4	4.4
Resistance of Net (Kg)	-	13771
Resistance Doors (Kg)	-	3510
Height of mouth (m)	4.80	3.91
Distance between doors (m)	187	181
Opening of Wings (m)	-	46.3

Conclusions

Development of this calculation tool introduces a substantial improvement in estimating gear resistance when considering the set of forces acting on a flexible structure displaced in the space. For such, we consider the shape said structure develops until reaching an equilibrium state upon being subjected to a dynamic system that is dependent on said spatial configuration.

The net's resistance is calculated considering the local constructive dimensions, bearing in mind for each zone the number and size of meshings and wire diameter.

The summary of the comparative data shows that in calculating the distance between doors, the results of the model differ between 2.5 and 4.5% from the data provided by shipowners, with the biggest differences represented in the vertical opening of the mouth, with a range between 2.0 and 20.4%.

It has been identified that it is necessary to advance in the behavior and spatial positioning of the cables that comprise the flanges, whose final state severely conditions the estimation of the vertical opening, a fundamental efficiency parameter for fishery types.

The introduction of improvements in identifying coefficients of meshing opening and in the adjustment of its sizes and wire diameter at localized level will permit refining the calculation of the net's resistance, whose contribution to the gear's global resistance is determinant in the final value.

Bibliography

DICKSON, W. (1980). *Trawl drag area meshing.* Bergen, Noruega, Noruega: Research, The Institute of Fishery Technology.

FERRO, R. S., & HOU, E. H. (1984). *A selected review of hydrodynamic force coefficient data on stranded wires used in fishing gears*. Scottish Fisheries Research, Aberdeen.

FRIDMAN, A. (1986). *Calculations for fishing gear designs (Vol. 1)*. (FAO, Ed.) Farnham, Surrey, Inglaterra: Fishing News Books Ltd.

FRIDMAN, A. L. (1969). *Theory and design of commercial fishing gear.* Moscow: Pischevaya Promyshlennost.

NOMURA, M., & YAMAZAKI, T. (1975). *Fishing Techniques.* Tokio: Japan International Cooperation.

WILEMAN, D. A., & HANSEN, K. (1988). *Estimation of the drag of trawls of known geometry.* Hirtshals, Dinamarca: Danish Fisheries Technology Institute.

Analysis of radar cross section assessment methods and parameters affecting it for surface ships

Análisis de Métodos de Evaluación de la Sección Transversal de Radar y de los Parámetros que Inciden en Ella para Buques de Superficie

Vladimir Díaz Charris [1]
José Manuel Gómez Torres [2]

Abstract

This article presents an analysis of the different modeling methods for predicting the radar cross section of surface ships. In the analysis, we studied the effect of different factors in vessel construction regarding the amount of electromagnetic energy returning to a radar source, such as the handling of shapes, use of different materials, and vessel size. We can see the different evaluation methods of the radar cross section and the software tools available to determine an appropriate methodology for adoption by the Colombian Navy and their subsequent integration with the design process and optimization of warships.

Key words: Radar Cross Section, RCS, vessels, RAM, absorbent, prediction, Navy.

Resumen

En este artículo se presenta un análisis de los diferentes métodos de modelado para la predicción de la sección transversal de radar (RCS) de buques de superficie. Dentro del análisis, se estudia el efecto de los diferentes factores constructivos del buque sobre la cantidad de energía electromagnética que regresa a una fuente de radar, como son el manejo de formas, el uso de diferentes materiales y el tamaño del buque. Se aprecian los diferentes métodos de evaluación de la sección transversal de radar y las herramientas de *software* disponibles con el fin de determinar una metodología adecuada para su adopción por parte de la Armada de Colombia, y su posterior integración con el proceso de diseño y optimización de buques de guerra.

Palabras claves: Sección Trasversal de Radar, RCS, buques, RAM, absorbente, predicción, Armada.

Date Received: November 1st, 2011 - *Fecha de recepción: 1 de Noviembre de 2011*
Date Accepted: January 18th, 2012 - *Fecha de aceptación: 18 de Enero de 2012*

[1] Mechatronic Engineer, M.Sc.(c) Electronic Engineering, DIDESI Researcher, COTECMAR, Colombia. e-mail: vdiaz@cotecmar.com
[2] Naval Electronic Engineer, MSME & MSSE, DIDESI researcher, COTECMAR, Colombia. e-mail: jmgomez@cotecmar.com

Introduction

For the design of warships and military aircraft it is very important to have tools to predict or estimate the Radar Cross Section (RCS) during the preliminary design phase because it is not economically viable to do so with models or demos. Thus, we get clear information for the design of shapes of low or high radar detection and what shapes are compatible with the structural and hydrodynamic requirements. From the study of the state-of-the-art of managing the RCS (*Díaz, Domínguez, and Saravia, 2012*), we identified the factors that most affect the RCS of ships and other military vehicles, as well as the most frequent techniques used for their reduction.Among the factors identified are size, shape, and the vehicle's materials and coatings. Among the techniques for reducing the RCS, we identified the use of radar-absorbing materials (RAMs) and the managing of shapes (Shaping); they are shown in relation to the use of stealth technology (Stealth).

From identifying factors and techniques that influence RCS, different methods and simulation tools are explored to evaluate RCS of warships and investigate the relative impact of different factors and techniques described about their RCS, through experiment design.

Development

Radar Behavior

To analyze radar behavior, we used the radar equation relating the radar's range to the transmission, reception, antennae, target, and environmental characteristics. This equation is used to determine the maximum range at which radar can detect a target and be useful to understand the factors affecting the performance of the radar (*Skolnik, 2001*).

A typical scenario of a bistatic radar is shown in Fig. 1, where the TX box represents the radar transmitter, the RX box the radar receiver, while the gray object on the right represents the goal or target. Both transmitting and receiving antennae are closely located to each other; therefore, it is assumed that the range to the target is equal to R.

The simple radar equation is described below:

$$P_T = \left(\frac{P_t G_t}{4\pi R^2}\right)\left(\frac{\sigma}{4\pi R^2}\right)\left(\frac{G_r \lambda^2}{4\pi}\right) \quad (1)$$

Where P_r is the power received by the radar in (watts). P_t is the transmission power in (watts). G_t is the Gain of the transmitting antenna. G_r is the gain of the receiving antenna, σ the radar cross section (RCS) (m^2), λ the wavelength of the radar operating frequency (m), and R is the range between the radar and the target (m).

It takes into account that the first term in parentheses represents the power density of radar in the objective (watts/m^2). The product of the first and the second terms in parentheses represents the power density in the radar receiver due to the reflection or scattering that occurs in the target. The third term in parentheses represents the amount of reflected power captured by the opening receiving antenna.

In the case of the mono static radar, where the radar uses the same antenna for transmission and reception, G_t is equal to G_r and by establishing $G_t = G_r = G$, the equation can be written as:

Fig. 1. Typical Radar Scenario of Objectives. (Jenn D. C., 1995)

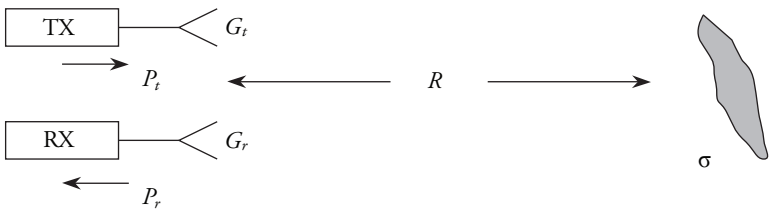

$$P_t = \frac{P_t G^2 \sigma \lambda^2}{(4\pi)^3 R^4} \quad (2)$$

The radar's maximum range, R_{max}, is the distance beyond which the target cannot be detected. This occurs when the P_r received signal is equal to the minimum detectable S_{min} signal. Substituting $P_r = S_{min}$ in equation (1.2) and rearranging terms, yields:

$$R_{max} = \left[\frac{P_t G^2 \sigma \lambda^2}{(4\pi)^3 S_{\min}} \right]^{1/4} \quad (3)$$

Although this form of radar equation (1.3) excludes many important factors and generally predicts high values for the maximum range, it represents the relationship between the maximum RCS radar and the target.

As shown in equation (1.3) of the radar, the RCS is a property of the object or target dispersing the radar signal, representing the magnitude of the radar signal echo returned by that object. It can be defined as:

$$\sigma = \frac{\text{Power reflected to receiver per unit solid angle}}{\text{Intensity power density / 4p}} \quad (4)$$

Clearly, the RCS of a target is a measure of the scattered power in a given direction when the target is illuminated by an incident wave normalized to the power density of the incident field. The purpose of normalization is to remove the effect of the range and, thus, obtain a value of SCR that is independent of the distance between the target and the light source (*Garrido, 2000*).

Some factors that determine the amount of electromagnetic energy returning to the source are (*Maritime Safety Information, 2009*):

- The material and geometry of the target in which it is made.
- The absolute size of the target.
- Relative transmitter/receiver position to the target.
- The relative size of the target in relation to the wavelength of the illuminating radar.
- The incidence angle, which is the angle at which the radar sends waves to a particular portion of the target that depends on the shape and orientation of the target to the radar source.
- The reflected angle, which is the angle at which the reflected wave leaves the target and is directly related to the angle of incidence.
- Signal strength of the radar transmitter.
- Distancebetween radar and target.

Frequency Behavior

To perform the prediction, it is necessary to know what the behavior of RCS in frequency reading is. There are three frequency regions in which a target RCS is quite different, as shown in Fig. 2. These

Fig. 2. RCS of a sphere (Jenn D. C., 1995)

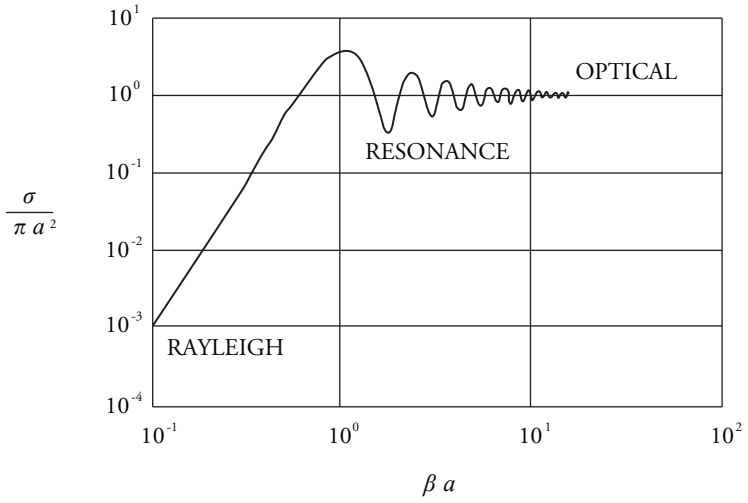

regions are defined depending on the target size in terms of the incident wavelength as: low-frequency region or Rayleigh region, resonance region or Mie region, high-frequency region or optical region.

- Low-frequency region or Rayleigh ($2\pi/\lambda < 1$), where the induced current in the body of the target is approximately constant in amplitude and phase.
- Resonance or Mie region ($2\pi/\lambda \approx 1$). The phase variation of the current through the body of the target is important and all parts contribute to the dispersion. Generally, λ against $2\pi/L$ will fluctuate.
- High-frequency or Opticalregion ($2\pi/\lambda > 1$). There are many cycles in the variation of the current phase through the target body and, consequently, the discrete field will be a highly dependent angle (*Jenn D. C., 1995*).

Methods to predict RCS

Methods are available to make RCS predictions,such as methods of moments, finite difference, microwave optics, and method of optical physics where many disadvantages can be found in each of them in terms of high computation requirements and increased runtime to perform the prediction;described as the best option is RCS prediction in the optical physics method consuming the least amount of computational resources and with less complexity (*Garrido, 2000*). It is necessary to validate, in any case, the accuracy for ranges of frequencies of interest and the size of the ships to consider.

Modeling and visualization of radar targets

Several types of modeling and visualization of radar exist such as geometric modeling of solids, modeling by borders, modeling by Curved Patches, and Modeling by Facets, which are techniques for predicting radar cross section that require a realistic model of the target to impose boundary conditions of the electromagnetic problem on its surface.

The most common method used today is modeling by borders through flat facets in which the modeled surface is more similar to the real and results in much higher prediction (*Rius Casals, 1991*).

The main drawback of modeling with flat facets is that the performance of the model is difficult when the radar target presents very complex surface shapes, as shown in Fig. 3, where the wings and aircraft turbines have hundreds of facets to achieve its real constitution.

To achieve a precise model, the facets should be approximated to the actual surface as much as necessary at the expense of raising the number of facets used. The large number of facets, each characterized by the spatial coordinates of its vertices, constitutes an extremely large amount of information to process, requiring a considerable computational effort even with high-frequency techniques, although much less than the level required by discretization with low-frequency methods.

Fig. 3. Boeing 727 modeled with flat facets (Rius Casals, 1991)

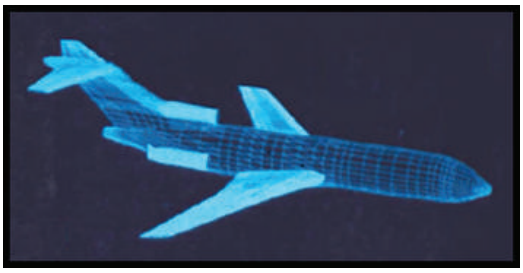

Physical optical model

It is another of the techniques most commonly used today to predict cross section of complex radar targets and it is obtained by consistently adding the contributions of each of the illuminated areas (*Garrido, 2000*).

The method of modeling by facets allows easily adding the diffraction in edges by analyzing the wedges that form adjacent facets. These wedges may correspond to the edges of the real model, such as the trailing edge of the wings on an airplane or artificial edges due to the creation of facets of the real curved surface.

The main limitation of the geometrical optics approximation is to assume infinite frequency. The physical optics approximation introduces

appropriate dependence on the frequency via the application of the theorem of equivalence: it calculates the fields radiated by the induced currents on the surface of the object. To find out about these the approximation of the tangent plane, it is used on the illuminated surface and assumed null in the shadow area. This is equivalent to performing the integral of radiation only on the illuminated surface disregarding hidden surfaces.

Because the physical optics method approximates the currents on the surface of the object, for currents that would be on an Infinite tangent plane, it correctly predicts the first-order reflection in large areas, while it incorrectly deals with the surfaces of small radius of curvature and the diffraction in edges and vertices. This provides good results with radar targets of large dimensions, in which the reflection on the surface of the fuselage is dominant.

Methods of reduction and control of RCS

Techniques and tactics are used to reduce RCS such as:

Management of Shapes
It is best done at the design stage to ensure no large angular sources of RCS like orthogonal corners. Subsequently, the reduction of micro-geometry techniques can be applied; it offers a reduction in RCS by eliminating or re-designing exposed subsystems to concentrate the radar signature in some directions under threat, leaving RCS low elsewhere. Careful design can substantially reduce RCS by using shaping, the preparation of surfaces, minimizing the number of openings, and contraction of weapons and sensors within the structure when not in use (*AirPlane Design, 2011*).

Fig. 4 describes the difference in the scattering of the radar signal in some types of shapes.

Radar absorbent material (RAM)
Radar-absorbing materials in the form of surface coating or structural materials play an important role in complementing or enhancing RCS reduction.Radar echo includes direct specular reflections, diffractions from edges, multiple reflections and drag waves, which propagate along the surface of the body and emerges at the opposite edge.

These materials are presented in many forms depending on the mode of application and on the place and environment in which they have to work. For example,aircraft materials will be resistant to erosion, differential pressure, and attacks, while ships have to work in aggressive marine environments and must withstand day-to-day operations therein.

Fig. 4. Signal dispersion regarding target shape (Microwaves 101, 2012)

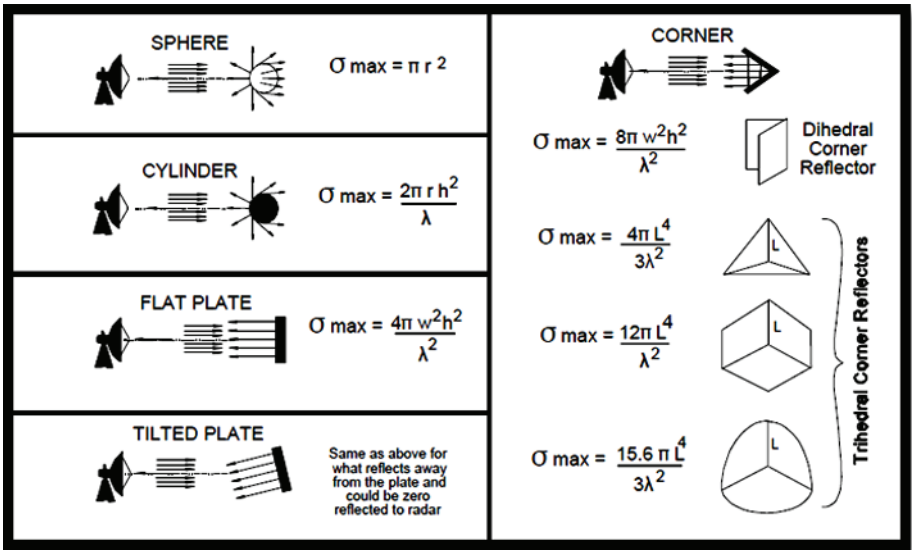

There are radar absorbent panels that are easily transported and are designed to be temporarily affixed to the structure of the vessel; they absorb the radar energy in broadband. In addition, there are Radar-Absorbent layers lighter than the panels, the slabs of Radar absorbent, the absorbent materials in spray for difficult access areas or in those on which it is difficult to apply other types of materials like masts of vessels or air and gas intakes and outlets. These materials tend to be heavier than the prior. Light foams are also used in areas where transparency at the output of radar waves is necessary (domes, antennae, etc.) (*Sahajanand, 2011*) and radar reflective film used in aircraft crystals, helicopters and command bridges on ships that can be applied and replaced with ease.

When shapes can no longer be modified orwhen modifying them is an excessive cost, it is necessary to use radar-absorbing materials (RAM). With these, RCS and detection distance can be significantly diminished.For this reason, if the RCS of a typical frigatecan be 25,000 m^2, a reductionof the RCS of the same frigateby 600 m^2 is possible by using certain radar-absorbing materials.

In the design of these materials, we will have to consider the frequencies normally used by surveillance and lighting radars. In general, the 6-18 GHz band covers most of the known anti-vessel missile systems. However, on other platforms, like tanks, the frequency is about 98 GHz.

Passive Cancellation

It is a form by which its basic concept is to introduce a source echo whose amplitude and phase can be adjusted to cancel another echo of origin. This can be achieved by relatively simple objects, provided that a charge point is available that can be identified in the body, and the size and shape of the inner cavity can be designed to present optimal impedance at the opening. Unfortunately, for simple bodies, it is always extremely difficult to generate the unit of frequency required for these incorporated impedances and the reduction obtained for a frequency in the spectrum disappears quickly as frequency changes. In addition, typical weapons platforms have hundreds of wavelengths in size and hundreds of echo sources. It is clear that it is not practical to design a treatment of cancellation of passives for each of these sources. In addition, the cancellation can return to reinforcement with asmall change in the frequency or viewing angle. Consequently, passive cancellation for the most part has been ruled out as a useful technique in reducingRCS (*Knott, Shaeffer, &Tuley, 2004*).

Active Cancellation

Also known as the active load, active cancellation is even more ambitious than the passive load. In essence, the goal is to deliver radiation to coincide with the time at input pulse whose amplitude and phase cancels the reflected energy. This implies the goal being "smart" enough to detect the angle of arrival, intensity, frequency, and waveform of the incident wave.It should also be smart enough to know its own echo characteristics for that particular wavelength and angle of arrival fast enough to generate the waveform and frequency. This system must also be versatile enough to adjust and emit a pulse of amplitude and phase at the appropriate time. Obviously, the relative difficulty increases the active cancellation more frequently, as centers of dispersal of the in and out of phase with the smallest appearance changes and where dispersion patterns are more complex and, therefore, the active cancellation is best suited for low-frequency RCS reduction (*Knott, Shaeffer, & Tuley, 2004*).

Items to obtain an RCS minimum (Knott, Shaeffer, and Tuley, 2004)

a. Avoid creation of design with strong characteristics to reflections in the direction of the radar

- Use non-metallic materials
- Absorb instead of reflectthe radar energy
- Mask or cancel any remaining reflection

In creating the design, the following should be considered:

- Avoid using large flat surfaces
- Avoid the curve of the exhaust surface and other parts with concave shapes, or convex shapes because they would be reflexive
- Avoid shape discontinuities such as corners and abrupt change in the profile, blending and smoothing all appendages and joints in the surface

- Use Flat Panel Design (FPD), which consists of multiple surfaces that reflect each in a different direction and is less likely to betray the position. Fig. 5 shows the difference of the reflection of radar waves between commercial aircraft and modern combat aircraft.

Fig. 5. Design of flat planes

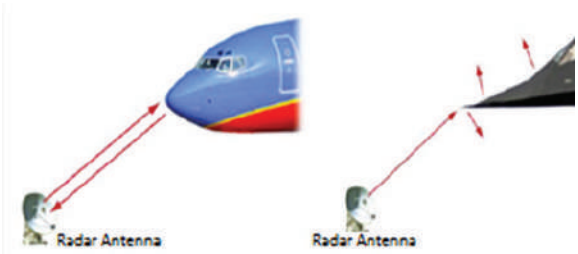

- Incoming cavities or structures have a high RCS. Input and exhaust pipes must be moved to lower surfaces; in the case of vessels, where they can be detected far from the body.
- The radome or the antenna that stands out is a good source of reflection. Therefore, there is a need to use radio equipment in millimetric waves with size reduction on the antenna, as well as the use of flat arrangements, which have low RCS or use retractable antennas.

Other production factors that reduce RCS:

- Sides of the hull with a given outward angle
- Sides of the superstructure angled inwardly
- Bulkheads of the superstructure directed in four preferred directions
- Avoid dihedrals and trihedrals
- Equipment on deck, as well as its base, must be analyzed in such a way as to reflect the least possible
- Elimination of candlesticks

Software

Within the search of computational tools that allow predicting RCS, various software have been developed for the military by companies in different countries like Germany, England and the United States.Below is a preview of the different software:

POFACETS 3.0: Software developed in 2000 under the Matlab platform, see Fig. 6; it allows approximation of RCS by using the physical optics method, via facets and models created manually or imported from existing CAD &RCS software; Cifer, Acads, Autocads (.Stl) and Pdetools MATLAB and can export files to and ACADS CIFE.

Allowing single static combinations, which could be described as a "transceiver" where the transmitting antenna is the same receiving the signal, and bistatic which is the combination of dual antenna, transmitter, and receiver.

Conversions among software versions, unit conversions, adding of new material data, among many other functions (*Chatzigeorgiadis, 2004*).

Fig. 6. POFACETS Main Screen(Chatzigeorgiadis, 2004)

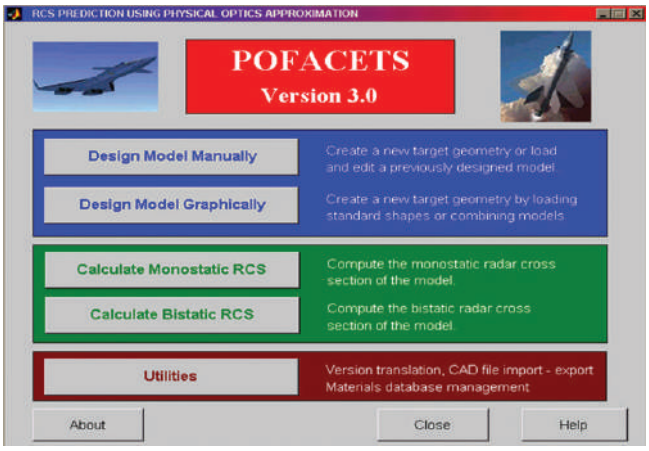

EPSILON

Software developed by ROKE in the UK in 2008, see Fig. 7. The most rigorous, accurate, and easy-to-use RCS developer in its class. It is a software that predicts the RCS of large direct targets electrically from a computational model. EPSILON is a versatile tool, which approximates models of real-life scenarios, enabling customers to quickly evaluate signatures of targets and investigate how these signatures vary according to the shape and orientation of its design. This allows multiple designs to be evaluated for selection of the most cost-effective solution.It can also be embedded with simulation tools to offer high-performance approximations of radar targets for combat analysis. No other platform is required and it does not consume high computational resources. It uses the four methods described in this article and does not have limitations on maximum size, materials, and geometric models, compatible with CAD files, DXF, 3D Studio, and others (*ROKE, 2012)*.

Typical applications for Epsilon include conventional RCS predictions, concept optimization of new platforms for stealth, improvement, and redesign of existing platforms, generation of models for physical simulation, and radar target imaging tests.

Other applications include major platforms such as aircraft, ships, tanks, spacecraft, secondary field equipment; trucks, generators, tents, weapons and weapon launch systems, antennae, buildings, and structures.

Fig. 7. EPSILON – Software Visualization(ROKE, 2012)

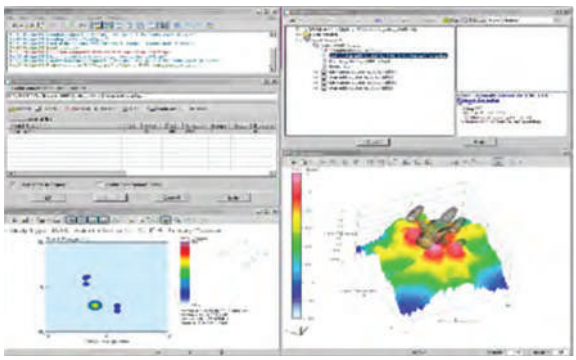

CADRCS

Software created in 1999 for RCS simulation. It is the only software that allows continuous evaluation of stealth ships, aircraft, and other military buildings during the construction phase. It provides high-resolution RCS simulation based on information from CAD files, see Fig. 8.

A friendly tool under the Windows operating system; based on graphical displays that allow precise enabling of areas reflected by radar waves and also provides images of mono-pulses, showing the objects that the radar is aimed at. It also displays the Polar view of RCS in square meters, with modification of factors that affect the signal, see Fig. 9. 3D calculation techniques used in this highly advanced software are based on 20-year experience in RCS measurements. The calculation time depends on the reflection profile of the object, the accuracy desired, and the RAM capacity of the PC. The theory used in CADRCS is unique and has not been published (*CADRCS, 2012*).

Fig. 8. Sample 3D model viewing RCS (CADRCS, 2012)

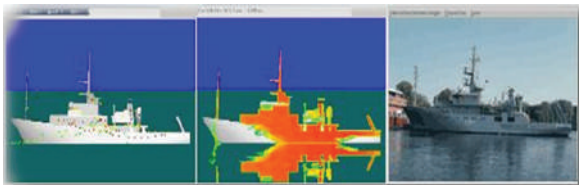

Fig. 9. Monitor Display andpolar graph of RCS (CADRCS, 2012)

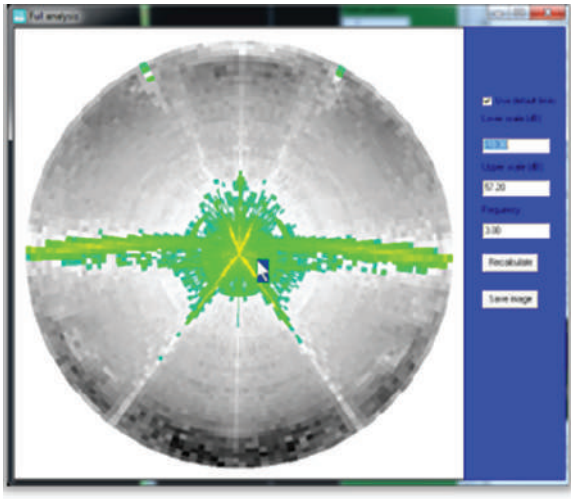

Fig. 9. Monitor Display andpolar graph of RCS (CADRCS, 2012)

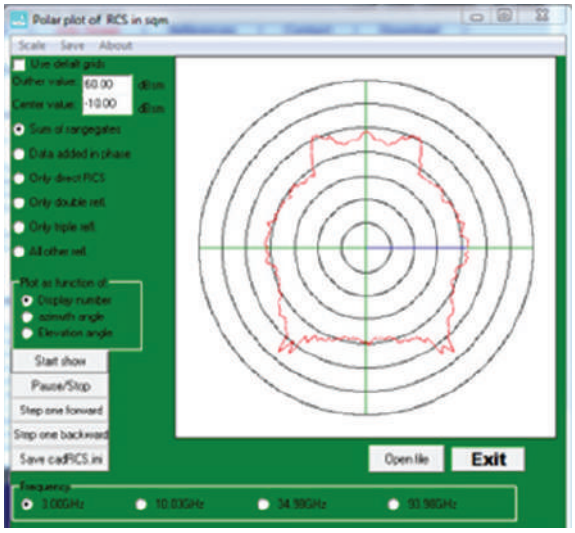

CST, Computer Simulation Technology Microwave Studio

The developer of integral equations of CST Microwave Studio is a new module for approximation of 3D analysis of electrically large structures, see Fig. 10. It is based on the multilevel fast multipolemethod (MLFMM) and it is used for analysis of patterns for fittings and radiation of antennae. Typical applications include location of antennae in aircraft and cross section of radar objects of high dispersion calculations.

Within the results offered by CST are the polar graphs, as shown in Fig. 11 and output of text files for export to other kinds of software.

This software allows discretization by the moments method, integral formulation of surfaces combined with the MLFMM, surface mesh that generates less mesh cells than common volume methods, the computational effort with MLFMM is effectively proportional to the size of the problem.

Fig. 10. Main Screen CST MICROWAVE STUDIO®

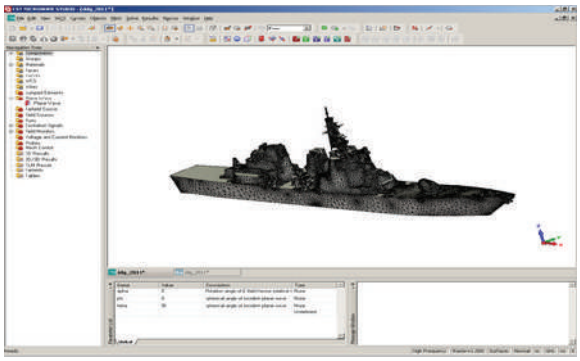

Fig. 11. RCS Results for 1,4, and 5 GHz

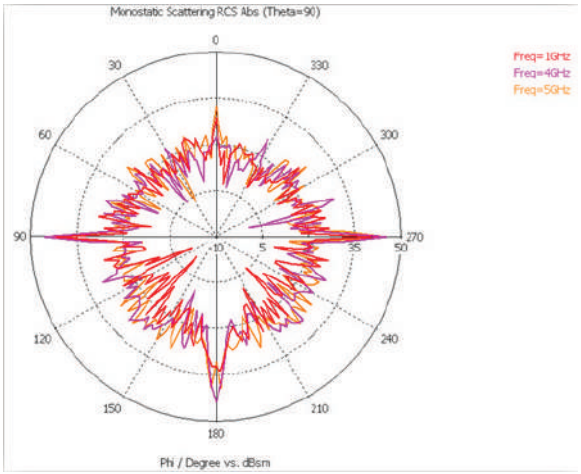

Methodology

A series of tests are designed to validate the results given by the POFACETS, CADRCS software. The 3D models of ships made in the COTECMAR shipyard are used. Riverine support light Patrol boat (PAF-L) and Riverine support heavy Patrol boat (PAF-P), where modifications to the hull are made to vary the angle of incidence of the radar rays and simulation with different types of materials to observe the behavior of the RCS.

The models used are described below:

We describe as NORMAL the ship unmodified in shape, and as FLAT the ship with bulkheads and sections perpendicular to the surface.

The fact that the PAFP and PAFL have different displacements, allows noting the relationship between size and RCS and also observing its behavior.

NORMAL PAF-L

Dimensions: Width: 7 m., Length: 30 m., Spot: 10.61 m.

Fig. 12. CAD Model of NORMAL PAF-L

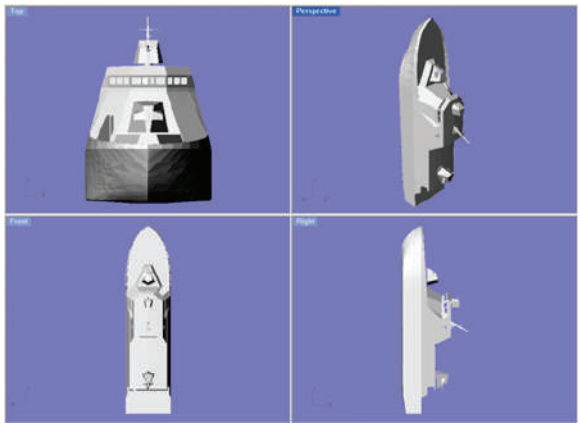

FLAT PAF-L

Dimensions: Width: 7 m., Length: 30 m., Spot: 10.61 m.

Fig. 13. CAD model of FLAT PAF-L

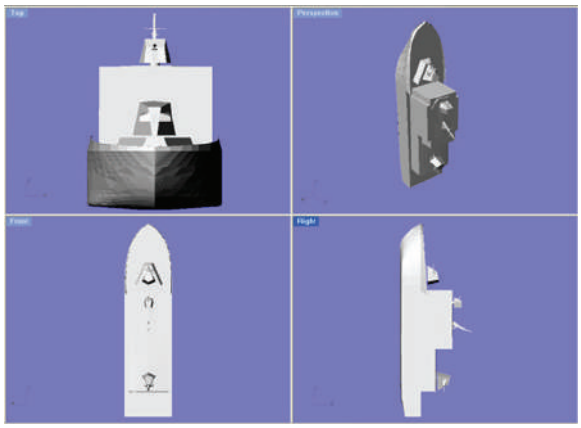

To make the comparison among software, the same CAD models of the same vessel were simulated at the same frequency by selecting the Test Material REL. PER = 1in POFACETS,as well as in CADRCS.

Also, due to the unique format of each software to obtain data in flat files, a program in Labview, RCS2Polar.vi, was designed to be able to read and compare them. The software has two tabs of graphical and numerical comparison: Images and Data respectively, opening of two .txt files in parallel, one for the POFACETS software and the other for CADRCS, differentiating each graph in dB or m2 with a different color.

NORMAL PAF-P

Dimensions: Width: 9.7 m., Length: 41 m., Spot: 11.9 m.

Fig. 14. CAD Model of NORMAL PAF-P

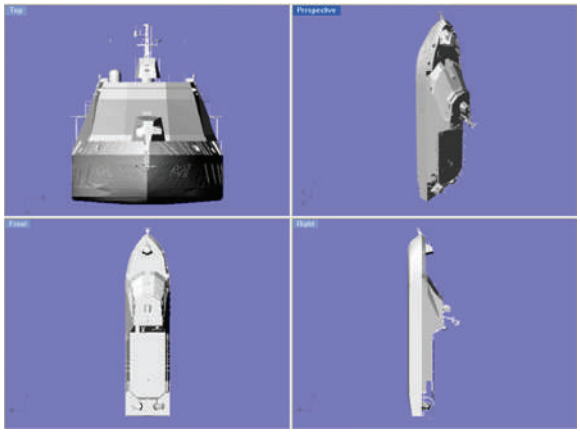

FLAT PAF-P

Dimensions: Width: 9.7 m., Length: 41 m., Spot: 11.9 m.

Fig. 15. CAD Model of FLAT PAF-L

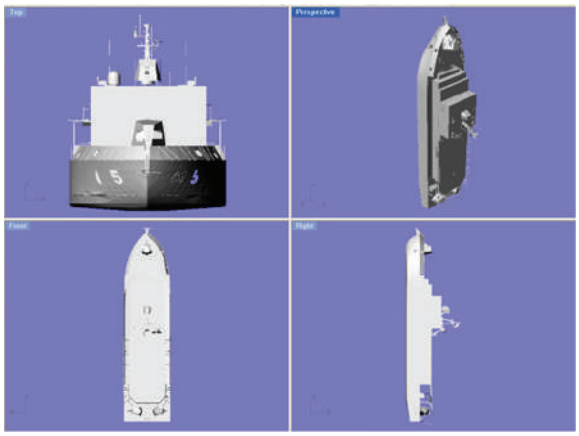

Comparison among software is performed at different frequencies because these use different methods to calculate RCS, then each method, therefore, uses different techniques where the value of the frequency directly affects both precision

Fig. 16. Screen in Labview software

Fig. 17. Data in Labview software

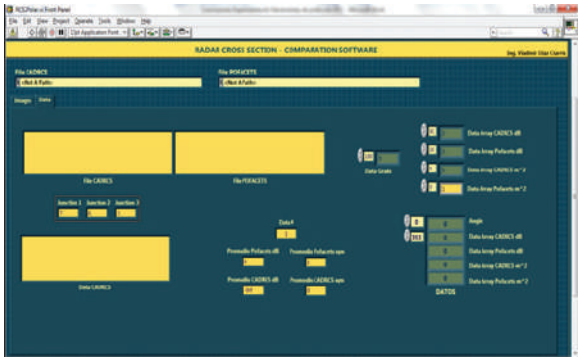

of the result and simulation time. Here are some graphs of simulations at different frequencies 1-16 GHz with results given in dB.

Fig. 18. Graphical comparison screen at 1 GHz in Labview

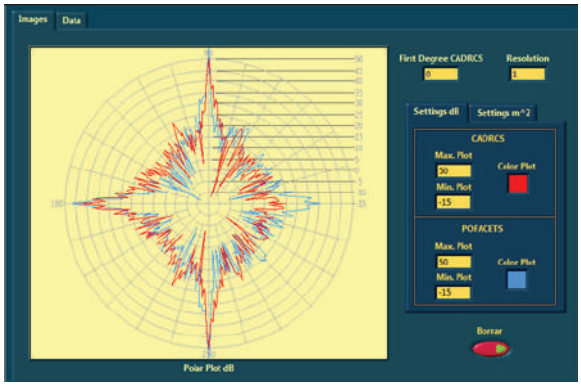

Fig. 19. Graphical comparison screen at 2 GHz in Labview

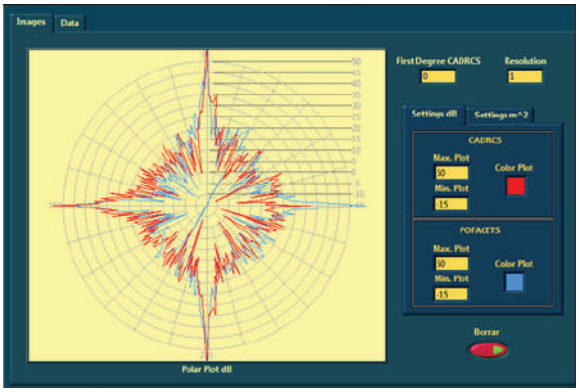

Fig. 20. Graphical comparison screen at 14 GHz in Labview

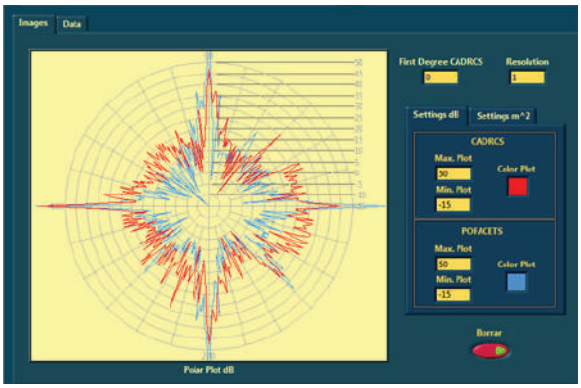

Fig. 21. Graphical comparison screen at 16 GHz in Labview

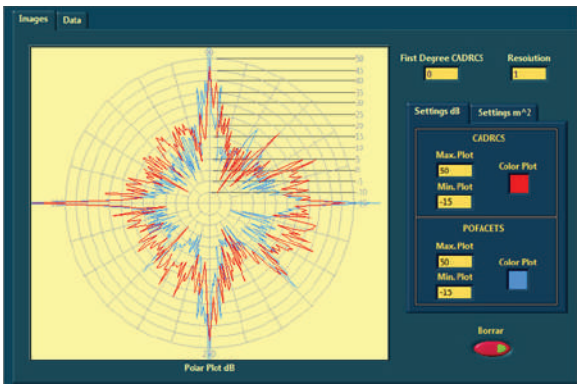

After various tests, we observed that in many angles of the ship a great similarity can be seen in values that RCS takes and found what sides are more feasible to be detected by a radar with its respective frequency.These polar images shown allow visually determining and analyzing the most critical points of the two results obtained: Red for CADRCS and blue for POFACETS. Each previous simulation is taken to one degree of resolution; therefore, there are 360 samples per simulation and its units are given in dBm.

On the other hand, within the RCS2Polar.vi software there is a polar chart that shows exactly the same data obtained in the two simulations but in m^2units (m^2). This chart allows easily determining the critical angles where it is necessary to apply RCS reduction techniques.

Evaluation of RCS

A possible event is determined to establish the need for the use of RCS reduction techniques in the design of ships. For this, a missile attack is evaluated; in this case an OTOMAT missile was selected and the AS-4 for surface-to-surface warfare and air-surfacewarfare, respectively, given their widespread use in armed forces worldwide and the ease of access to information in databases.

Missile Characteristics

- OTOMAT (SSM) – Band X 8 At 12 GHz (*Knott, Shaeffer, & Tuley, 2004*)

Fig. 22. OTOMAT SSM Missile (Pakistan Defense, 2011)

- AS-4 (ASM) 14 – 15GHZ (*Forecast International, 2011*)

Fig. 23. AS-4 ASM Missile Defense

To determine the radar frequency at which to perform the tests, various bands and applications of these in military operations are consulted resulting in the study of Band I / J (X Band Radar & Ku). This is a relatively popular radar band for military applications such as airborne radars for the exercise of functions of intercepting, hunting, and attack of enemy combatants and targets on land and sea. The size of the very small antenna provides good performance and, hence, its frequent use in missiles (*Wolff, 2011*).

Some aircraft like the Sukhoi have Kh-59MK anti-ship missiles with increased range. Its active ARGS-59 radar seeker has a maximum detection range of 25 km against 5000 m^2 RCS targets and 15km against 300 m^2 RCS targets.The cruising altitude of the Kh-59M is about 7 m above water or 50-1000 m above the ground. It can be launched at speeds of 600 to 1000 km /h at altitudes of 0.2 to 11 km [15].

The following tests were carried out in the POFACETS software, given that the results with this software are very similar to those obtained with CADRCS, and offers freedom of license, easy modification of type of material in its database and allows easily performing simulations and changes and quickly.

Results

Tests are developed with the following configuration:

Fig. 24. Monostatic RCS calculation setting

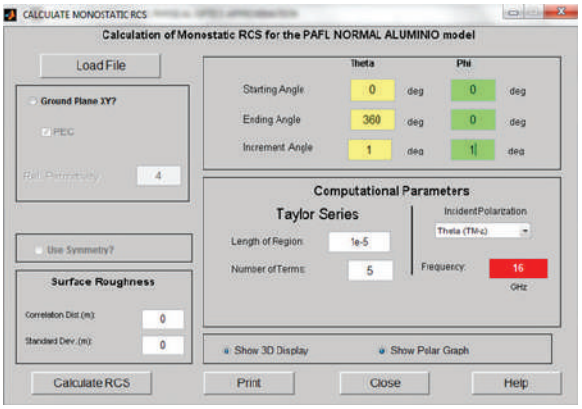

The increased resolution of one degree is configured, the start angle: 0, final angle: 360 to theta, frequency 16 GHz test set and 3D model and polar plot display features activated. Simulation of four designs of vessels for steel, and Eglass with Polyethylene Fiber materials.

Fig. 25. Graphical RCS polar PAF-L Normal Eglass

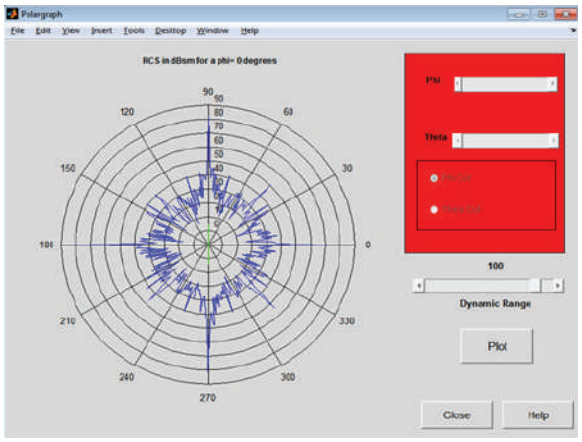

For each model simulations with RCS values of 360°, weproceed to obtain a characteristic value of these 360°, data with which we will compare the results of the experimental design, and the 90° angle value is selected being the starboard angle, one of the sides together with port side where the highest amount of RCS is reflected.

Fig. 26. Graphical RCS Polar PAF-L Plana Eglass

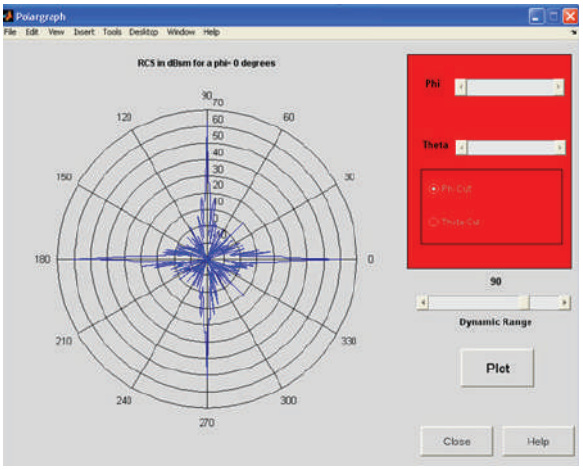

The data are shown in the following table:

Table 1. Simulation Results

No.	Displacement	Shaping	Material	RCS [dB]
1	PAFL	NO	Eglass Polyethylene	74.7641
2	PAFL	NO	Steel	88.4554
3	PAFP	YES	Eglass Polyethylene	68.4404
4	PAFL	NO	Eglass	84.8577
5	PAFL	YES	Steel	85.1996
6	PAFP	YES	Steel	82.1301
7	PAFP	NO	Eglass	87.8019
8	PAFP	NO	Steel	91.3989
9	PAFP	YES	Eglass	78.5349
10	PAFP	NO	Eglass Polyethylene	77.707
11	PAFL	YES	Eglass Polyethylene	63.8995
12	PAFL	YES	Eglass	81.5965

Fig. 27. Pareto chart of Transformed Estimates

Term	Orthog Estimate
Materials [Eglass Polyethylene]	-6,365918
Shapes Handling [SI]	-3,765333
Materials [Fiberglass]	1,979133
Displacement (162,373)	0,0603367

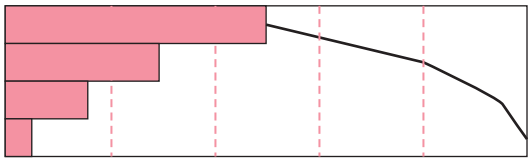

With the JMP 9.0 software, which allows for statistical analysis of the data, a series of tests are stipulated that permit full analysis of the different variables affecting the variation of RCS in a ship. For this, handling of shapes is initially set, making modifications to the PAF-P and PAF-L, to its main outer structure, turning the superstructure into faces perpendicular to the surface, followed by handling of materials; steel, fiberglass E-glass, and a composite between E-glass and polyethylene, and ending by comparing the sizes of the two vessels; displacement.

The Pareto diagram (see Fig. 27) can determine which is the most critical variable or greater impact on the RCS obtained and, in this case, if there are relationships between variables that influence the increase or decrease of the RCS. From the results, it can be seen that using composite materials like Eglass with polyethylene; fiberglass with polyethylene, allows for greater reduction in the RCS of a vessel, followed by Shapes Handling, proper shapes handling in the hull design of the vessel allows for a considerable reduction of the amount of energy reflected to enemy radars. Then, by handling these two variables the behavior of the model can be determined.

Another type of composite material,fiberglass, also called glass-reinforced plastic (*Mayer, 1993*) reflects the importance of using such materials in the manufacture of the superstructure, given that it absorbs large amounts of radar power in comparison to naval steel, it has great strength, light weight, and supports drastic weather variations.

Finally, it is remarkable that RCS behavior does not vary significantly with respect to the difference in displacement between the PAF-L and the PAF-P.

Conclusions

Given the results of this research, we can see that using POFACETS software as a tool to predict radar cross section is suitable for the development and scope of the objectives of this research. However, it should be noted that large global computational tools are available, which are used in the shipbuilding industry that allow more accurately predicting RCS in warships, considering factors like reflection of radar waves in the sea, conditions of the sea state, and more features such as ability to detect "hot spots" and ray tracing to identify parts of the structure that generate them.

Most computational tools for predicting RCS use prediction methods associated with physical optics because it is a high-frequency approximation that provides the best results, it does not consume excessive computational resources, and simulation time is relatively short compared to other methods like moments and the finite difference, which are used in software presented in this research. Nonetheless, the big disadvantage that leads to using other methods different other than physical optics to predict RCS, is that this method only works for high frequencies of detection.

Variables were identified that especially influence in the radar cross section of the type of shape of the superstructure and the hull, the type of material used in the construction of the vessel and its likely displacement, which in the experiments performed revealed that the type of material used has the most influence on the RCS followed by the handling of shapes, and – finally – displacement. In particular, evidence of the importance of using composite materials with lining in the manufacture of the superstructure of a vessel, such as fiberglass with

polyethylene, because they absorb great amount of radar energy in comparison to other materials as the sole use of fiberglass and steel, have high resistance, light weight, and support drastic climate variations ideal for everyday naval operations.

The result of this research focused on using the knowledge acquired during its development in future designs of surface platforms with low radar cross section, which can be done by applying RCS reduction techniques, focusing on the use radar absorbing materials (RAM) in those parts of the ship that require such and the proper handling of shapes in designing the hull and superstructure, which allows significant reductions in the amount of energy reflected to enemy radars.

Bibliography

AIRPLANE DESIGN. (2011). AirPlane Design PJ Gates - Ship Detection and Counter Detection. Obtained from http://www.airplanedesign.info/

CADRCS, C. (2012). PC, MAC, and GNU/LINUX BASED SOFTWARE FOR RADAR CROSS SECTION SIMULATION. Accessed in October 2011.

CAMTECH Camouflage Technology. (2005). SPECTRO DYNAMIC SYSTEMS. Accessed inOctober 2011, from www.camouflage.com.au/SPECTRO/Solve%20Low%20Observe.htm

CHATZIGEORGIADIS, F. (2004). Development of Code For a Physical Optics Radar Cross Section Prediction and Analysis Application. Naval Postgraduate School.

CHEVALIER, F. L. (2002). Principles of Radar and Sonar signal processing.London: Artech House.

DÍAZ, V., DOMINGUEZ, K., & SARAVIA, J. (2012). Estado Del Arte Del Manejo De La Seccion Transversal De Radar.

DVICE. (2009). DVICE SWEDEN. Accessed inOctober 2011, from www.dvice.com/archives/2009/02/sweden-creates.php

DVICE. (2012). DVICE. Accessed inOctober 2011, from www.dvice.com/archives/2009/02/top-secret-navy.php

FORECAST INTERNATIONAL. (2011). The Market for Anti-Ship. Revista(http://www.forecastinternational.com/samples/F658_CompleteSample.pdf).

GARRIDO, E. J. (September 2000). Graphical User Interface for a Physical Optics Radar Cross Section Prediction Code. Master's Thesis. Monterey, California: Naval Postgraduate School.

GATES, P. (2012). Ship Detection and Counter Detection. www.airplanedesign.info, www.ausairpower.net

gCaptain. (11 February 2009). Visby Class – Stealth Ship Of The Swedish Navy. Accessed inOctober 2011, from www.gcaptain.com/visby-class-stealth-ship-of-the-swedish-navy?6484

JENN, D. C. (1995). Radar and Laser Cross Section Engineering. Washington D.C.: AIAA Educations Series.

JENN, P. D., GARRIDO, C. E., & CHATZIGEORGIADIS, M. F. (2004). Software: Pofacets 3.0. Monterey, California: Naval Postgrade School - Philippine Navy - Hellenic Air Force.

KNOTT, E. F., SHAEFFER, J. F., & TULEY, M. T. (2004). RCS. Technology & Engineering.

LUCERNHAMMER. (2010). Accessed inOctober 2011, from http://lucernhammer.tripointindustries.com/

MARITIME SAFETY INFORMATION. (2009). CHAPTER 1 — BASIC RADAR PRINCIPLES AND GENERAL

CHARACTERISTICS. http://msi.nga.mil/MSISiteContent/StaticFiles/NAV_PUBS/RNM/310ch1.pdf.

MAYER, R. M. (1993). Design with reinforced plastics.

MICROWAVES 101. (2012). Microwaves101. Accessed inOctober 2011, from www.microwaves101.com

NET RESOURCES INTERNATIONAL AIR-FORCE. (2012). Air-Force Technology. Accessed inOctober 2011, from www.airforce-technology.com

NET RESOURCES INTERNATIONAL NAVAL. (2011). Naval - Technology. Accessed inOctober 2011, from http://www.naval-technology.com/projects/lafayette/lafayette1.html

NOTICIAS 24. (2008). Missiles Fire and Forget. Noticias 24.

ORBIT-FR. (2012). Accessed inOctober 2011, from www.orbitfr.com

PAKISTAN DEFENSE. (2011). Pakistan Defense. Obtained from http://www.defence.pk/forums/bangladesh-defence/168816-bangladesh-army-52.html

REVISTA NAVAL. (2012). Revista Naval. Accessed inOctober 2011, from www.revistanaval.com/articulos/tecnologia_stealth.htm

RIUS CASALS, J. M. (1991). Sección recta de blancos radar complejos en tiempo real. Departament de Teoria del Senyal i Comunicacions. Catalunya, España: Universitat Politècnica de Catalunya.

ROKE. (2012). EPSILON. Accessed inOctober 2011, from www.roke.co.uk/epsilon/

SAHAJANAND. (2011). Sahajanand Laser Technology Limited. Accessed inOctober 2011, from http://www.sltmicrowave.com/products.php?tab=1&#Conical_Rubber_Based_Radar_Absorbent_Material

SIEPEL. (2011). Absorbants électromagnétiques. Accessed inOctober 2011, from http://www.siepel.com/fr/siepel-france/produit/absorbants-%C3%A9lectromagn%C3%A9tiques

SKOLNIK, M. I. (2001). Introduction to Radar Systems 3rd Edition. New York: McGraw Hill.

TAYLOR, M. (2012). Soviet Missiles. Obtained from http://personal.inet.fi/cool/foxfour/sovmis/sovmis-as.html

VIRTUAL MARINE ARSENAL. (2007). Virtual Marine Arsenal. Accessed inOctober 2011, from www.bodrum-bodrum.com/vorteks/arsenal/stealth.htm

WOLFF, C. (2011). Radartutorial. Accessed inOctober 2011

Editorial Guidelines for Authors

Thematic Interest

The *Ship Science and Technology* Journal accepts for publication original engineering contributions in English language on ship design, hydrodynamics, dynamics of ships, structures and materials, vibrations and noise, technology of ship construction, marine engineering, standards and regulations, ocean engineering and port infrastructure, as well as results of scientific and technological research. Every article shall be subject to consideration by the Editorial Council of The *Ship Science and Technology* Journal deciding on the pertinence of its publication.

Typology

The *Ship Science and Technology* Journal accepts to publish articles classified within the following typology (COLCIENCIAS 2006):

- *Scientific and technological research articles*. Documents presenting detailed original results of finished research projects. Generally, the structure used contains four important parts: introduction, methodology, results, and conclusions.
- *Reflection Articles*. Documents presenting results of finished research as of an analytical, interpretative, or critical perspective of the author on a specific theme, resorting to original sources.
- *Revision Articles*. Documents resulting from finished research in the field of science or technology in which published or unpublished results are analyzed, systemized, and integrated to present advances and development trends. These are characterized by presenting an attentive bibliographic revision of at least 50 references.

Format

All articles must be sent to the editor of The *Ship Science and Technology* Journal accompanied by a letter from the authors requesting their publication.
Every article must be written in *Microsoft Word* in single space and sent in magnetic form.
Articles must not exceed 10,000 words (9 pages).
File must contain all text and any tabulation and mathematical equations.
All mathematical equations must be written in *Microsoft Word Equation Editor*. This file must contain graphs and figures; additionally, they must be sent in a modifiable format file (soft copy). Also, abbreviations and acronyms have to be defined the first time they appear in the text.

Content

All articles must contain the following elements that must appear in the same order as follows:

Title
It must be concise (no more than 25 words) with appropriate words so as to give readers an idea of the contents of the article. It must be sent in English and Spanish language.

Author and Affiliations
The author's name must be written as follows: last name, initial of first name . Affiliations of author must be specified in the following way and order:

- Business or institution (including department or division to which he/she belongs).
- Street mailing address.
- City (Province/State/Department).
- Country.

Abstract
A short essay of no more than one hundred fifty (150) words, specifying content of the work, scope, and results. It must be written in such a way so as to contain key ideas of the document. It must be sent in English and Spanish language.

Key Words
Identify words and/or phrases (at least three) that recover relevant ideas in an index. They must be sent in English and Spanish language.

Introduction
The text must be explanatory, clear, simple, precise, and original in presenting ideas. Likewise, it must be organized in a logical sequence of parts or sections, with clear subtitles to guide readers. The first part of the document is the introduction. Its objective is to present the theme, objectives, and justification of why it was selected. It must contain sources consulted and methodology used, as well as a short explanation of the status of the research, if it were the case, and form in which the rest of article is structured.

Body Article
It is made up of the theoretical framework supporting the study, statement of the theme, status of its analysis, results obtained, and conclusions.

Equations, Tables, Charts ang Graphs
All of these elements must be numbered in order of appearance according to their type and must have their corresponding legends, along with the source of the data.

Equations must be numbered on the right hand side of the column containing it, in the same line and in parenthesis. The body of the text must refer to it as "(Equation x)". When the reference starts a sentence it must be made as follows: "Equation x". Equations must be written so that capital letters can be clearly differentiated from lower case letters. Avoid confusions between the letter "l" and the number one or between zero and the lower case letter "o". All sub-indexes, super-indexes, Greek letters, and other symbols must be clearly indicated. All expressions and mathematical analyses must explain all symbols (and unit in which they are measured) that have not been previously defined in the nomenclature. If the work is extremely mathematical by nature, it would be advisable to develop equations and formulas in appendixes instead of including them in the body of the text.

Figure/Fig. (lineal drawings, tables, pictures, figures, etc.) must be numbered according to the order of appearance and should include the number of the graph in parenthesis and a brief description. As with equations, in the body of the text, reference as "(Fig. X)", and when reference to a graph is the beginning of a sentence it must be made as follows: "Fig. x".

Charts, graphs, and illustrations must be sent in modifiable vector file format (*Microsoft Excel, Microsoft Power Period*, and/or *Microsoft Vision*).

Pictures must be sent in TIF or JPG format files, separate from the main document in a resolution higher than 1000 dpi.

Foot Notes
We recommend their use as required to identify additional information. They must be numbered in order of appearance along the text.

Acknowledgment
Acknowledgments may be made to persons or institutions considered to have made important contributions and not mentioned in any other part of the article.

Bibliographic References

The bibliographic references must be included at the end of the article in alphabetical order and shall be identified along the document. To cite references, the Journal uses ISO 690 standards, which specify the mandatory elements to cite references (monographs, serials, chapters, articles, and patents), and ISO 690-2, related to the citation of electronic documents.

Quotations
They must be made in two ways: at the end of the text, in which case the last name of author followed by a comma and year of publication in the following manner:

"Methods exist today by which carbon fibers and prepregs can be recycled, and the resulting recyclate retains up to 90% of the fibers' mechanical properties" (*Davidson, 2006*).

The other way is:
Davidson (2006) manifests that "Methods exist today by which carbon fibers and prepregs can be recycled, and the resulting recyclate retains up to 90% of the fibers' mechanical properties".

List of References
Bibliographic references of original sources for cited material must be cited at the end of the article in alphabetical order and according to the following parameters:

In the event of more than one author, separate by commas and the last one by an "and". If there are more than three authors write the last name and initials of the first author and then the abbreviation "*et al.,*".

Books
Last name of author followed by a comma, initial(s) of name followed by a period, the year of publication of book in parenthesis followed by a comma, title of publication in italics and without quotation marks followed by a comma, city where published followed by a comma, and name of editorial without abbreviations such as Ltd., Inc. or the word "editorial".

Basic Form:
LAST NAME, N.I. *Title of book*. Subordinate responsibility (optional). Edition. Publication (place, publisher). Year. Extent. Series. Notes. Standard Number.

Example:
GOLDBERG, D.E. *Genetic Algorithms for Search, Optimization, and Machine Learning*. Edition 1. Reading, MA: Addison-Wesley. 412 p. 1989. ISBN 0201157675.

If a corporate author
Write complete name of entity and follow the other standards.

Basic form:
INSTITUTION NAME. *Title of publication*. Subordinate responsibility (optional). Edition. Publication (place, publisher). Year. Extent. Series. Notes. Standard Number.

Example:
AMERICAN SOCIETY FOR METALS. *Metals Handbook: Properties and Selection: Stainless Steels, Tool Materials and Special-Purpose Metals*. 9th edition. Asm Intl. December 1980. ISBN: 0871700093.

When book or any publication have as author an entity pertaining to the state, write name of country first.

Basic form:
COUNTRY, ENTITY PERTAINING TO THE STATE. *Title of publication*. Subordinate responsibility (optional). Edition. Publication (place, publisher). Year. Extent. Series. Notes. Standard Number.

Example:
UNITED STATED OF AMERICAN. EPA - U.S. Environmental Protection Agency. Profile of the Shipbuilding and Repair Industry. Washington D.C. 1997. P. 135.

Journal Article

Basic form:
Last name, N.I. Title of article, *Name of publication*. Edition. Year, issue designation, Pagination of the part.

Graduation Work

Basic form:
Primary responsibility. *Title of the invention*. Subordinate responsibility. Notes. Document identifier: Country or issuing office. *Kind of patent document*. Number. Date of publication of cited document.

Example:
CARL ZEISS JENA, VEB. *Anordnung zur lichtelektrischen Erfassung der Mitte eines Lichtfeldes. Et-finder*: W. FEIST, C. WAHNERT, E. FEISTAUER. Int. Cl.3 : GO2 B 27/14. Schweiz Patentschrift, 608 626. 1979-01-15.

Presentation at conferences or academic or scientific event

Basic form:
LAST NAME, N.I. Title of the presentation. In: Sponsor of the event. *Name of the event*. Country, City: Publisher, year. Pagination of the part.

Example:
VALENCIA, R., et al. Simulation of the thrust forces of a ROV En: COTECMAR. P*rimer Congreso Internacional de Diseño e Ingeniería Naval CIDIN 09*. Colombia, Cartagena: COTECMAR, 2009.

Internet

Basic form:
LAST NAME, N.I. *Title of work*, [on-line]. Available at: http://www.direccion_completa.com, recovered: day of month of year.

Example:
COLOMBIA. ARMADA NACIONAL. Cotecmar gana premio nacional científico, [web on-line]. Available at: http://www.armada.mil.co/?idcategoria=545965, recovered: 5 January of 2010.

Acceptance

Articles must be sent by e-mail to the editor of The *Ship Science and Technology* Journal to otascon@cotecmar.com or in CD to the journal's street mailing address (Cotecmar Mamonal Km 9 Cartagena Colombia), accompanied by the "Declaration of Originality of Written Work "included in this journal.

The author shall receive acknowledgement of receipt by e-mail. All articles will be submitted to Peer Review. Comments and evaluations made by the journal shall be kept confidential. Receipt of articles by The Ship Science and Technology Journal does not necessarily constitute acceptance for publishing. If an article is not accepted it shall be returned to the respective author. The Journal only publishes one article per author in the same number of the magazine.

Opinions and declarations stated by authors in articles are of their exclusive responsibility and not of the journal. Acceptance of articles grants The Ship Science and Technology Journal the right to print and reproduce these; nevertheless, any reasonable petition by an author to obtain permission to reproduce his/her contributions shall be considered.

Further information can be obtained by:
Sending an e-mail to sst.journal@cotecmar.com
Contacting Oscar Dario Tascon (Editor)
The Ship Science and Technology (Ciencia y Tecnología de Buques) office located at: Cotecmar Mamonal Km. 9, Cartagena Colombia.
Phone Number: 57 - 5 - 6685377.

SHIP
SCIENCE & TECHNOLOGY
CIENCIA & TECNOLOGÍA DE BUQUES

Statement of Originality of Written Work

Title of work submitted

_____

_____

_____

I hereby certify that the work submitted for publication in The *Ship Science and Technology* journal of Science and Technology for the Development of Naval, Maritime, and Riverine Industry Corporation, COTECMAR, was written by me, given that its content is the product of my direct intellectual contribution. All data and references to material already published are duly identified with their respective credits and are included in the bibliographic notes and quotations highlighted as such.

I, therefore, declare that all materials submitted for publication are completely free of copyrights; consequently, I accept responsibility for any lawsuit or claim related with Intellectual Property Rights thereof.

In the event that the article is chosen for publication by The *Ship Science and Technology* journal, I hereby state that I totally transfer reproduction rights of such to Science and Technology for the Development of Naval, Maritime, and Riverine Industry Corporation, COTECMAR. In retribution for the present transfer I agree to receive two issues of the journal number where my article is published.

In witness thereof, I sign this statement on the _____ day of the month of _____ of year _____, in the city of _____ .

Name and signature: Identification document:

_____ _____

Publindex
Indexación - Homologación

COTECMAR
COLOMBIA

Red Colombiana de Revistas de Ingeniería

Km. 9 Vía Mamonal - Cartagena, Colombia
www.shipjournal.co

Vol. 6 - n.° 11
July 2012

Project and Construction of Oceanographic and Faisheries Research Vessels in Spain
José Fernando Núñez Basáñez

Analysis and Prediction of Welding Distortion in complex Structures Using Elastic Finite Element Method
Adán Vega Sáenz, Carlos Plazaola, Ilka Banfield, Sherif Rashed, Hidekazu Murakawa

Study of the weldability of Aluminum Alloy 5083 H116 with Pulsed Arc GMAW (GMAW-P)
Cueca, F., Morales, A., Muñoz, R., Patarroyo, A., Rojas, F., Solano, E.

Shooting Simulator for Fluvial Combat Training
Carlos F. Rodríguez, José Tiberio Hernández, Pablo Figueroa

Side-boat tow to Test the Influence of Flaps in a 2-meter Planing Craft Model
José R. Marín, Daniela A. Benítes

Dynamic modeling of trawl fishing gear components
Jorge Freitas Pereira

Analysis of radar cross section assessment methods and parameters affecting it for surface ships
Vladimir Díaz Charris, José Manuel Gómez Torres

COTECMAR

www.shipjournal.co